Hydrogasification of Carbon Catalyzed by Nickel

Yoshiyuki Nishiyama and Yasukatsu Tamai

Chemical Research Institute of Non-Aqueous Solutions,
Tohoku University, Katahira, Sendai, 980 Japan

Introduction

Gasification of coals to produce high-Btu gases is receiving extensive attentions. Catalysis at gasification stage is investigated by several workers(1), but the catalytic processes, especially the interaction between coal and catalyst, are not well understood. In the preceding report from this laboratory, it was shown that some of the transition metals catalyze the hydrogasification of active carbons and that methane was formed in two or three stages. When Ni was used, the first stage reaction occurred at a temperature region around 550°C and the second one above 800°C. It would be interesting if the low temperature reaction can be incorporated in a coal conversion process. In this presentation, a study to clarify the nature of the reactions is described, putting emphasis on the behavior of Ni.

Experimentals

Two types of activated carbon were used; one in a granular form (AC-G) and the other a powder(AC-P). They were impregnated with a Ni salt, normally $Ni(NO_3)_2$ if not stated otherwise, from aqueous solution. Gasification was conducted mainly in a thermobalance and the specimen, 0.1-0.5 g, was heated in an atmospheric flow of hydrogen at a constant heating rate(denoted as HR) up to 1000°C and the amount of methane formed was analyzed by a gas chromatograph. Gasification at elevated pressures were done in a fixed bed reactor. In this case, the temperature was raised to 900°C in 80 min and kept for 1 hr.

The dispersion of Ni on carbon surface was examined using X-ray diffraction, scanning electron microscope and a magnetic measurement. In the last one, the magnetization of the specimen was measured in hydrogen atmosphere by Faraday method using a permanent magnet. The apparant magnetic susceptibility given below, χ_a, is supposed to be proportional to the magnitude of magnetization at a constant field.

Results

Types of reactions concerned

A typical methane formation profile is illustrated in Fig. 1. Of the two active regions, the lower one between 400 and 700°C is referred to as R-1 and the other, the higher one above 800°C, as R-2. In the results given below, conversion to methane is denoted by X.

Features of R-1 reaction

[1] Temperature dependence. One of the marked character of R-1 is its transient nature, i.e., the specimen lost its activity when heated above 650°C whether the heating accompanied gasification or not, but a re-impregnation of Ni to the deactivated specimen restored the reactivity(Table 1). Even when the temperature was kept within the active region, the rate decreased rather rapidly, as shown by one of the broken lines, A, in Fig. 1, as if a limited portion of carbon could be gasified.

[2] Pressure dependence. R-1 had a negative dependence on the hydrogen pressure above 1 atm(Fig. 2).

[3] Dependence on Ni content. Fig. 3 shows that X(R-1) is small up to 2 % of Ni for AC-P and beyond this limit, the conversion increases steeply with Ni content. For another carbon, similar patterns were

observed, but the extent of Ni content within which the activity was insignificant depended on surface state of carbon. For example, a nitric acid treatment of AC-G(in 13.5 N acid at 20°C for 3 hr) increased the amount of inactive Ni to 4 % when this was 1.5 % for untreated specimen(AC-G). The concentrations of surface acidic sites titrated with NaOH were 52 and 9 mmol/100g for treated and untreated carbon, respectively. This suggest that the inactive Ni atoms are trapped at active sites.

[4] Effect of Ni salts. Table 2 shows a comparison of Ni salts used as Ni source. $Ni_3CO_3(OH)_4$ from aqueous ammonia solution and $Ni(NO_3)_2$ were active for R-1, whereas $NiCl_2$ was almost inactive under normal conditions. Interestingly, X(R-1) of $NiCl_2$-impregnated specimen varied with the condition to reduce the salt. The activity increased by a prolonged reduction at lower temperatures(Table 3). These results can be understood by a variation in the dispersion of Ni.

Features of R-2 reaction

[1] Dependence on temperature and pressure. R-2 is an ordinal reaction in that it proceeds at nearly constant rate at a constant temperature though the rate increased somewhat at the initial period and decreased gradually with the carbon burn-off and that the rate varied reversibly with temperature. R-2 had a positive order with respect to hydrogen pressure(Fig. 2).

[2] Dependence on Ni content. In contrast to R-1, X(R-2) increased with Ni content at first but leveled-off soon, as shown in Fig. 3.

[3] Effect of Ni salt and the surface state of carbon. R-2 had no preference to the species of Ni salt to be impregnated(Table 2). Also, the surface treatment of carbon had negligible effect on X(R-2).

Dispersion of Ni on carbon surface

[1] X-ray diffraction. The breadth of (111) diffraction of Ni showed a trend that the smaller the average crystallite size, the larger the X(R-1), and that growth of Ni crystallites occurred after R-2 took place(Table 2), but this method is insensitive to the smaller part of crystallite and is inappropriate to follow the changes during R-1.

[2] Microscopic observation. From observations by a SEM, slight change in the distribution of Ni was noted after the completion of R-1. Upon heating to R-2 region, vigible Ni particles appeared on the whole surface(Fig. 4).

[3] Magnetic measurement. Fig. 5 demonstrates typical changes in χ_a at the initial and the final stage of R-1. The turns at 70-200°C was ascribed to the adsorption of hydrogen at lower temperatures. The figure indicates that Ni in unreacted specimen is in a superparamagnetic state(3),which was converted into a ferromagnetic state by heating. The χ_a at 100°C from descending curve or its extrapolation was used as a measure of the dispersion of Ni and is given as χ° in Table 4, together with the activity in R-1. The conversion into a ferromagnetic state occurred even without gasification reaction. If a plot is made from Table 4, it can be shown that the remaining activity of specimens preheated to various degree is nearly proportional to the change in χ° by further heating. In another experiment, a specimen was heated repeatedly to the predetermined temperature which was raised in succession and the weight and χ_a were measured at room temperature(Fig. 6). Both of these changed concurrently at the same temperature regions. The χ_a decreased during or after R-2, which seems to suggest a change in the bonding state of Ni, probably due to the dissolution of carbon or some component of ash concentrated on carbon surface.

Discussions

From the results given above, it can be concluded that the deactivation by heating above the R-1 region is due to a change in the dispersion of Ni, i.e., an aggregation to a larger particles. Fig. 6 and Table 4 seem to suggest that the catalytic action is related to the migration of Ni atoms and smaller particles on carbon surface. The migration itself is, perhaps, a thermal motion, not associated with the gasification reaction. The dependence of R-1 activity on Ni content indicates that those atoms strongly held at active sites are immobile and are inactive for R-1. Ni particles continue to grow during R-2, but this seems to be caused by the disappearance of the substrate.

Two types of possible mechanism of catalytic gasification are frequently discussed: (A) hydrogen dissociates on the catalyst surface and spills over to carbon surface, and (B) catalyst modifies the C-C bonds to enhance the reactivity. The present results are insufficient to draw a conclusion about the mechanism, but it seems improbable that (A) type action is working in R-1, as this has negative dependence on hydrogen pressure. For R-2, on the other hand, (A) type action can account the pressure dependence as well as the insensitiveness to Ni content and to the state of dispersion, although other possible explanations may exist. The decrease in χ_a at R-2 region need further study and it is not clear at present whether this change has any correlation with the gasification reaction.

References

(1) J. L. Johnson, Cat. Rev., 14, 131 (1976).
(2) A. Tomita and Y. Tamai, J. Cat., 27, 293 (1972).
(3) P. W. Selwood, "Adsorption and Collective Paramagnetism", Academic Press, New York (1962).

Table 1 Activities in R-1*

Specimen	X(R-1)
Unreacted	30.2 %
Reacted once	0.7
Re-impregnated	27.7
Preheated in He**	3.1

* AC-P, 5 % Ni. HR=5°C/min.
** at 600°C for 2 hr.

Table 2 Comparison of Ni salts*

Salt	Ni content	X(R-1)	X(R-2)	Crystallite size after reduction	R-1	R-2
$Ni(NO_3)_2$	4.3 %	5.8 %	7.0 %	35 Å	40 Å	260 Å
$NiCl_2$	4.1	0.8	6.4	200	200	230
$NiBr_2$	4.3	0.9	5.4	200	-	490
$Ni_3CO_3(OH)_4$**	4.1	6.3	4.8	260	300	320
$(CH_3COO)_2Ni$**	3.9	1.2	6.8	165	-	190

* AC-G, HR=2.3°C/min.
** Impregnated from aqueous ammonia solution.

Table 3 Effect of reduction temperature

Conditions	X(R-1)	Crystallite size
240°C, 5 hr	1.2 %	- Å
257°C, 14.7 hr	2.7	125
263°C, 8 hr	1.1	135
284°C, 3 hr	0.8	140
const. rise**	0.9	200

* AC-G impregnated with $NiCl_2$ (4.1 % Ni).
** HR=2.3°C/min.

Table 4 χ° and R-1 reactivity*

Ni content	Treatment**	χ°	X(R-1)
1 %	300°C, 2 hr	3.2 esu/g Ni	1.2 %
1	450°C, 2 hr	3.7	0.5
1	600°C, 2 hr	5.5	0.1
5	300°C, 2 hr	2.3	30.2
5	450°C, 0 hr	3.9	25.2
5	450°C, 2 hr	4.2	24.0
5	600°C, 2 hr	8.0	0.7
5	600°C, 2 hr in He	8.9	3.1

* AC-P, HR=5°C/min.
** In hydrogen except for the last line.

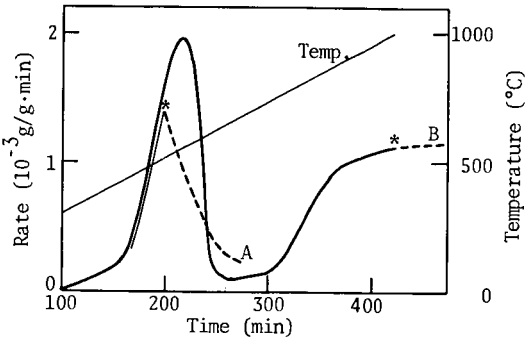

Fig. 1 Methane formation profile (AC-G)
Solid line: HR=2.3°C/min,
Broken lines: Temperature was kept constant from the points marked by asterisks. A at 560°C and B at 1000°C.

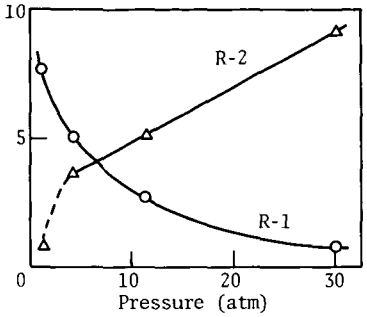

Fig. 2 Pressure dependence (AC-G,7%Ni)
R-1: conversion in %.
R-2: maximum rate at 900°C in 10^{-3} g/g·min.

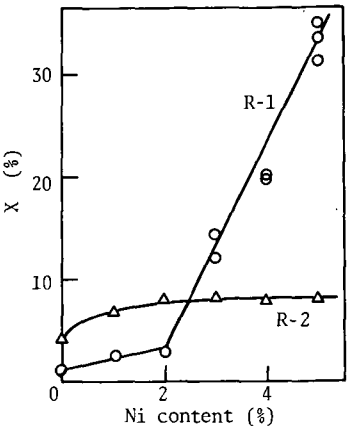

Fig. 3 Conversion vs. Ni content
Specimen: AC-P, HR=5°C/min.

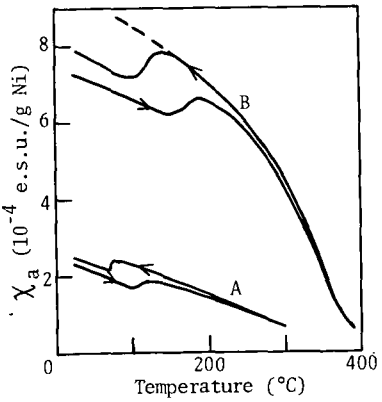

Fig. 5 Apparant magnetic susceptibility of AC-P with 5 % Ni
Specimens were heated in hydrogen for 2 h, A: at 300°C, B: at 600°C before measurement.

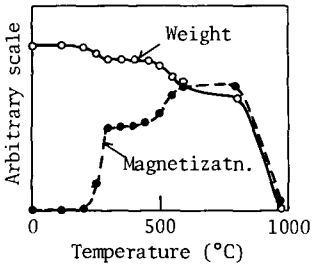

Fig. 6 Changes in weight and magnetization
Specimen: $NiCl_2$-impregnated (5 % Ni)

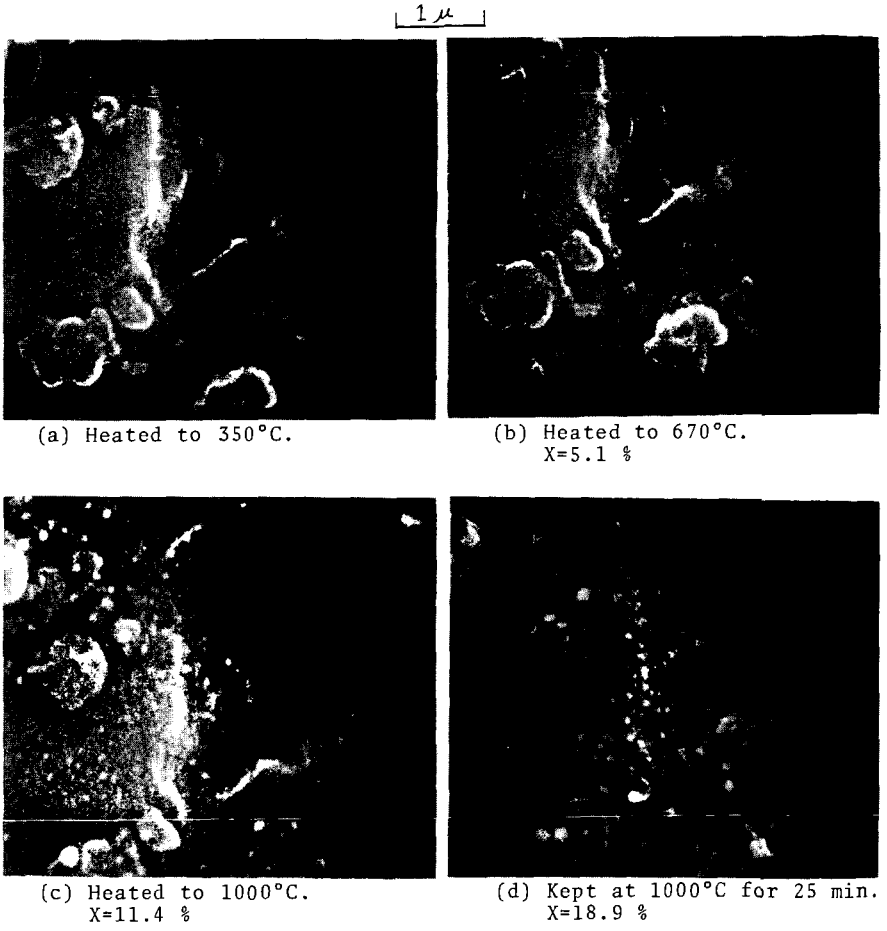

(a) Heated to 350°C.

(b) Heated to 670°C.
X=5.1 %

(c) Heated to 1000°C.
X=11.4 %

(d) Kept at 1000°C for 25 min.
X=18.9 %

Fig. 4 Photographs of an AC-G specimen with 7 % Ni(as an average for a batch of the specimen), heated repeatedly in hydrogen HR=5°C/min.

SCANNING ELECTRON MICROSCOPE STUDY ON THE CATALYTIC GASIFICATION OF COAL

Akira Tomita, Kazutoshi Higashiyama and Yasukatsu Tamai

Chemical Research Institute of Non-Aqueous Solutions,
Tohoku University, Katahira, Sendai 980, Japan

INTRODUCTION

In previous papers (1,2), it has been reported that coals pretreated with liquid ammonia can be gasified more easily than untreated coals, especially when they are impregnated with nickel catalysts. The effectiveness of nickel catalyst varies with such parameters as the method of nickel loading, the kind of nickel salt, the condition of reduction of salt to metallic state, and others. According to circumstances, nickel does not necessarily act as effective catalyst. In order to obtain a higher catalytic activity, it is essential to understand how a nickel particle catalyzes the gasification reaction. Some particles may be active, and others may be less active. We then have to find the way of nickel loading to produce only such active particles. Thus, we can maximize the catalytic activity of nickel for coal gasification. The microscopic observation is known to be one of the most useful tool for understanding the behavior of metal catalyst on carbon gasification (3,4,5). Scanning electron microscope (SEM) studies on catalytic coal gasification have been made by several groups of workers in recent years (6, 7). These studies have dealt almost exclusively with the static state of catalyst. We wish to report here dynamic behaviors of catalyst on coal gasification observed by the SEM coupled with the energy dispersive analysis of X-rays (EDAX).

This technique would be useful in the following aspects. The movement of nickel particles can be monitored by examining the specimens before and after gasification. The relationship between the catalytic activity and the size or shape of nickel particle can be checked. A semi-quantitative analysis is possible with respects to the presence of mineral matter and its catalytic activity on the gasification. The interaction of nickel with other elements can be examined. The sulfur poisoning of nickel catalyst is the most important interaction among all. The present method, however, has some limitations in addition to the dangers implicit in the use of microscopy, which Thomas called as the twin evils of electicism and tendentiousness (3). The first limitation is that we did not observe the change of coal surface at reaction conditions , but at room temperature. Some changes might occur during the cooling stage. The second one is the neglect of possible catalytic activities of fine particles of diameter less than 100 nm. In spite of these limitations, we believe that this technique may give useful informations about the catalytic behavior of nickel particles.

EXPERIMENTAL

Coal samples used in this study were the same as in the earlier work (2). Ammonia treatment was carried out at 373 K and 10 MPa for 1 hr. About 1 wt% of nickel was impregnated on coal from an aqueous solution of hexaamminenickel(II) carbonate. Details on these pretreatments and analyses of coals were reported elsewhere (8). We would like to use the abbreviations for coal samples with different pretreatments; UN for raw coal, UC for raw coal with nickel catalyst, and TC for ammonia treated coal with nickel catalyst. The same nomenclatures are also used for the chars therefrom. For the SEM observations, five coal particles of 1 - 2 mm in size were mounted on a cylindrical graphite holder which is fit for the SEM equipment. Graphite paste was used to adhere the coal particles to the holder.

Figure 1 illustrates the reactor assembly. Two graphite sample holders were put on a rectangle quartz dish with a size of 20 by 40 mm. The dish can be moved horizontally by a quartz tube with a hook. In this quartz tube, a thermocouple was inserted to monitor the reaction temperature. The temperature difference between the tip of this thermocouple and the coal sample was less than 5 K. The furnace temperature was controlled by another thermocouple. For steam generation, a small evaporator with an electric heating wire was utilized. It evaporates water fed from a microfeeder at a constant rate. Exposed parts of tubings were also wound with a heating wire in order to prevent a steam condensation.

Coal samples on a graphite holder were examined under an SEM, a Hitachi-Akashi MSM 4C-101, to which an EDAX, a Horiba EMAX-1500, was attached. Then, the holder was put on a quartz dish and placed in the reactor. The initial position of the dish was outside of the furnace. After an evacuation of the system, nitrogen gas was introduced at the flow rate of 200 cm^3(STP)/min. When the furnace temperature reached 773 K, the quartz dish was pushed into the center of the furnace. It was pulled out after the devolatilization for 1 hr. Samples were then carefully examined by SEM and EDAX. The graphite holder were returned to the quartz dish in the reactor. The evacuation of the system was followed by the introduction of nitrogen and reacting gas. In case of steam gasification, the flow rate of nitrogen was kept at 40 cm^3(STP)/min and the flow rate of steam was 150 cm^3(STP)/min. When the temperature and the gas flow rate became stationary, the quartz dish was pushed in. After the required time of gasification, the coal sample was pulled out to be examined. Similar procedures were repeated for several times to follow the morphlogical changes at the same sights on char surface. In case of hydrogasification, the flow rate of hydrogen was 200 cm^3(STP)/min. Some photographs were taken for coal samples gasified in the thermobalance reported earlier (2).

The conversion of coal at each stage was determined in a different series of experiments. Coal particles of about 200 mg were placed on a quartz dish without graphite holders. The devolatilization and gasification were carried out under the same reaction conditions as before. At the end of each stage, the weight was measured and the conversion was calculated on a dry ash free basis.

RESULTS AND DISCUSSIONS

We would like to mention first about the result of observation on coals without any heat treatment. Figure 2 shows the surface of Shin-Yubari coal cut by a microtome in order to check whether the nickel salt penetrated into the inside of particle. Three points should be noted here. First, the ammonia treated coal has cracks of various widths, whereas the untreated coal has no cracks. We present here only one particle for each, but this tendency was quite general one. The crack formation was particularly remarkable for lower rank coals. Second, the presence of nickel salt was recognized either on the external surface as in (b) or along the cracks as in (d). In these two photographs, the concentration of nickel was analyzed along the upper stright line, and it was shown as a notched line. These facts indicate that the nickel salt on a UC sample exists mainly on the external surface, whereas that on a TC sample exists not only on the external surface but also in the inside of coal particle. Third, there were many ellipsoidal holes of a diameter of about 10 μm on the cut surface. Flakes with a thickness of 1 μm were made during the course of cutting by a microtome, and it was also examined on SEM. We found that the flake consisted of many granular particles supported on a thin film. These particles might come out from the holes mentioned above. It can therefore be presumed that these holes are made because of the heterogeneity of coal in mechanical strength. Similar holes were observed for all other types of coal.

Table I. Successive Gasification of Leopold Coal

Stage	Gas	Temperature (K)	Reaction Time (hr)	Conversion (%, daf) UN	UC	TC
1	N_2	773	1.0	26	25	23
2	H_2O	1023	0.5	37	37	37
3	H_2O	1023	0.5	40	41	42
4	H_2O	1023	0.5	42	45	47
5	H_2O	1073	0.5	49	55	56
6	H_2O	1073	1.0	60	67	71

As an example of catalytic coal gasification, we present here the result on steam gasification of Leopold coal. The heat treatment procedures and the conversion on a dry ash free basis are summarized in Table I. The conversion was in accordance with that obtained earlier in a thermobalance (2). Figure 3 shows a typical behavior of nickel catalysts during steam gasification. At the first stage, where the coal was devolatilized in nitrogen, most nickel exist as flakes. Some granular nickel particles are seen in Figure 3(a). An X-ray diffraction analysis revealed that the state of nickel at this stage was already metallic. The dispersion of nickel is not homogeneous, and the accumulation of nickel along cracks is observed. A lesser amount of nickel is found on the flat surface at the upper left side of the photograph. At the second stage, most of flakes have changed to particles. The size of particle seems to be around a few microns so far as judging from Figure 3(b). However, in fact, each particle consists of a number of much smaller particles which are bundled in a wooly substance. In the upper left corner, many nickel particles appeared and they catalyzed the gasification around them, resulting in the formation of holes. Most of these particles disappeared in their own holes at the third stage (c). At the fifth stage (d), the surface becomes rough and rough. The nickel particles start to agglomerate. The ditch becomes wide. EDAX examined the nickel and sulfur concentration for the whole field of view in this series. It can be said that the nickel content decreased at the third stage perhaps due to the submersion of particles into holes. The sulfur content also decreased at this stage. The mechanism whereby this occurs is unclear. One possible explanation may be the desulfurization by an excess amount of steam and/or hydrogen. Figure 4 shows somewhat less common example. At the devolatilization stage, fine particles with diameters of less than 0.1 μm gather to form a long, narrow strip. Fine cracks were observed on and near this strip. Some of them were perpendicular to the strip. After the gasification for 0.5 hr, a deep ditch appeared where fine particles had existed. Comparing with the depth of holes dug by an ordinal spherical particle shown on a flat surface, we may presume that the fine particle is much more active as a gasification catalyst. After the second stage, the gasification reaction proceeds in a similar manner as shown in Figure 3. In some cases, needle crystals containing nickel and a considerable amount of sulfur were observed after devolatilization. These were not so active.

Low magnification photographs of Leopold-UC coal and the first stage char are shown in Figure 5. A cubic particle swells upon devolatilization. The degree of swelling can be estimated by measuring the size of particle before and after the heat treatment. Usually, TC samples do not swell and some of UC samples swell as this particle does. Most of UN coal particles swell to some extent (FSI is $1\frac{1}{2}$). Such suppression effect on caking property by the present pretreatment has been found for a variety of coals. Almost no nickel particles were observed on the hemispherical portion of char in Figure 5(b), which had bubbled out from the inside of coal. In order to check the uncatalyzed gasification rate, the change in this portion was followed throughout the series of steam gasification shown in

Table I. Practically no change was observed. Ash particles containing iron catalyzed the gasification, although the effect as catalyst was much smaller than that of nickel. Other ash particles containing aluminum, silicon, potassium, or calcium were found to be catalytically inactive.

Figure 6 shows two examples of the fate of nickel catalyst. Both samples are Leopold TC char gasified in steam at 1123 K for 2 hr. The conversion was 92 %. The first photograph indicates the accumulation of nickel and ash on the external surface of char particle at such a high conversion. Spot analyses by EDAX revealed the composition of ash as follows: A, nickel; B, nickel and sulfur; C, nickel; D and E; aluminum, silicon, nickel, iron and sulfur; F, iron; G, little sulfur, which means the main element is carbon. The blackish part which can be seen through the cleavage of ash layer is nearly pure carbon. The contact of this carbonaceous portion with nickel catalysts seems to be poor. The ash layer may be a resistance for gas diffusion. These facts imply the difficulty of catalyst utilization at high conversion. The second photograph shows the interior of Leopold char. This surface was exposed by cutting a char particle by a razor blade. The inside of char is very porous. In these macropores, few nickel particles were recognized. In accord with the observation in Figure 2, some nickel particles were found in the inside of TC char, but none in the inside of UC char. Anyhow, the amount was quite small compared with that present on the external surface. All other chars from different coals also have similar macropores. The amount of nickel in these macropores are also limitted. In order to utilize nickel catalyst efficaciously, we should make all possible efforts to impregnate nickel salt not only on the external surface but also in the inside of coal particle.

Figure 7 exhibits some reactions of nickel with other elements in coal. A somewhat peculiar form of nickel is shown in the first photograph which was taken from Zollverein TC char. The intensity of EDAX tells us that a stick-shaped part is made from iron with a small amount of nickel, and that a ball-shaped part is made from nearly an equal amount of nickel and iron. The slender the stick, the larger the ratio of iron to nickel. The bigger the ball, the larger the nickel content. We think these are some compound resulted from the reaction of nickel and iron, although an X-ray diffraction study of char could not identify it. There is no evidence so far that they catalyze the gasification reaction. The reaction with sulfur is more important in connection with the catalyst poisoning (7). Sulfur exists all over the coal particle, and this reaction was observed quite frequently in case of steam gasification. As is shown in the line profiles of nickel and sulfur in Figure 7(b), some nickel particles contain a considerable amount of sulfur, while the others do not. The concentration of sulfur is not homogeneous even in a single particle. The catalytic activity of nickel does not seem to have a strong dependence on the sulfur content. We can find many nickel particles which is still active in spite of the contamination with sulfur. In the case of hydrogasification at 1273 K, the sulfur on nickel was quickly taken away as hydrogen sulfide. Essentially no sulfur remained after a few stages of hydrogasification.

CONCLUSIONS

A nickel catalyzed gasification of coal has been investigated by means of SEM and EDAX. We followed the movement of catalyst by observing the fixed sight before and after gasification. The most important finding is that nickel particles do not exist in the interior of coal particle so far as the present method of impregnation is utilized. Nickel particles on the external surface are found to be very active as catalysts. In other words, true reaction rate for catalytic gasification is much greater than non-catalytic reaction rate. If we can only find an appropreate method of impregnation to put nickel salt into the inside of

coal, the catalytic effect would be significantly improved. The next important result is the fact that the catalytic activity of nickel varies with the form of nickel particle. Very fine particle, for example, are much more active than the others. Thus, the second subject that we should challenge is to find an impregnation method which can disperse most nickel in the form of such very fine particles.

REFERENCES

1. Matida, M., Nishiyama, Y., and Tamai, Y., "Gasification of Coals Treated with Non-Aqueous Solvents. 1. Liquid Ammonia Treatment of a Bituminous Coal," Fuel, 56, 171 (1977).
2. Tomita, A., Oikawa, Y., Kanai, T., and Tamai, Y., "Gasification of Coals Treated with Non-Aqueous Solvents. 6. Catalytic Steam Gasification at Atmospheric Pressure," presented at the Annual Meeting of CSJ, Yokohama, April, 1978.
3. Thomas, J. M., "Microscopic Studies of Graphite Oxidation," in P. L. Walker, Jr., Ed., "Chemistry and Physics of Carbon," Vol. 1, Marcel Dekker, New York (1965), p 121.
4. Tomita, A. and Tamai, Y.,"An Optical Microscopic Study on the Catalytic Hydrogenation of Graphite," J. Phys. Chem., 78, 2254 (1974).
5. Baker, R. T. K., "Catalysis in Action," Chem. Eng. Prog., April 97 (1977).
6. Gardner, N., Samuels, E., and Wilks, K., "Catalyzed Hydrogasification of Coal Chars," in L. G. Massey, Ed., "Coal Gasification," American Chemical Society, Washington, D. C. (1974), p 217.
7. Rai, C. and Hoodmaker, F., "Effect of Coal Sulfur on Catalyst Activity in the Direct Production of Hydrocarbons from Coal-Steam Systems," AIChE Symposium Series, 72, 332 (1976).
8. Tomita, A., Tano, T., Oikawa, Y., and Tamai, Y., "Gasification of Coals Treated with Non-Aqueous Solvents. 5. Properties of Coals Treated with Liquid Ammonia," presented at the Annual Meeting of CSJ, Yokohama, April, 1978.

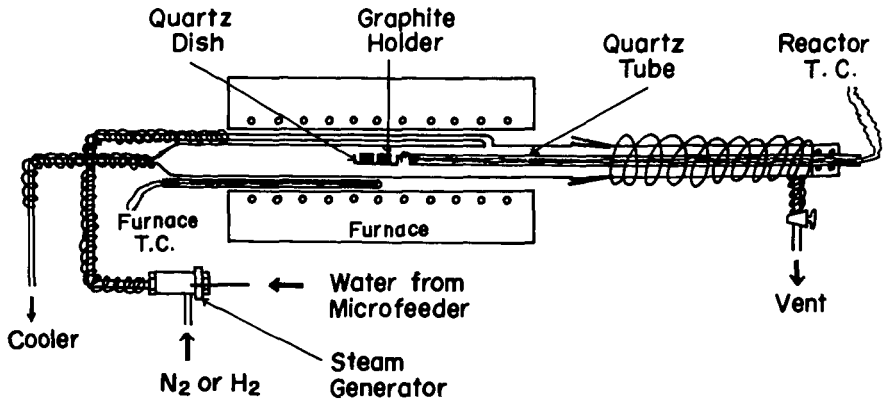

Fig. 1. Schematic diagram of apparatus

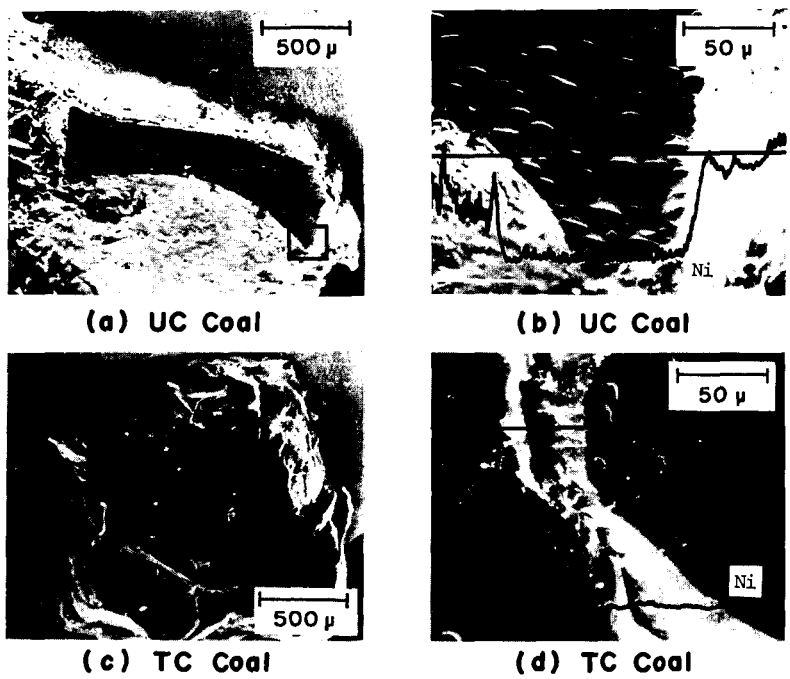

Fig. 2. Nickel Impregnated Shin-Yubari Coal

(a) 1st Stage

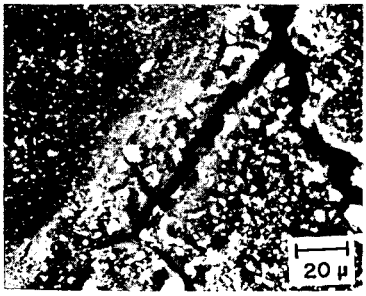

(b) 2nd Stage

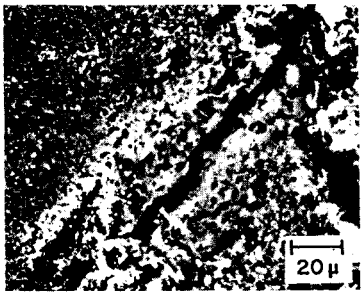

(c) 3rd Stage

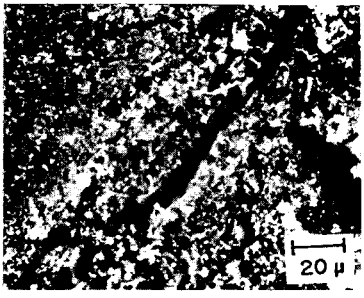

(d) 5th Stage

Fig. 3. Leopold TC Char (1)

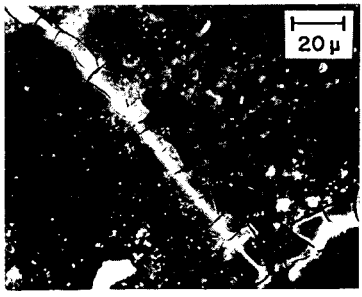

(a) 1st Stage

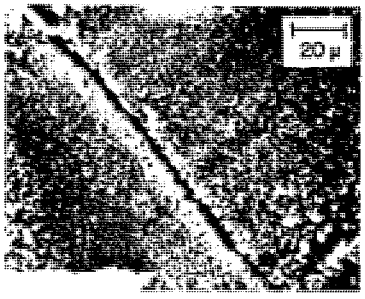

(b) 2nd Stage

Fig. 4. Leopold TC Char (2)

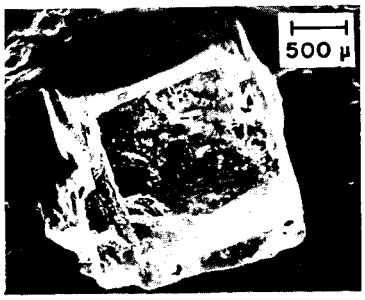

(a) Raw Coal

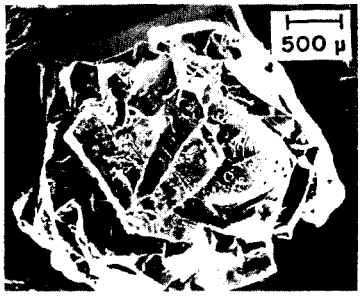

(b) 1st Stage Char

Fig. 5. Leopold UC Coal and Char

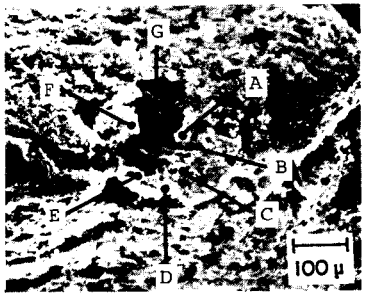

(a) Accumulation of Ash

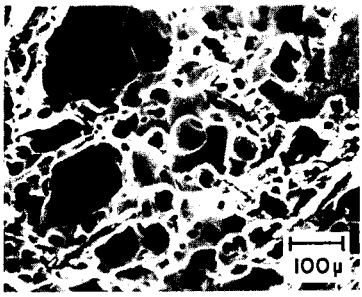

(b) Interior of Char

Fig. 6. Leopold Char at a Conversion of 92%

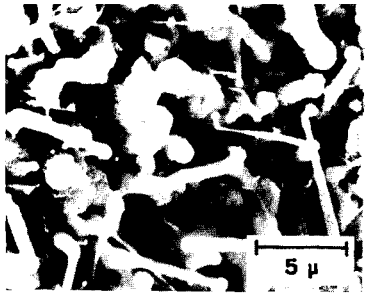

(a) Reaction with Fe

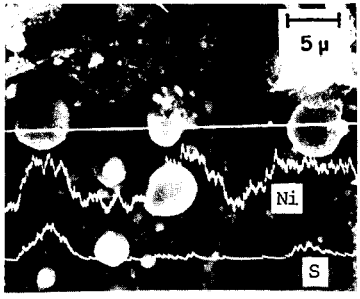

(b) Reaction with S

Fig. 7. Reaction of Nickel

COAL LIQUIDS HYDROGASIFICATION: EXPERIMENTS AND MECHANISM

H. N. Woebcke, P. E. Koppel, and P. S. Virk
Stone & Webster Engineering Corporation, P.O. Box 2325, Boston, MA 02107

Experimental data are presented for the hydrogasification of coal-derived liquids at conditions of temperature, pressure and residence time respectively 1200-1700F, 740-1500 psig, and 10-120 s, with hydrogen-to-substrate ratios from 0.8 to 2.0 times stochiometric. The coal liquids originated from hydroliquefaction of Pennsylvania and Wyoming coals; both full range 300-1200F and low boiling 400-650F fractions were employed, all samples being characterized by elemental analysis and NMR spectroscopy. Hydrogasification was performed in a packed tubular flow reactor with sequential effluent quenching and analysis by GCMS to yield information on products from C1(methane) to C14(phenanthrene). Theoretically, it was postulated that the hydrogasification mechanism involves two steps, namely (i) hydrodealkylation of substituted alkyl-aromatics to their nude polynuclear aromatic parent plus gas and (ii) fragmentation of the unsubstituted polynuclear aromatics to progressively smaller aromatic molecules and further gas. The theory predicts that the kinetics of both steps should be governed by the delocalization energy of the aromatic nuclei involved; at the conditions of the present experiments, step (i) should be appreciably faster than step (ii). The experimental data for gas, benzene and naphthalene yields were well rationalized by the theory. Further, the present theoretical framework can be applied to infer hydrogasification behavior of any aromatic feedstock from its NMR analysis, using the aromaticity and ring-breakdowns provided by the latter.

METHOD FOR REACTIVATION OF A CATALYST USED IN STEAM REFORMING OF HYDROCARBONS

J.Kimoto,K.Yamauchi,M.Morimoto,M.Yamada and F.Noguchi

Research Center, Osaka Gas Co., Ltd., 6-19-9 Torishima Konohana-ku Osaka 554, Japan

1. Introduction

Osaka Gas Company,Ltd. has been bringing in LNG, a clean fuel, from overseas since late 1972. With the necessity of the fact that our company smoothly converts its system from manufactured gas to natural gas distribution,the establishment of SNG(Substitute Natural Gas) production technology is essential if any possibility of a short supply of LNG is taken into account.

We have already developed the MRG(Methane Rich Gas) process, a low temperature steam reforming process, jointly with Japan Gasoline Company(JGC). Although this process, a SNG process using LPG or Naphtha with a nickel type reforming catalyst, is of good efficiency, it is considered that a SNG process with a better reforming catalyst can be expected to be of higher efficiency. As the result of extensive investigation, we have recently succeeded in developing a new steam reforming catalyst completely different from conventional catalysts. This catalyst,SN-108, has many excellent characteristics as compared with conventional steam reforming catalysts. In particular, it is a great advantage that this catalyst can be reactivated perfectly by the newly developed method.

It is our intention to explain pricipally about the characteristics of SN-108 and the method for reactivation.

2. Catalyst

The conventional catalysts used in low temperature steam reforming of hydrocarbons are usually nickel type.
On the other hand, SN-108 has a γ-Alumina oxide core impregnated with active metal which is not nickel.
The characteristics of SN-108 are as follows.

(1) High activity and long life.
(2) Resistance to the deposition of carbonaceous materials.
(3) Operable in the low temperature range and with a low steam to carbon ratio,such as 1.5 and 0.7 respectively at 1st and 2nd stage of two stages reactors.
(4) Handling is simple and no hydrogen reduction is reguired.

In addition to these characteristics,SN-108 can be completely reactivated by the specified method which we have recently developed. Furthermore, it has been found that SN-108 has a good performance in gasifying heavier distilates such as kerosene,gas oil,V.G.O. etc.

SN-108 has already been used for three winter seasons in a commercial plant of a daily output of 200,000 Nm^3/day to reform straight run naphtha having an end point 180°C (Test Naphtha) and also subjecting to reactivation during this period.
In these operations,the characteristics of SN-108 has been comfirmed. Fig.1 shows the catalyst deterioration with passing of time in the third operation. The reaction conditions are as follows.

steam / carbon ratio : 1.5
reaction pressure and temperature : 12 Kg/cm^2 G, 490°C

3. Reactivation

3.1 Method of reactivation

Typical conventional procedures for reactivation are treatments with hydrogen,steam or oxigen,which are mainly effective for the elimination of carbonaceous materials deposited on the catalysts. Our new reactivation system consists of two stages of chemical treatment essentially different from conventional ones. It is particularily noted that the combination of two chemical treatments is essential for the performance of reactivation.
The system cycle may be repeated depending on the extent of catalytic activity deterioration. Even if the catalytic activity deteriorates completely after being used, it is recovered to the state of flesh catalyst by 6 to 8 treatments.

Fig.2 shows the general process flow.

3.2 Effect of reactivation

1. Sample

The sample to be reactivated is the catalyst which had been used in a commercial plant for 4300 hours to reform Test Naphtha with steam and whose activity deteriorated completely.

2. Catalytic activity

Fig.3 shows the temperature profiles of steam reforming reaction using Test Naphtha. It can be found that the catalytic activity is recovered depending on the number of treatment.

3. Catalytic properties

Table 1 shows the typical catalytic properties of fresh catalyst,used catalyst and reactivated catalyst.

Table 1. Typical property of tha catalyst

	property \ sample	fresh cat.	used cat.	reactivated cat.
catalyst	carbon content (wt%)	0.2	6.0	3.0
	sulfur content (wt%)	0.00	0.09	0.00
	relative active metal content	1	1	1
carrier	crush strength (kg)	20	7.3	7.0
	surface area (m^2/g)	140	90	95
	pore volume (cc/g)	0.46	0.38	0.38

4. Chemical state of active metal

Fig.4 shows XPS spectra of the three kinds of catalysts. It became clear that the active metal consists of three kinds of chemical state,the relative ratios of three states change after being used and the chemical state of used catalyst is recovered to the almost same state of fresh catalyst by reactivation.

3.3 Mechanism of reactivation

In general,catalytic steam reforming reactions of hydrocarbons result in deposition of various materials such as carbonaceous and sulfurous materials on the catalyst. In addition,these reactions often result in a sintering of active metal particles causing their mutual cohesion,whereby the size of active metal particles enlarged and the dispersibility consequently lowered. Further,the physical or chemical constitution and behaviour of active metal may be gradually changed during the catalytic reactions. From the results in Table 1,it became clear that carbonaceous and sulfurous materials on the catalyst were eliminated by reactivation. Especially sulfurous materials was removed completely. Moreover,the observations by transparent electron-microscope gave the fact that there existed some sintered active metal particles on the catalyst after being used which disappeared after reactivation. Furthermore,as indicated in Fig.4,active metal of used catalyst was recovered to the chemical state of active metal of fresh catalyst. Consequently it may be concluded from these facts that our reactivation method is effective for the reduction or elimination of all of these adverse factors.

It may be noted,as stated in section 3.1,that conventional reactivation treatment with hydrogen,steam or oxigen is effective for the removal of carbonaceous material deposited on the catalysts,but not for the elimination of sulfurous materials and the recovery of chemical constitution of active metal. We have already found that conventional reactivation method has completely no effect on the recovery of the catalytic activity of SN-108 and furthermore our reactivation method is not effective for the recovery of the activity of conventional nickel type catalysts.

4.Summary and Conclusions

We have developed the new catalyst,SN-108,for low temperature steam reforming of hydrocarbons which has various excellent characteristics as compared with conventional nickel type catalysts. In particular,SN-108 is operable with a extremely low steam to carbon ratio,which enables SNG process with the catalyst to be of much higher efficiency. Furthermore,we have developed the new reactivation method for SN-108 essentially different from conventional methods and succeeded in commercializing this method. We believe that the process with SN-108 can make the great many of advantages in the field of steam reforming of hydrocarbons.

In Japan where stringent environmental protection regulations are being enforced,there has been a trend of using lighter fuel oil and it is considered inevitable that there will be greater surplus hereafter of residual oil. With this background,we will continue to investigate the catalytic activity and the reactivation method for SN-108 with residual oil.

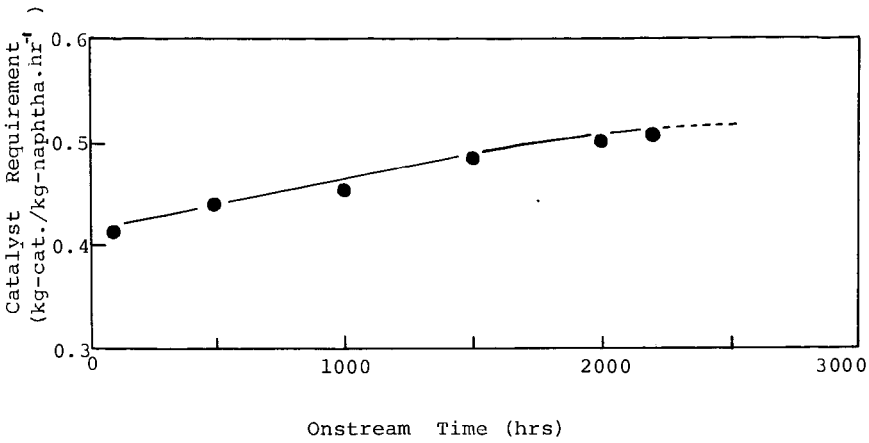

Fig.1 Activity deterioration curve of SN-108

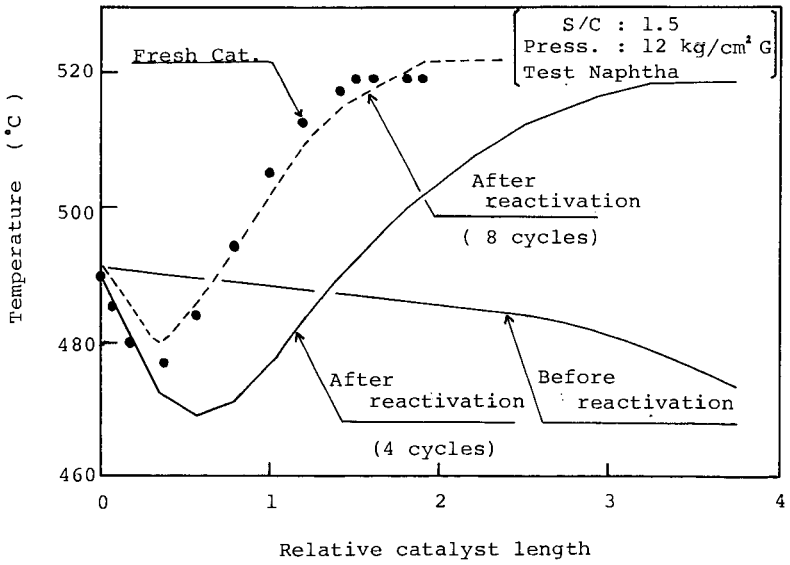

Fig.2 Recovery of the catalytic activity

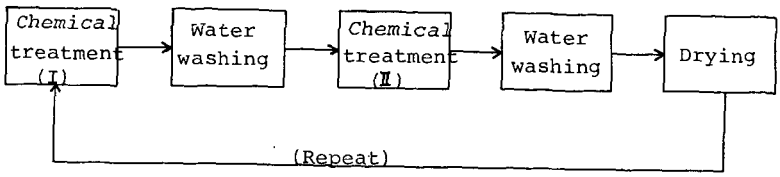

Fig.3 General process of reactivation

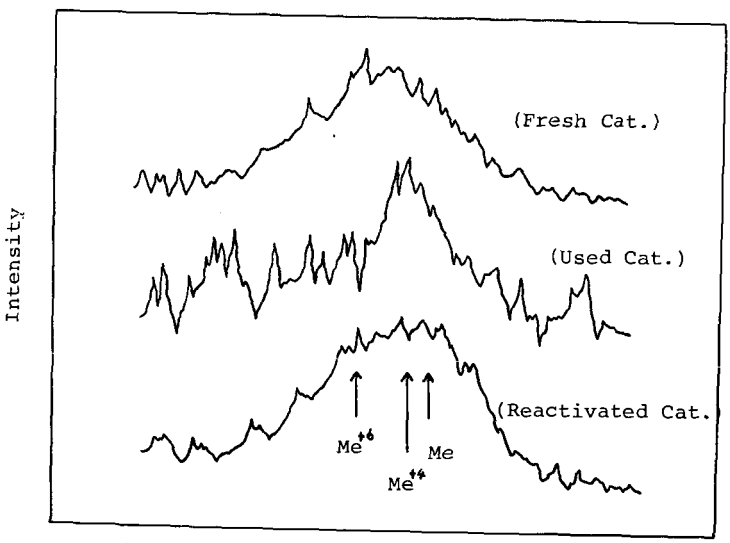

Fig.4 XPS spectra of active metal

Fluidized Bed Combustion of Residual Oils

Y. Morita, T. Kimura, H. Ikeda, Y. Kondo and E. Kikuchi

Department of Applied Chemistry, School of Science and Engineering, Waseda University, 3-4-1 Okubo, Shinjuku-ku, Tokyo 160, Japan.

INTRODUCTION

Shortage of crude oil plus the lack of progress in the development of stack gas clean up systems have sparked interest in processes that generate electric power by the fluidized bed combustion of residual oil and coal with high sulfur and nitrogen content. Many development works on the fluidized bed combustion of fossil fuels have been carried out by various organizations in U.S.A. and other countries. In all of these works, dolomite or limestone has been used as a bed material because these substances have ability to absorb H_2S or SO_2 released during combustion. Furthermore, reduced NOx emission can be achieved by the lower operating temperature in fluidized bed combustion than conventional combustors(1,2).

The authors have investigated the combustion of various residual oils in the fluidized bed of a dolomite at 700 ∿ 1000°C and atmospheric pressure. By use of the dolomite, heavy residual oils of low reactivity such as an Arabian Light vacuum residue could be burnt with combustion efficiency higher than 98% above 850°C. It was also shown that the dolomite was effective to reduce the concentration of SOx and H_2S in flue gases to very low levels at temperatures below 900°C. The purpose of the present work was to investigate catalytic reduction of NOx (mostly fuel NOx) by ammonia using a fluidized bed of the dolomite loading various kinds of metal oxide.

EXPERIMENTAL

Figure 1 shows a schematic diagram of the fluidized bed combustion system. The combustor was made of 50 mm φ i.d. SUS 27 stainless steel tube and its bed depth was 400 mm. Stainless steel beads (3 mm φ) were packed at the conical-bottom of the combustor as bed support and gas distributor. Feed oil (Arabian Light vacuum residue) was introduced at the bottom of the fluidized bed through an atomizer from a microfeeder. To prevent coke plugging in the feed pipe, the atomizer was cooled by circulating a coolant. The bed material was first heated externally to a desired temperature in a stream of air and then the residual oil was fed. After combustion started, external heating was cut off. To remove the heat evolved, water was circulated in a coil of 6 mm φ o.d. SUS 27 stainless steel tube which was immersed in the fluidized bed. After a certain period of combustion, ammonia was admitted to the combustion system at the upper level of fluidized bed from a cylinder which contained 5% ammonia in nitrogen.

After the condensation of steam in an ice-trap, the flue gas passed through a solution of 3% hydrogen peroxide to absorb SOx and through a solution of ammine complex of zinc to absorb H_2S. The SOx in the solution was titrated by barium acetate using Arsenazo III as an indicator. The H_2S concentration in the solution was determined by I_2 titration using sodium thiosulfate. The flue gases were periodically sampled to determine their compositions. The NOx concentrations were measured as nitrous ions by means of photometric analyzer using naphthyl ethylene diamine. Compositions of gaseous products, methane, carbon monoxide and dioxide were determined by means of gas chromatography.

Dolomite from Kuzuo (Tochigi Prefecture) was used after calcined at 700°C ($CaCO_3 \cdot MgO$). Its composition (wt%) was as follows: CaO 65.4, MgO 33.4, SiO_2 0.8, Al_2O_3 0.3, and Fe_2O_3 0.1. The dolomite was impregnated with an aqueous solution of Fe, Co, Cu, or Cr nitrate. These were finally calcined at 900°C prior to reaction.

RESULTS AND DISCUSSION

Table I shows the catalytic activity of some typical bed materials for the reduction of NOx emitted during combustion of the residual oil. The concentration of added NH_3 (1050 ppm) was calculated from the volume of flue gases (wet basis) and feed rates of ammonia. Combustion was carried out at the optimum operating conditions for the dolomite: bed temperature, 850°C; excess air, 20%; residence time, 0.57 sec. The concentrations of NOx in the absence of ammonia were almost independent of the kind of bed materials (near 320 ppm). The NOx concentrations decreased on addition of NH_3 to the combustion system. As shown in Table I, Fe_2O_3-dolomite was the most active among the bed materials tested.

Table I. Catalytic Activity of Some Bed Materials for the Reduction of NOx by NH_3

	Dolomite	Fe_2O_3-Dolomite	CuO-Dolomite	Cr_2O_3-Dolomite	CoO-Dolomite
C(a)	328	305	313	348	303
C(b)	246	149	184	246	192
X (%)	25.0	51.1	41.2	29.3	36.6

C(a) and C(b) are the concentrations of NOx in flue gases in the absence and presence (1050 ppm) of ammonia, respectively. And X is % reduction of NOx defined by $[C(a)-C(b)]\times 100/C(a)$. The content of metal oxides was 10 wt%.

Figure 2 shows the effect of bed temperature on the reduction of NOx by ammonia in the fluidized bed combustion using Fe_2O_3-dolomite containing 7.5 wt% of Fe_2O_3. When NH_3 was absent, the NOx emission increased with increasing bed temperature. The NOx emission, however, decreased in the temperature range of 700 ∿ 950°C in the combustion with NH_3 added. The catalytic reduction of NOx by NH_3 was enhanced remarkably as the bed temperature increased. At 950°C, the NOx concentration was reduced from 337 to 116 ppm by the catalytic reduction with NH_3.

Excess air was found to be a critical factor for the catalytic reduction of NOx on the Fe_2O_3-dolomite. With stoichiometric amount of air, the NOx concentration was not reduced by the addition of NH_3. However, the NOx concentration decreased with increasing amount of excess air and it was leveled off at about 10% excess air.

Figure 3 shows the effect of NH_3 concentration on the NOx emission. The NOx concentration decreased with increasing concentration of added NH_3. The lowest NOx emission of 57 ppm was attained when 2000 ppm NH_3 was added at 850°C, 10% excess air and 0.61 sec residence time.

Figure 4 shows that combustion efficiency was also improved by loading Fe_2O_3 on the dolomite in the range of combustion temperature from 700 to 950°C. Here combustion efficiency was defined as percent carbon in the oil converted to carbon dioxide. Combustion efficiency increased with increasing bed temperature and reached 100% at 950°C on both bed materials. The Fe_2O_3-dolomite was more effective

for combustion at lower temperatures than the dolomite. Combustion efficiency also increased with increasing excess air and it exceeded 99% at 10% excess air without formation of carbon monoxide and methane.

Figure 5 shows the effect of bed temperature on the emission of SOx and H_2S during combustion in the fluidized bed of the Fe_2O_3-dolomite. The results on the dolomite fluidizing were also shown in Figure 5. Concentrations of (SOx + H_2S) in flue gases were as low as 10 ppm in the temperature range of 700 ∿ 900°C but they increased abruptly as the bed temperature further increased as described by Moss (3) and Roberts (4). The mode in variation of (SOx + H_2S) emission with bed temperature in the Fe_2O_3-dolomite and the dolomite bed were similar. This suggests that the sulfur removing efficacy of the Fe_2O_3-dolomite is completely due to the dolomite.

CONCLUSION

The concentration of NOx emitted during the combustion of the vacuum residual oil was reduced when NH_3 was added to the fluidized bed of Fe_2O_3-dolomite. Furthermore, combustion efficiency higher than 99% was attained above 800°C. Simultaneously concentrations of (SOx + H_2S) in the flue gases were kept at very low level by the action of dolomite which might absorb SOx and H_2S. The optimum operating conditions for the Fe_2O_3-dolomite fluidized bed were determined as follows: bed temperature, 850°C; excess air, 10%; residence time, 0.61 sec. Under these conditions, the concentrations of (SOx + H_2S) and NOx were as low as 10 ppm and 57 ppm, respectively.

REFERENCES

(1) Nack, H., Kiang, K.D., Liu, K.T., Murthy, K.S., Smithson, G.R., and Oxley, J.H., Int. Fluid. Conf.(U.S.A.) 2, 339 (1976).
(2) Beer, J.M., Sym. Int. Combust. (U.S.A.) 16, 439 (1977).
(3) Moss, G., Int. Conf. Fluid. Combust. D2-1 (1975).
(4) Roberts, A.G., Stantan, J.E., Wilkins, D.M., Beacham, B., and Hoy, H.R., Int. Conf. Fluid. Combust. D4-1 (1975).

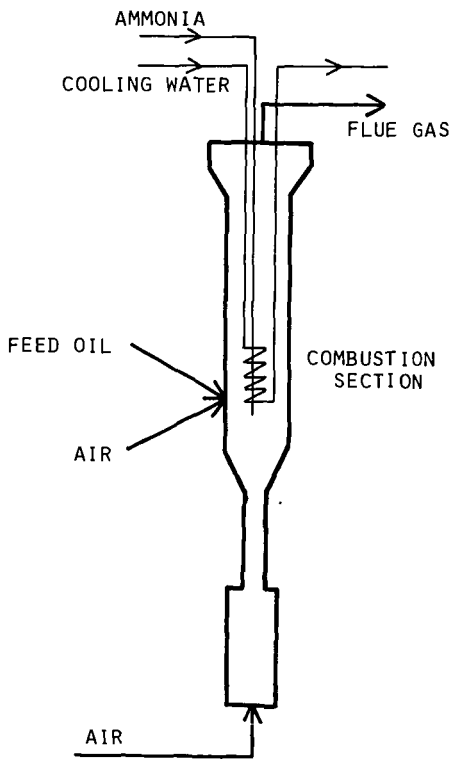

Figure 1. Diagram of Combustor Assembly

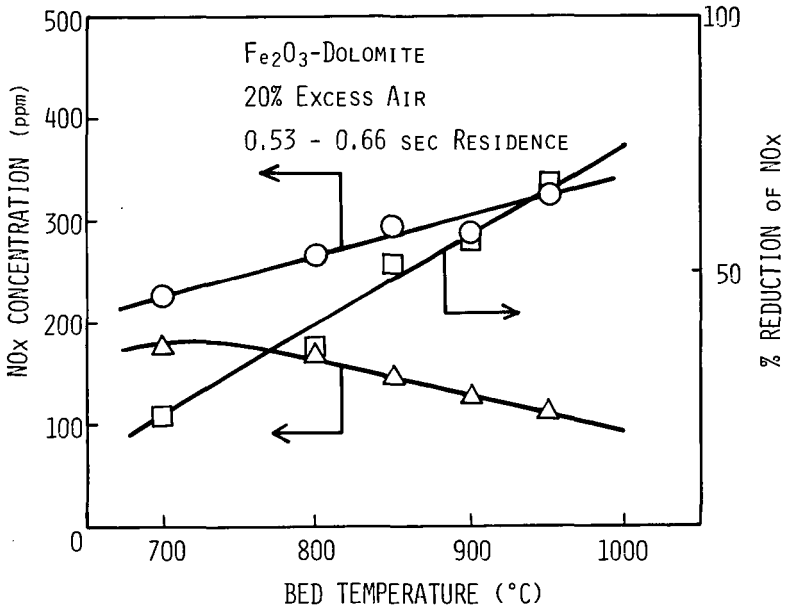

Figure 2. The Effect of Bed Temperature on the the Reduction of NOx by NH_3.

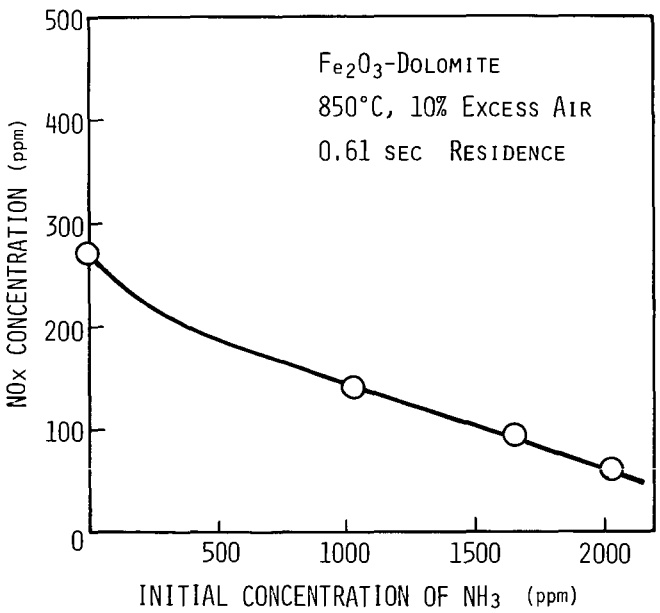

Figure 3. The Effect of NH_3 Concentration on the Reduction of NOx by NH_3.

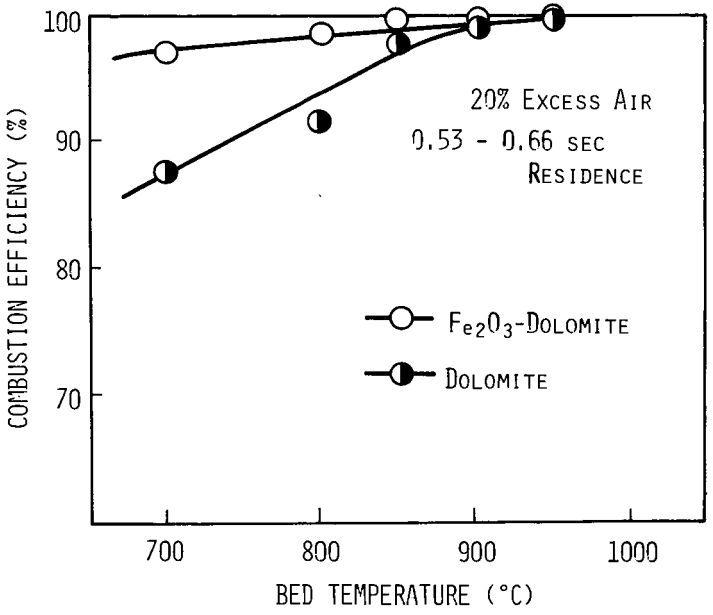

Figure 4. Relationships between Combustion Efficiency and Bed Temperature

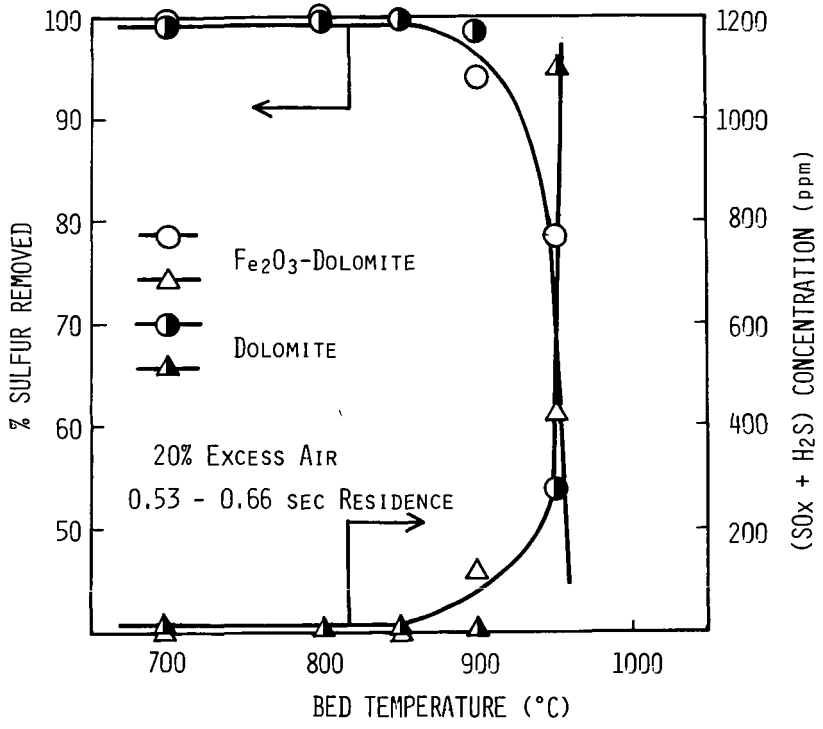

Figure 5. Sulfur Removing Efficacy of Fe_2O_3-Dolomite and Dolomite as a Function of Bed Temperature.

CHEMISTRY OF COAL ASH MELTING IN GASIFICATION AND COMBUSTION

Karl S. Vorres

Institute of Gas Technology
3424 South State Street
Chicago, IL 60616

INTRODUCTION

Coal deposits occur in a number of localities within the United States. The mineral matter in the coal varies with the location but is usually made up of quartz, pyrite, clay, shale and smaller amounts of other materials. The relative amounts of the mineral matter in the parent coal will vary from one region to another and within regions, as well as individual coal seams. During combustion or gasification, the mineral matter will contact other types of mineral matter resulting in a coal ash of different properties than the parent mineral species.

Our reliance on coal for production of energy via combustion or synthetic fuels will necessitate the ability to operate under a wide range of conditions. The boilers that generate electric power are in some cases designed to reject coal ash in the form of a molten slag. Some gasifiers are intended to operate with a continuous flow of molten ash from the gasifier to a collection zone. Continuing reliable operation of this equipment requires the ability to sustain an ash viscosity within a range to permit the ready removal of the ash material.

The determination of viscosity of the ash from coal is an expensive and time-consuming operation. A number of efforts have been made to correlate this property with the chemical composition. Different types of correlation have been suggested for use with coal ash of different ranges of compositions. It is desirable to have some understanding of the chemistry of the interactions that occur within the melt in order to more fully understand the melting behavior of this material and to make effective predictions of that behavior from the chemical composition.

ASH CATION PROPERTIES

The species that make up a coal ash after it has been in the reactor are usually metal oxides. This discussion assumes the coal ash materials are, or have been, converted to oxides. In a general way the behavior of the different ions can be viewed as the result of the important properties of charge and size that the positive ions or cations possess.

One of the more important properties is that of the size or radius. A listing of cation radii is given below for the important metal ion species in coal ash.

Si^{+4}	0.42	Fe^{+2}	0.74
Al^{+3}	0.51	Na^{+1}	0.94
Fe^{+3}	0.64	Ca^{+2}	0.99
Mg^{+2}	0.67	K^{+1}	1.33
Ti^{+4}	0.68		

These cation radii according to Ahrens (1) are given in angstrom units, Å (10^{-8} cm). The largest ion is roughly three times the size of the smallest.

A number of correlations of behavior have been made with the base-to-acid ratio of the oxide mixtures. The acids have been defined as oxides of Si, Al, and Ti. The bases have been identified as the oxides of Fe, Ca, Mg, Na, and K. The listing of radii does not readily divide the group into acids and bases. Iron is listed twice because it can occur in melts in two oxidation states.

In melts and other liquid solutions there is a tendency for the smaller more highly charged positive ions to draw the larger negatively charged ions into a complex ion. For coal ash this complex could have a general formula, MO_x^{-n}, where x oxide ions are coordinated around an M ion and the overall negative charge is n units. The coordination number, x, is determined primarily by the ratio of the radii of the M and O ions. The value of 1.40 angstroms was assigned to the oxide ion. A coordination number of 4 is observed for Si and Al. The coordination number of 6 is observed for the rest of the ions except K which has the number of 8 in these systems. In some cases Al may also be found with a coordination number of 6.

The other property of importance in the coal ash cations is that of charge. The charge affects the relative capacity to attract the negative ions to the cation. The capacity is also affected by the size of the ion. The ionic potential, defined as the ratio of cation oxidation state or valence to the ionic radius, gives a measure of the ability of the cation to attract the anion. A high ionic potential indicates an ability to compete effectively with other ions of lower ionic potential for a limited supply of oppositely charged ions. The values of the ionic potentials calculated from the ionic radii given earlier are listed below.

Si^{+4}	9.5	Fe^{+2}	2.7
Al^{+3}	5.9	Ca^{+2}	2.0
Ti^{+4}	5.9	Na^{+1}	1.1
Fe^{+3}	4.7	K^{+1}	0.75
Mg^{+2}	3.0		

Examination of these values quickly indicates that the highest values belong to the acid group of Si, Al, and Ti, while the lower values are associated with the bases. This grouping and the physical interpretation of the ionic potential lead to the suggestion that this parameter is a physical characteristic which can be useful in quantifying acid and base behavior. To the extent that this is true, then this parameter should also be useful in further efforts to correlate coal ash chemical compositions with melting, viscosity and other properties associated with ash deposition in the process.

The ionic potential is an indication of a cation's capacity to form a complex ion such as SiO_4^{-4}. This capacity may be limited by the availability of oxide ions as in coal ash systems. In the compound SiO_2 each Si is expected to have

four oxide ions around it. This can only be accomplished if oxygen ions are shared between different Si ions. This tetrahedral coordination occurs both in the solid and liquid state and requires sharing of oxide ions in all cases. The sharing of oxide ions leads to the formation of polymeric aggregates in the liquid state. Individual angular SiO_2 groups may join in chains, sheets, or other arrangements. These groupings require additional oxide ions for termination of the polymer. Oxides of ions of lower ionic potential than Si can provide these oxide ions. The groupings will terminate more frequently and the average polymer or aggregate size would decrease as more oxide ions became available. Al ions occur in many mineral species with Si and are able to take the place of Si in the polymeric groupings. In a similar fashion it is expected that they would be able to participate in the polymer formation in the melt. Alkali metal oxides could most readily supply oxide ions since they have the lowest ionic potentials. The alkali cations would find positions between the polymeric chains or other groupings involving Si and Al. At equilibrium, complexes will be formed due to attractive forces and disrupted by thermal energy. A population of complexes of various sizes would be expected for a given composition. The larger the aggregates, especially chain types, the greater the number of opportunities for interaction between them and to increase the viscosity.

The effectiveness of the addition of other cations to reduce the viscosity for reliable slag formation depends on the rate of mixing of the additives, the dissociation of the cations and oxide ions and the diffusion of these ions into the melt. These steps are typically much slower than the acid-base reaction in water solutions typified by titration.

A flux such as fluorite, CaF_2, is added in some cases to decrease the viscosity of a melt. This material provides a supply of anions with a size comparable with oxide ions. The fluoride radius is 1.36 Å compared to 1.40 for oxides. Fluorite is even more electronegative than oxide and both can serve as chain terminators. The addition of calcium fluorite instead of the oxide provides twice as many anions for each calcium ion, effectively doubling the capacity to limit polymer formation.

In coal ash melts, the role of an acid is that of a complex ion or polymer former. The tendency for polymer formation increases with ionic potential. The bases serve as oxide ion donors. The tendency to yield oxide ions is greatest for those with lowest ionic potential. The oxide ions are attracted by cations with the highest ionic potential in the system to form polymers, terminate polymer groupings and diminish viscosity. The cations with low ionic potentials exist as unattached hard spheres and can facilitate slippage between the polymer groups.

THE ROLE OF IRON

Ferric and ferrous ions have significantly different ionic potentials (4.7 and 2.7). The ferric ion falls between the values for the acid group and the basic group. The importance of iron is associated with its unique ability to alternate between the two valence states, the different behavior associated with

each state and its significant contribution to the composition of many coal ashes. Iron acts as either an acid or a base depending on its charge. The intermediate values for ionic potential indicates that ferric iron would be a weak acid and ferrous would be a moderate base.

The combustion process in boilers produces a coal ash with a mixture of the two states. Analyses have indicated that about 20% is present as ferric ion while the remainder was ferrous. In some slagging gasifiers elemental iron has been observed. Since the majority of the iron was present as ferrous ion it was appropriate to classify the iron oxides with the bases (assuming that a single classification had to be made) even though the oxide is identified as Fe_2O_3 in earlier correlations. The gaseous environment determines the equilibrium oxidation state of the ion in coal ash systems. Iron is an important component of most Eastern coal ashes, usually following Si and Al in abundance. The behavior of the coal ash system depends on the oxidation state of the iron. Viscosity studies show a reduction of coal ash viscosity for reducing conditions with a reduction of the ratio of ferric to ferrous iron. (2) This observation is consistent with the role of a complex former for the acidic ferric iron and an oxide donor role for the ferrous iron.

Figure 1 (3) indicates the liquidous relationships in the alkali and alkaline earth-silica systems. A comparison of the depression of the melting point for different alkali metal oxides indicates that the depression is greatest for the ions with lowest ionic potential or strongest bases. A similar relationship holds for the alkaline earths. In general, for this series of bases the melting point depression increases with decreasing ionic potential.

Table 1 (4) indicates the analysis of a series of coal ashes and gives the ash fusion temperatures. The indicated initial deformation temperature of 2900°F is just below 1600°C for the low-volatile bituminous coal. This material is essentially a two-thirds SiO_2/one-third Al_2O_3 mixture. An examination of the Al_2O_3-SiO_2 equilibrium diagram indicates that this softening temperature would be close to the eutectic melting temperature. One would then expect a very much higher liquid temperature.

Table 1 also gives the ash analyses of a series of high-volatile bituminous coal taken from three Eastern fields and one Western field. The SiO_2 contents of three of the four are close to 48%. The Al_2O_3 contents diminish from about 23% to 11%. The TiO_2 remains relatively constant in the range 0.6 to 1.0%. The Fe_2O_3 content is indicated from about 29.3 down to 7% which would indicate a wide range of behavior depending on the gaseous environment. The sum of SiO_2 and Al_2O_3, the dominant acid species, is greatest for the Ohio coal and the highest oxidizing fluid temperature is observed for this material. The next highest sum is for the Illinois coal and this one has the next highest oxidizing fluid temperature. The remaining two (Utah and West Virginia) have similar total Si and Al contents. However, the iron content is much lower for the Utah coal than for the West Virginia coal. In an oxidizing environment this means that the total acid content would be higher for this coal and a higher oxidizing fluid temperature is observed for the West Virginia fuel.

An examination of the phase equilibrium diagram for the system $FeO-Al_2O_3-SiO_2$, Figure 2 (5), shows that in the region of about 50% SiO_2, 25% Al_2O_3, 25% FeO, which corresponds fairly closely to the Ohio coal, one would expect a liquidus temperature of about 1450°C (2642°F) which is in good agreement with the fluid temperature in the reducing environment for the Ohio coal ash. The lowest temperature on the diagram is at the eutectic between fayalite, tridymite and iron cordierite. The indicated temperature is 1083°C or 1980°F which is in general agreement with the observed initial deformation temperature for the reducing environment. The minimum temperature would correspond to a localized region in a sample where this phase could form through diffusion of different constituents with the required composition for formation of that material.

The composition of the Illinois coal ash is similar; however, this material does contain a significant amount of calcium oxide which is expected to reduce the melting temperature below that observed for the Ohio coal. The two temperatures are similar but are somewhat less for the Illinois material.

The West Virginia coal is richer in Fe_2O_3 according to the analysis. Again, refering to the $FeO-Al_2O_3-SiO_2$ phase equilibrium diagram and normalizing the content of these three constituents, the material falls in the same general region in the phase diagrams as the Ohio and Illinois coals. However, the melting temperature expected appears to be about 1540°C or about 2430°F. This temperature is somewhat higher than the observed reducing fluid temperature, however there is also about 4% calcium oxide, 1.2% magnesium oxide, and smaller amounts of other bases which contribute to the reduction in observed temperature.

The observed reducing initial deformation temperature is similar for the three coals from Ohio, West Virginia and Illinois. The same equilibrium phase diagram would apply to all three and would reflect the earlier mentioned minimum temperature.

The Utah coal is richest in SiO_2, CaO, and Al_2O_3. In the phase equilibrium diagram for this system, Figure 3 (6), the normalized composition for this ash lies in the pseudo-wollastonite region. From this normalized composition the melting temperature to be expected is about 1280°C or 2336°F. The solid species would be a wollastonite ($CaO \cdot SiO_2$). This temperature is about 80° above the observed fluid temperature in a reducing environment, indicating that the iron has the ability to depress the melting point by this amount in conjunction with the other basic materials. The oxidation of the iron is able to elevate the fluid temperature as indicated, through production of the acid ferric ions and associated change in oxide ion availability.

BIBLIOGRAPHY

1. Ahrens, L. H., Geochim. Cosmochim. Acta., 2, 155 (1952).

2. Steam, Its Generation and Use, Publ. by the Babcock & Wilcox Co., N.Y., pp. 15-16 (1978).

3. Phase Diagrams for Ceramists, E. M. Levin, H. F. McMurdie & F. P. Hall, Fig. 128, pp. 66 (1956). Am. Ceram. Soc., Columbus, Ohio.

4. Ref. 2, pp. 15-20.

5. Ref. 3, Fig. 696, pp. 241 (1964 edition).

6. Ref. 3, Fig. 631, pp. 220 (1964 edition).

Table 1

Ash content and ash fusion temperatures of some U.S. coals

Rank:	Low Volatile Bituminous	High Volatile Bituminous			
Seam	Pocahontas No. 3	No. 9	Pittsburgh	No. 6	
Location	West Virginia	Ohio	West Virginia	Illinois	Utah
Ash, dry basis, %	12.3	14.10	10.87	17.36	6.6
Sulfur, dry basis, %	0.7	3.30	3.53	4.17	0.5
Analysis of ash, % by wt					
SiO_2	60.0	47.27	37.64	47.52	48.0
Al_2O_3	30.0	22.96	20.11	17.87	11.5
TiO_2	1.6	1.00	0.81	0.78	0.6
Fe_2O_3	4.0	22.81	29.28	20.13	7.0
CaO	0.6	1.30	4.25	5.75	25.0
MgO	0.6	0.85	1.25	1.02	4.0
Na_2O	0.5	0.28	0.80	0.36	1.2
K_2O	1.5	1.97	1.60	1.77	0.2
Total	98.8	98.44	95.74	95.20	97.5
Ash fusibility					
Initial deformation temperature, F					
Reducing	2900+	2030	2030	2000	2060
Oxidizing	2900+	2420	2265	2300	2120
Softening temperature, F					
Reducing		2450	2175	2160	
Oxidizing		2605	2385	2430	
Hemispherical temperature, F					
Reducing		2480	2225	2180	2140
Oxidizing		2620	2450	2450	2220
Fluid temperature, F					
Reducing		2620	2370	2320	2250
Oxidizing		2670	2540	2610	2460

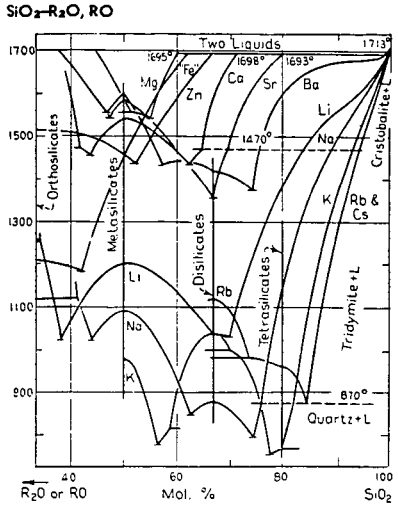

Figure 1. Liquidus Relations in the Alkali and Alkaline Earth-Oxide-SiO_2 Systems

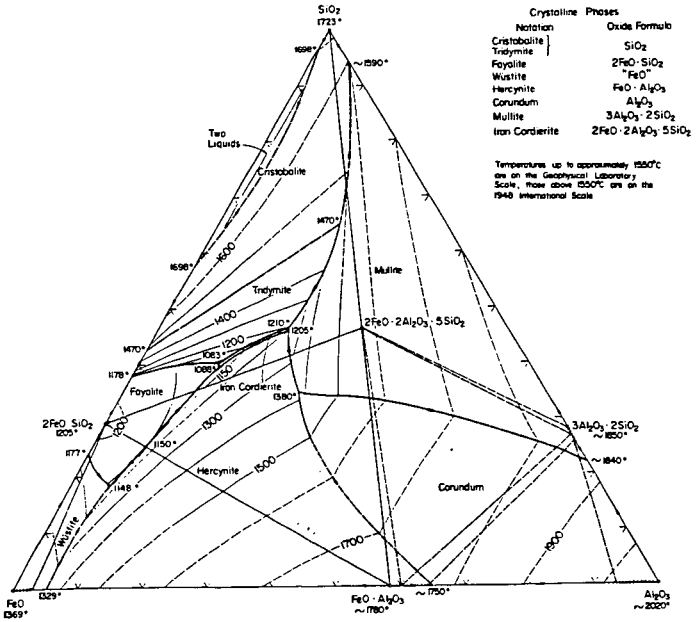

Figure 2. Composite "FeO"-Al_2O_3-SiO_2 System

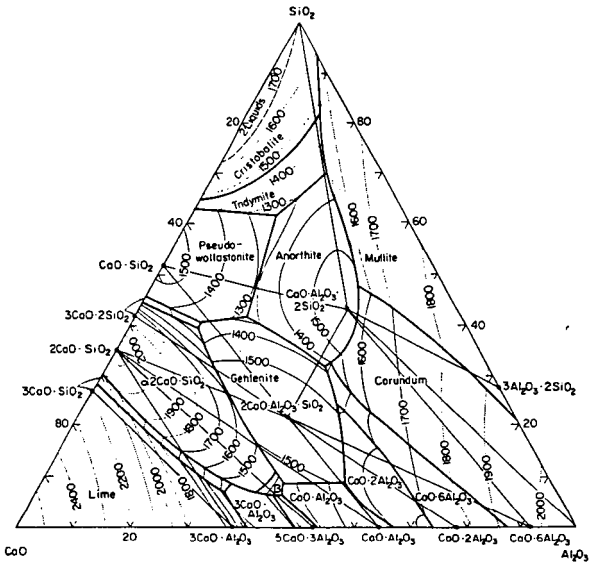

Figure 3. $CaO-Al_2O_3-SiO_2$ System

CALCIUM CARBONATE DEPOSIT FORMATION DURING THE LIQUEFACTION OF LOW RANK COALS

J. B. Stone, K. L. Trachte and S. K. Poddar

Exxon Research and Engineering Company
P. O. Box 4255; Baytown, Texas 77520

Introduction

During the liquefaction of low rank coals, that is subbituminous or lower, the calcium humates in the coal decompose to form calcium carbonate solids. These solids have been identified in the reactor solids from pilot plant runs and could be a significant operational problem in commercial sized equipment. The purpose of this paper is to present our operating experience and proposed solutions to this problem as it applies to the Exxon Donor Solvent, or EDS, Process. The units used in the EDS development program range from 3 gram batch reactors to a one ton-per-day process development unit.

In the EDS Process, which is shown in Figure 1, crushed coal is slurried with a hydrogen donor recycle solvent and liquefied in a tubular upflow reactor to which molecular hydrogen has been added. The liquefaction operating conditions are about 840°F and 2000 psig. The liquefaction reactor product is separated into a light hydrocarbon gas stream, the spent solvent, which is recycled and upgraded in a catalytic hydrogenation unit, the total liquid product and a residual bottoms slurry which is processed in a Flexicoker to produce process fuel and some additional liquid product. The ash residue from the Flexicoker is landfilled. The plant is balanced in that the solvent, hydrogen and process fuel needed are generated by the process. For an Illinois No. 6 bituminous coal approximately 2.7 barrels of liquid are produced per ton of dry coal. Liquid yields from a balanced plant processing lower rank coals are less because of their lower carbon content.

Source of Calcium Carbonate Deposits

Most of the calcium in low rank coals is in the form of salts of humic acids. These calcium humates are represented in Figure 2. These humates decompose in the liquefaction reactor to form calcium carbonate. The exact mechanism for calcium carbonate formation is not known, but all of the components of the calcium carbonate within the dashed lines are readily available. The calcium is ionically bonded to carboxylic acid and sometimes phenolic groups in the coal. Since these groups are weak acids, the calcium can be ion-exchanged. There are also other calcium salts present in coal. Calcite and gypsum are found predominately in higher rank coals, bituminous and above, and are stable under liquefaction conditions. The three coals studied in greatest detail for calcium carbonate deposition are: a Wyoming subbituminous coal from the Wyodak mine, a North Dakota lignite from the Indian Head Mine and a Texas lignite from the Big Brown Mine.

Identification of Calcium Carbonate Problem

During the second quarter of 1975, a screening study was completed on the Wyoming subbituminous coal. Inspection of the reactors used in these runs revealed calcium carbonate deposition as wall scale. Since this was not a problem specific to the pilot units used, calcium carbonate deposition could have a significant impact on the operation of a commercial unit. A study was then initiated to identify the magnitude of this deposition problem.

The bench scale and pilot units used in the calcium carbonate deposition study range from 3 gram batch tube autoclave reactors to a one ton-per-day Pilot Plant. Each of these units plays an integral part in the testing of solutions to the calcium carbonate problem. Some solutions can easily be tested in the batch reactor; whereas other solutions must be tested in a flow unit. The liquefaction product from the batch reactor is separated with a hydrocarbon solvent wash and the residue is analyzed for calcium carbonate by X-ray diffraction and thermo-gravimetric analysis. In the flow units, the residual bottoms can be tested similarly as in the batch case. But more importantly, the reactor solids from these units can be analyzed for particle size, calcium carbonate content and calcium carbonate growth patterns and crystal forms. The larger units, the 50- and 100-pound-per-day Recycle Coal Liquefaction Units (RCLU) and the one ton-per-day Coal Liquefaction Pilot Plant (CLPP), are completely integrated pilot plants with distillation and recycle solvent hydrogenation sections. A smaller Once-Through Coal Liquefaction Unit (OTCLU) uses a simulated recycle solvent and has no distillation or solvent hydrogenation facilities.

Types of Deposit Forms

Calcium carbonate deposition occurs as scale on the liquefaction reactor wall and free-flowing solids or oolites. Wall scale is very easy to detect in the liquefaction reactor solids by its characteristic shape. Oolite solids are particles of the coal mineral matter, clays, silicas, etc., which have a uniform layer of calcium carbonate growing around them. These oolites are predominately concentrated in mesh size fraction one size larger than the feed coal. For example, in the small pilot plants which use minus 100 mesh coal, the oolites are concentrated in the 50 to 100 mesh size. Similarly, for the large pilot plant using minus 30 mesh coal, the oolites are concentrated in the 16 to 30 mesh range. These oolites would be expected to grow larger during much longer runs, because they would not be swept out of the reactor by the normal fluid flow.

The predominant form of the calcium carbonate growth does depend on the coal from which it was formed. With the Wyoming subbituminous coal, the wall scale formed is primarily vaterite which is rarely found in nature. The growth on the oolites is primarily calcite and some wall scale, at times, is also calcite. For North Dakota lignite, on the other hand, scale and oolites in the first stages of the reactor are always calcite and in the latter stages of the reactor sodium magnesium carbonate (eitelite). The forms of the calcium carbonate deposits for the Texas lignite are essentially the same as those for the Wyoming coal.

Most of our operating experience with low rank coals has been the processing of Wyoming coal in the 50 pound-per-day RCLU pilot plant. After a run in this unit the reactor is removed and drained of solids and residual coal slurry. Methyl ethyl ketone washes and sometimes mechanical scraping are needed to remove the scale. The total solids are toluene washed to remove excess solvent, dried and sieved. For the RCLU unit, the wall scale is plus 50 mesh. Oolites are 50 to 100 mesh. Minus 100 mesh material is unreacted feed coal or coal mineral matter which has not yet formed oolites. The ranges of accumulation of calcium carbonate containing solids for the three coals studied are shown in Table 1. The accumulation is reported as pounds per 100 pounds of coal fed to compensate for the variations in run length. The only significant difference in the three coals is that the Texas lignite produces more oolites than the Wyoming coal. The oolite accumulation for the North Dakota lignite is not available because it was not possible to accurately sieve the reactor solids. The deposit accumulation is unaffected by changes in most liquefaction process variables, such as, temperature, space velocity, solvent quality, solvent boiling range and hydrogen gas rate. During high pressure operations (2500 vs. 1500 psig) there was a significant increase in oolite and wall scale accumulation.

Scanning Electron Microscope (SEM) photographs have provided invaluable information about the reactor solids recovered from the flow units. Most of the oolites have surfaces of calcium carbonate. This is identified by an X-ray spectrometer which is an integral part of the SEM. Some oolites have surfaces of iron sulfide crystals which are again identified by the X-ray. The iron sulfide surface is much more irregular in appearance than the calcium carbonate surface. Cross sections of these oolites reveal more information about the calcium carbonate growth. These cross sections show that calcium carbonate growth occurs on seeds of the coal mineral matter. There is also evidence of iron sulfide growth on the mineral matter seeds. The seed material can be iron sulfide itself, silica or clays or any part of the coal mineral matter. The iron sulfide growth is very regular and crystalline whereas the calcium carbonate growth is more evenly distributed.

The other type of calcium carbonate growth is wall scale. The reactor used in the 15 pound-per-day OTCLU is very amenable for detecting scale. It is a vertical hairpin tubing reactor which can be split along its length for a detailed inspection of any scale present. The reactor which is shown schematically in Figure 3 has eleven sections: six upflow and five downflow. The graph at the bottom of Figure 3 is a plot of the amount of calcium in the wall scale versus the reactor section number. Almost all of the calcium carbonate scale is in the first half of the reactor with the heaviest concentration in the 15 to 25 minute residence time range. This finding has been verified directionally in the pilot plants, although it is very difficult to detect the exact location of scale in the pilot plants. The SEM can also be used to detect the structure of the scale. The surface of the scale which is next to the reactor is smooth and is mostly iron sulfide and a slight amount of nickel sulfide. This is indicative of the fact that the sulfidation products of the wall are providing growth sites for calcium carbonate. The process side of the scale has a surface which is very similar to that of the oolites.

Solutions to Deposition Problem

Potential solutions to calcium carbonate deposition that we have investigated are mechanical or chemical in nature. The mechanical solutions tried are solids withdrawal and acid washing. The theory behind solids withdrawal is that since the oolites are free-flowing solids it should be very easy to withdraw them from the liquefaction reactor. Oolite growth can be controlled if the withdrawal rate is high enough so that the oolites do not have sufficient residence time for growth. Solids withdrawal has been very effective in controlling the growth of oolites in the one ton-per-day unit. A way to control wall scale growth is periodic acid washing of the reactor walls during reactor shutdowns. Several chemicals have been identified as ones which can effectively dissolve the calcium carbonate scale. A combination of solids withdrawal and acid washing is a very cost effective way of controlling calcium carbonate deposits. An uncertainty here is whether the scale would flake off the reactor walls and cause operational problems during the extended runs (6-12 months) in a commercial plant. This uncertainty will be tested during the operation of our 250 ton-per-day pilot plant now under construction.

The effect of solids withdrawal on solids accumulation and oolite growth in the one ton-per-day unit is shown in Table 2. During a four-day run without solids withdrawal, 1/4 percent of the coal fed remained in the reactor and of this amount, about one-third was larger than the feed coal, that is, plus 30 mesh. During a 16-day run with solids withdrawal, only nine-hundredths of one percent of the coal remained in the reactor, and essentially none of the oolites grew larger than the feed coal. Wall scale growth rates were about the same for both runs. This scale growth would amount to about 1/2 inch per year.

Chemical solutions to the calcium carbonate deposition problem can be classified as coal pretreatments or reactor additives. Coal pretreatments are ion exchanges in which the humate calcium which is the source of the calcium carbonate deposition is reacted with acids or metal salts. The resulting calcium salt would, of course, need to be stable in the liquefaction reactor for the exchange to be successful. A generalized mechanism for the ion exchange is:

$$MX \rightarrow M^{+2} + X^{-2}$$

$$M^{+2} + \sim Ca \sim \rightarrow \sim M \sim + Ca^{+2}$$

$$Ca^{+2} + X^{-2} \rightarrow CaX$$

Where the $\sim Ca \sim$ is a representation of the humate calcium.

The acids that we have concentrated most on and have been successful in ion exchanging with the calcium are sulfuric acid and sulfur dioxide. The sulfur dioxide readily dissolves in the coal's moisture and forms sulfurous acid. The HSO_3^- ion then diffuses through the coal pores to the site of the humate calcium where it exchanges with the calcium. Various metal salts have also been tried. In general, bivalent metal salts exchange very effectively with the humate calcium. Monovalent metal salts will also exchange if the resultant calcium (CaX) salt is very insoluble. For example, sodium carbonate will exchange more effectively than sodium sulfate because the resulting calcium carbonate is more insoluble than calcium sulfate. This insolubility provides an added driving force for the exchange. The metal salts would have an added advantage if the metal were catalytically active in liquefaction.

Coal pretreatments can be tested in the batch tube autoclave reactor because the form of the calcium has been changed, and it is only necessary to determine the amount of calcium carbonate in the liquefaction residue. Untreated Wyoming coal forms about 40% calcium carbonate on ash. Sodium sulfate is only partially effective in ion-exchanging with the calcium. The liquefaction residue contained about 20% calcium carbonate on ash (the remaining calcium is calcium sulfate). A run in the 15 pound-per-day unit did produce scale which confirms that sodium sulfate is only partially effective. Sulfur dioxide treated coal has only about 8% calcium carbonate on the ash of the residue. Ferrous sulfate and sulfuric acid are even more effective in exchanging with the calcium. After these pretreatments there is only 1% calcium carbonate in the residue ash. Reactor inspections after runs in the 15 pound-per-day unit revealed no scale for the sulfur dioxide, ferrous sulfate and sulfuric acid pretreatments. Sulfur dioxide and sulfuric acid treatments were also successful in preventing scale and oolite growth in the 50 pound-per-day RCLU.

Liquefaction reactor additives have different proposed mechanisms for success, but in general are not fully effective. Surfactants theoretically will disperse the calcium carbonate into a fine size so that it will flow out of the reactor before forming scale. It was difficult to find a surfactant that was stable under liquefaction conditions, but when we tried one that was, it had no effect on scale growth. There are two types of scavengers used: One to tie up the calcium, for example, collodial silica to form calcium silicate, and another to scavenge the carbon dioxide, for example magnesium oxide. Neither of these materials was effective in preventing calcium carbonate growth. Another possible mechanism for the colloidial silica to work is by providing many small sites for the calcium carbonate growth. This could prevent wall scale growth. Addition of two weight percent colloidial silica on coal did reduce scale formation in the 15 pound-per-day unit but did not eliminate it. Crystal modifiers have been used to shift the crystal form from vaterite to calcite but have had no effect on scale growth. Some reactor additives which have shifted the Wyoming coal wall scale from

vaterite to calcite are water, hydrogen sulfide and various chelating agents. The basic reason for the failure of these reactor additives is that the calcium carbonate formation occurs in the pores of the coal, and reactor additives reach only the coal particle surface at best.

SUMMARY

The major findings in our liquefaction work with low rank coals are that oolite formation and wall scale growth are primarily related to coal rank. We have detected both forms of calcium carbonate deposits with every low rank coal tested. As long as the calcium in the coal is present in the humate form, calcium carbonate deposition will occur. The physical withdrawal of solids from the liquefaction reactor can effectively control oolite accumulation and growth but not wall scale. Wall scale can be removed during reactor shutdowns by acid washing. Liquefaction reactor additives are generally ineffective in controlling calcium carbonate deposition. Coal pretreatment, that is, ion-exchange, can be very effective in altering the form of the calcium salt and thus prevent any type of calcium carbonate deposition in the liquefaction reactor.

ACKNOWLEDGEMENT

This work was performed at Exxon Research and Engineering Company's Baytown Research and Development Division in cooperation with the Corporate Research Laboratories as part of the Exxon Donor Solvent Coal Liquefaction Development Program. Funding for this program is shared by the U.S. Department of Energy, The Carter Oil Company (an Exxon affiliate), Electric Power Research Institute, Japan Coal Liquefaction Development Company, Ltd., Phillips Petroleum Company, and Atlantic Richfield Company. The authors gratefully acknowledge this support.

TABLE 1

RANGES OF CALCIUM CARBONATE SOLIDS ACCUMULATION

COAL TYPE	WYOMING SUBBITUMINOUS	NORTH DAKOTA LIGNITE	TEXAS LIGNITE
MINE	WYODAK	INDIAN HEAD	BIG BROWN
COAL COMPOSITION, WT% DRY COAL			
CALCIUM	1.22	1.31	2.2
SODIUM	.05	.84	.05
SOLIDS ACCUMULATION, LBS/100 LBS COAL FED			
TOTAL SOLIDS	0.35-0.57	0.22-1.1	0.49-2.0
OOLITES	0.07-0.27	NA	0.39-0.49
WALL SCALE	0.002-0.007	0.005-0.035	0.002-0.010
TOTAL SOLIDS COMPOSITION, WT%			
ASH	56-70	57-67	78-82
$CaCO_3$	24-83	17-49	67-74
$Na_2Mg(CO_3)_2$	-	24-46	-
$CaCO_3$ FORMS	CALCITE, VATERITE	CALCITE	CALCITE, VATERITE

TABLE 2

EFFECT OF SOLIDS WITHDRAWAL ON SOLIDS ACCUMULATION
ONE TON-PER-DAY UNIT, WYOMING COAL

	WITHOUT SOLIDS WITHDRAWAL	WITH SOLIDS WITHDRAWAL
INITIAL SOLIDS ACCUMULATION, WT% OF FEED COAL	0.25	0.09
PARTICLE GROWTH WT% OF REACTOR SOLIDS LARGER THAN FEED COAL	33	1
WALL SCALE GROWTH INCHES/DAY	.001	.0011-.0015

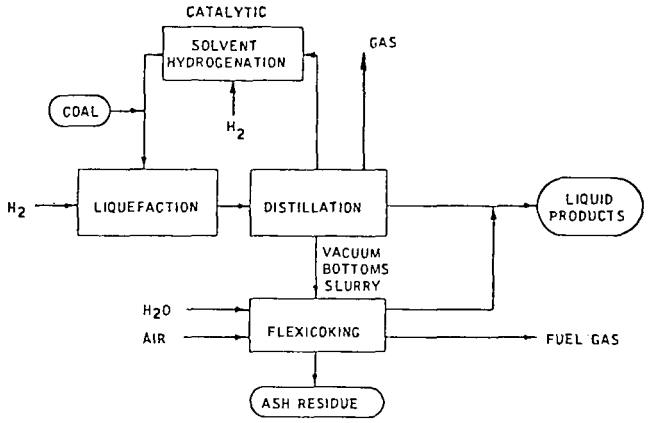

FIGURE 1. EDS PROCESS SCHEMATIC

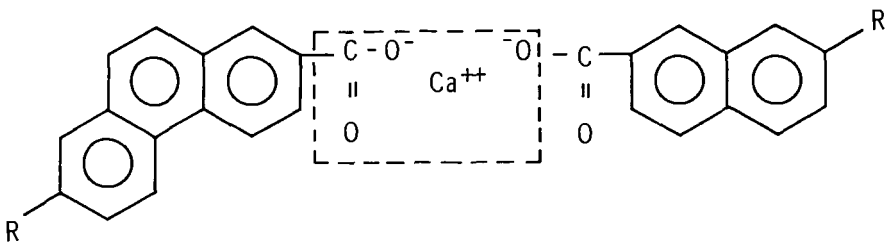

FIGURE 2. REPRESENTATION OF CALCIUM HUMATES

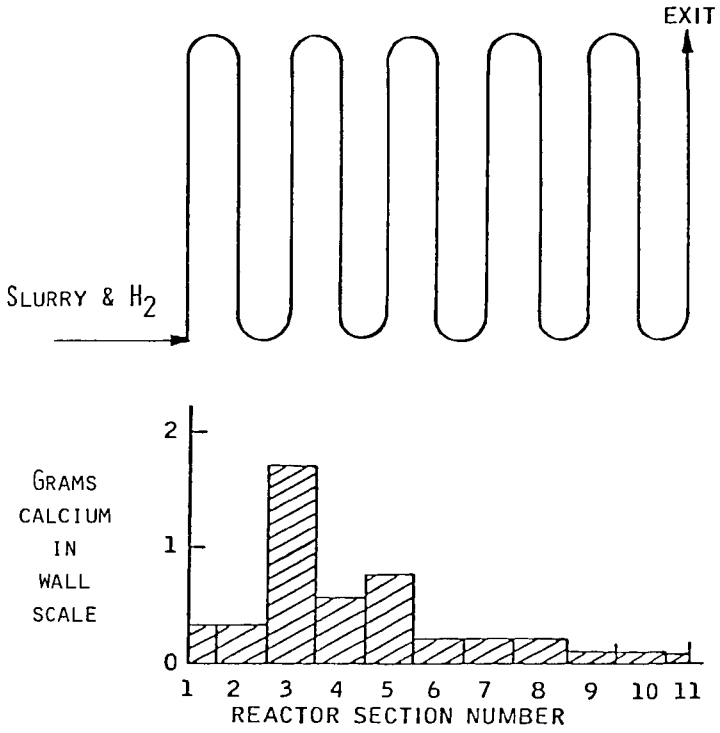

FIGURE 3. SCALE DISTRIBUTION IN A 15 LB/DAY UNIT

A ^{13}C, ^{2}H, ^{1}H NMR AND GPC STUDY OF STRUCTURAL EVOLUTION OF A SUBBITUMINOUS COAL DURING TREATMENT WITH TETRALIN AT 427°C

James A. Franz
Pacific Northwest Laboratory, P.O. Box 999, Richland, WA 99352

The recently developed magic angle/cross polarization Waugh-Pines techniques[1] promise to significantly advance the state of understanding of the statistical structure of coals. However, much work remains to be done in the area of detailed product characterization before predictable models of coal reactivity can be constructed. Although tetralin and other donor systems have been utilized in numerous studies, the results of Neavel[2] were among the first to demonstrate that certain coals can be rendered soluble in pyridine in >90% conversion in <5 min. Very little effort to characterize the evolution of coal structure over time during reductive thermolysis of coal has been made.

In this work the products from the thermal dissolution of subbituminous Kaiparowitz coal at 427°C in tetralin are examined by spectroscopic (^{13}C, ^{1}H, ^{2}H NMR, IR) molecular weight (gel permeation chromatography and vapor pressure osmometry) and elemental analysis and hydroxyl group analysis. The use of 1, 1-dideuterotetralin in conjunction with ^{2}H NMR to monitor the time dependence of introduction of deuterium into aliphatic and aromatic structures is presented. The tetralin-derived products were monitored versus time by glpc to determine the relationship between hydrogen uptake and coal product yields.

Reactions of Coal and Tetralin or 1,1-dideuteriotetralin

The procedure for these sections is similar to that of Neavel[2]: A 0.6 cm x 6.3 cm stainless steel tube equipped with threaded caps was charged with 0.15 g tetralin and 0.25 g coal or a 0.95 cm x 6.3 cm tube was charged with 1 g coal and 2 g tetralin. One or more tubes attached to a compressed air vibrator were plunged into a molten lead bath maintained at a temperature which would compensate for the heat uptake by the reaction vessel and stabilized as rapidly as possible at 427°C or 500°C. The sample tubes were withdrawn from the bath at various times from 2.5 min to 2 hr and quenched in water, the contents were washed out with 50 ml of THF and filtered through a 25 μm millipore filter. The insoluble material was dried and weighed. The THF soluble portions were analyzed directly by GPC in THF and the entire reaction mixture analyzed by gas chromatography (GLPC) to determine tetralin, naphthalene, methyl indane et al. The THF solutions were concentrated to 1-3 ml and combined with ~50 ml pentane. The resulting precipitate was repeatedly washed until no tetralin or naphthalene was detectable by GLPC of the pentane wash. This fractionation provides an excellent separation of coal from solvent-derived material. The pentane-insoluble, THF-soluble fractions were examined by vapor pressure osmometry, elemental analysis, GPC, hydroxyl group analysis and ^{13}C, ^{2}H and ^{1}H FTNMR.

Results and Discussion

As shown by Figure 1, subbituminous Kaiparowitz coal is rapidly converted to THF-soluble products at 427°C. The ultimate yield of 80% of THF-soluble products plus gases is achieved after approximately 35 min with most (75%) of the ultimate product forming within 10 min. A correction for ash content in the residues would increase the yields by approximately 8%. Vapor pressure osmometry of pyridine solutions of the THF-soluble fraction

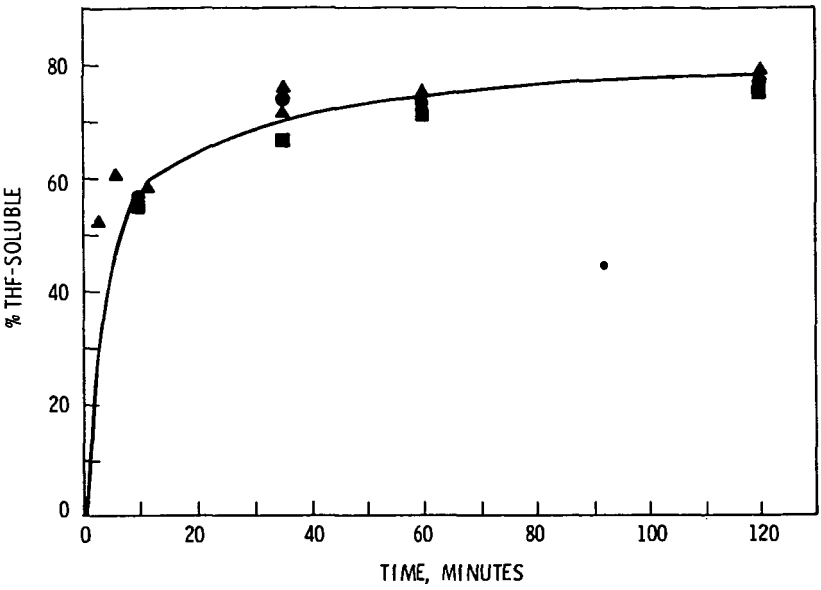

FIGURE 1. Percent THF-Soluble Product plus Gases from 427°C Reaction of Kaiparowitz Coal and Tetralin ■ = Total carbon rendered soluble ● = 1°/sec heatup rate ▲ = 15°C/sec heatup rate

shows a drop in number average molecular weight from approximately 1200 at 10 min to about 500 at 30 min and longer with a slight but reproducible increase after 2 hr reaction. Gel permeation chromatography of the entire reaction mixture in THF (including tetralin and tetralin derived products) shows the molecular size behavior versus time (Figures 2 and 3). Consistent with the vpo results, the principal peak occurs at molecular weight 1000 (polystyrene and polyethylene glycol standards). This peak decreases in size relative to major peaks at MW $\leq$ 500 so that by 35 min, molecular weights less than 500 dominate weight distribution occur in the first 15-20 min of reaction. After 35 min, the growth of the CA. 300 MW peak occurs only very gradually. The vpo results show an increase in molecular weight from CA. 500 to 600 between 1 and 2 hr. At 500°C the conversion of the higher molecular weight constituents to lower molecular weight products occurs more rapidly than at 427°C. Constituents with MW >10,000 are not observed at 500°C; however, even after 2 hr at 500°C there remains a substantial fraction of material of molecular weight >1000.

The conversion of aliphatic to aromatic structure occurs throughout the reaction. Figure 4 shows the ratio of aliphatic/aromatic hydrogen, deuterium and carbon versus time from integrals corrected for solvent absorptions. The carbon values are not quantitative, but qualitatively exhibit the same trend shown by the proton and deuterium data, with a decrease in C_{ali}/C_{arom} from 0.9 to 0.6 over a 2 hr reaction. The IR spectra of successive THF-soluble fractions shows the expected growth in aromatic CH stretch (3000-3100 cm^{-1}) relative to aliphatic CH stretch (2900-3000 cm^{-1}), and a notable increase in aromatic CH out-of-plane bending motion (700-850 cm^{-1}).

^{13}C NMR spectra for 10, 35, 60 and 120 min reactions were similar in most respects except for small changes in aromatic/aliphatic integrals. The aromatic region of a typical ^{13}C NMR spectrum (Figure 5) revealed a distinct region of absorption at δ 150-160 consistent with aryl ether and phenolic CO and a shoulder at 110-120 ppm typical of aromatic carbons adjacent to aromatic carbons bearing oxygen atoms.[3,4,5] The aryl ether and phenolic absorption accounts for 11%, 11%, 7% and 8% of the total aromatic integral of 10, 35, 60 and 120 min reactions, respectively. Since these are quaternary carbons with low or no NOEs, these percentages represent less than half of the actual percentages of aromatic carbons possessing oxygen substituents. Elemental analysis of the THF-soluble fractions (Table 1) reveals a rapid initial drop in oxygen content from CA. 17% in the coal to 14% in the THF-soluble fraction. The %O about 2% over a 2 hr reaction time in the THF-soluble fraction. The percent of oxygen in hydroxyl groups drops from CA. 30% to CA.15% over a 2 hr. reaction time indicating the incursion of dehydrocyclization-type reactions, consistent with the drop in aromatic CO observed by ^{13}C NMR.

Table 1. Elemental Analyses of THF-Soluble Fractions and Coal from the Reaction of 500 mg Tetralin and 250 mg Coal in 0.65 x 6.3 cm Reaction Vessels at 427°C

	Reaction Time, min	%C	%H	%N	%S	%O(diff)[a]	% ash	%OH[b]
Coal	--	71.0	5.19	1.1	0.3	17.1[a]	8.6	--
THF-Soluble Fractions	10	75.45	6.19	1.3	0.3	14.0	1.2	4.8
	35	76.22	6.32	1.43	0.2	13.9	1.0	4.2
	60	77.81	6.09	1.5	0.3	13.5	0.6	1.8
	120	79.49	6.01	1.7	0.12	13.3	0.8	2.2

(a) Oxygen analyses by difference in the presence of large ash residues are not reliable.
(b) Hydroxyl uncertainty is ±1%.

Hydrogen transfer during the reaction is very rapid during the first 15 min of reaction but levels off and becomes sluggish after 30 minutes, after the low energy processes of conversion of coal to preasphaltenes is succeeded by slower bond breaking processes leading to asphaltenes.

The analysis of tetralin, methylindane, and naphtahalene by GLPC during the reaction revealed that for every six carbon atoms in the total coal, 1.0, 1.2, 1.7 and 2.4 hydrogen atoms are transferred from tetralin at 5.5, 10, 35 and 60 minutes reaction time. Thus the hydrogen uptake per incremental increase in product yield is much lower in the initial 5 min of reaction than at succeeding times. This is consistent with the breaking of fewer bonds per weight of solvated material yielding radicals or ions which may abstract hydrogen or hydride from tetralin during the early stages of reaction.

The ^2H NMR results[6] (Figure 4) qualitatively support the concept of a rapid initial disruption of aliphatic structure in the early stages of conversion of coal to preasphaltenes. About 55% of the coal is dissolved within 10 minutes, deuterium incorporation occurring much more rapidly at aliphatic sites.

The ^1H NMR results reveal that the bulk of aliphatic hydrogen occurs at position β to aromatic rings ($ArCH_2\underline{CH_2}CH_3$) and cyclohexyl or internal methylenes of normal paraffins (δ 1-1.9) and at positions adjacent (α) to aromatic rings ($ArCH_2CH_2CH_3$)(δ 1.9-3.2). Aliphatic hydrogen is detectable in modest amounts assigned to diaryl substituted methylenes (α^2) (δ 3.2 - 4). As shown by Table 2, the percent of α and α^2 hydrogen doubles from 2.5 to 35 min, consistent with a significant increase in aromatic structure during the reaction.

TABLE 2. Distributions of Aliphatic Hydrogen versus Time from ^1H NMR Integrals of THF-Soluble Products (427°C) in Pyridine-d_5

Reaction Time (min)	Chemical Shift Ranges, δ(ppm)			
	δ0-1.0	δ1.0-1.9	δ1.9-3.2	δ3.2-4.0
2.5	18%	55%	24%	3%
10	13%	48%	34%	5%
35	10%	38%	44%	7%
60	9%	45%	39%	8%

Summary

The dissolution of subbituminous coal occurs very rapidly to produce predominantly phenolic aromatic or aryl ether structures associated with about an equivalent amount of aliphatic structure with molecular weights typically aroung 1000, and as high as 30,000. The ^{13}C NMR spectra show the products to possess a wide variety of structures in the chemical shift regions of diaryl and triaryl methanes and ethanes, cyclic and acyclic saturated hydrocarbons, with insignificant oxygenated aliphatic, carbonyl or quinoidal structure. Oxygenated aliphatics, if present, are destroyed in the first 10 min of reaction.[7] The hydrogen transfer process occurs initially at aliphatic sites but is soon incorporated in aromatic structure, as indicated by ^2H NMR results. The ^1H NMR results confirm the gradual production of aromatic structure during the reaction. The incursion of condensation reactions is reflected in a gradual upswing of average molecular weights beyond 1 hr reaction times, as well as a small but definite drop in hydroxyl group content in the coal products.

Acknowledgment

This work was supported by the Department of Energy, Division of Energy Research, Basic Energy Sciences Program, under contract EY-76-C-06-1830 with Battelle Memorial Institute. The author wishes to especially acknowledge the help of Mr. Gary L. Roberts for sample preparation, glpc and gpc analysis.

References

1. Bartuska, V. J., G. E. Maciel, J. Schaefer, and E. O. Stejskal, Fuel 56:354, 1977 and references therein.

2. Neavel, R. C., Fuel 55:237, 1976. For review of related earlier work, see loc. cit.

3. Levy, G. C. and G. L. Nelson, Carbon-13 Nuclear Magnetic Resonance for Organic Chemists, Wiley-Interscience, New York, N.Y., 1972.

4. Stothers, J. B., Carbon-13 NMR Spectroscopy, Academic Press, New York, N.Y., 1972.

5. Emsley, J. W., J. Feeney and L. H. Sutcliffe, High Resolution Nuclear Magnetic Resonance, Pergamon Press, New York, N.Y., vol 2, 1966.

6. For recent work in the use of ^{2}H nmr for characterization of batch hydrogenation, see Skowronski, R. P., J. J. Ratto, and L. A. Heredy, "Deuterium Tracer Method for Investigating the Chemistry of Coal Liquefaction - Annual Technical Progress Report for the Period July 1976 - June 1977," FE-2328-13, Atomics International Division, Rockwell International, Canoga Park, CA 91304, February 1978.

7. (a) Similar decreased in oxygen content have been reported in experiments using naphthalene or phenanthrene as a reaction medium: Whitehurst, D. D., M. Farcasiu, and T. O. Mitchell, "The Nature and Origin of Asphaltenes in Processed Coals," Electric Power Research Institute Report AF-252, Annual Report, February, 1976, Ch. 10, and references therein. (b) See ibid., p. 6-46 for comments on quinoidal functions.

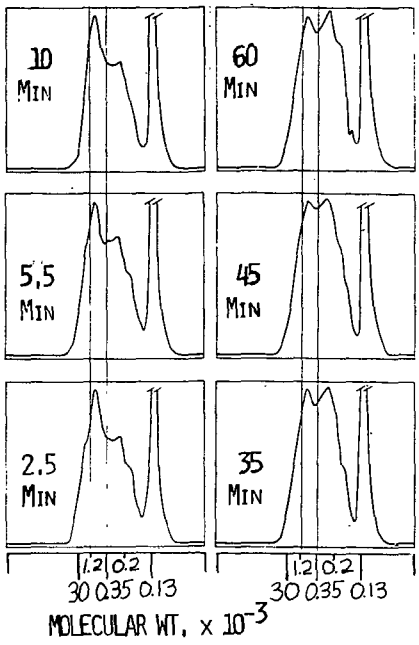

FIGURE 2. GPC trace of the THF solutions of products from the reaction of tetralin and coal at 427°C for varying periods of time. Tetralin and tetralin-derived products appear at MW 130.

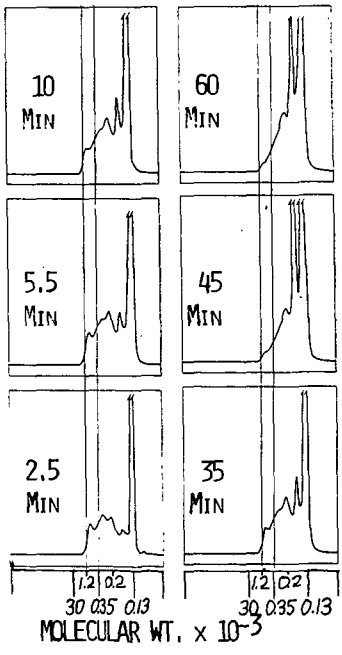

FIGURE 3. GPC trace of the THF solutions of products from the reaction of tetralin and coal at 500°C for varying periods of time. Tetralin and tetralin-derived products appear at MW 130.

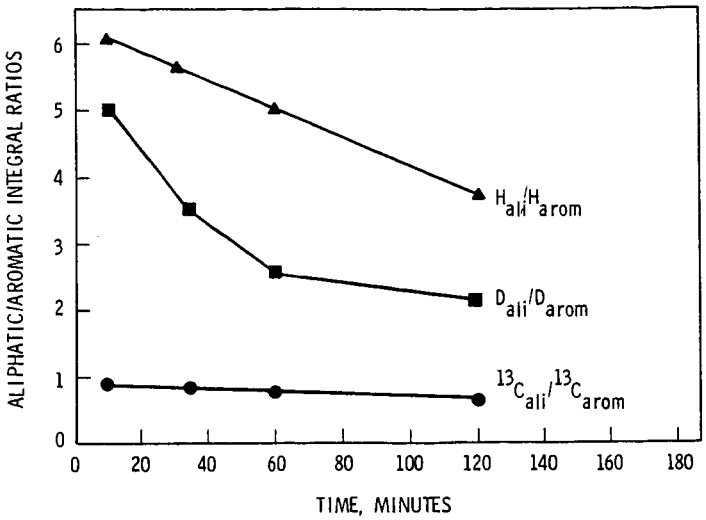

FIGURE 4. Aliphatic/Aromatic FTNMR Integral Ratios vs.Time for Reactions of Coal and Tetralin at 427°C. FTNMR spectra were determined at 79.54 MHz(^{1}H), 20.000 MHz (^{13}C) and 12.211 MHz (^{2}H) with a Varian model FT-80 multinuclear FTNMR spectrometer.

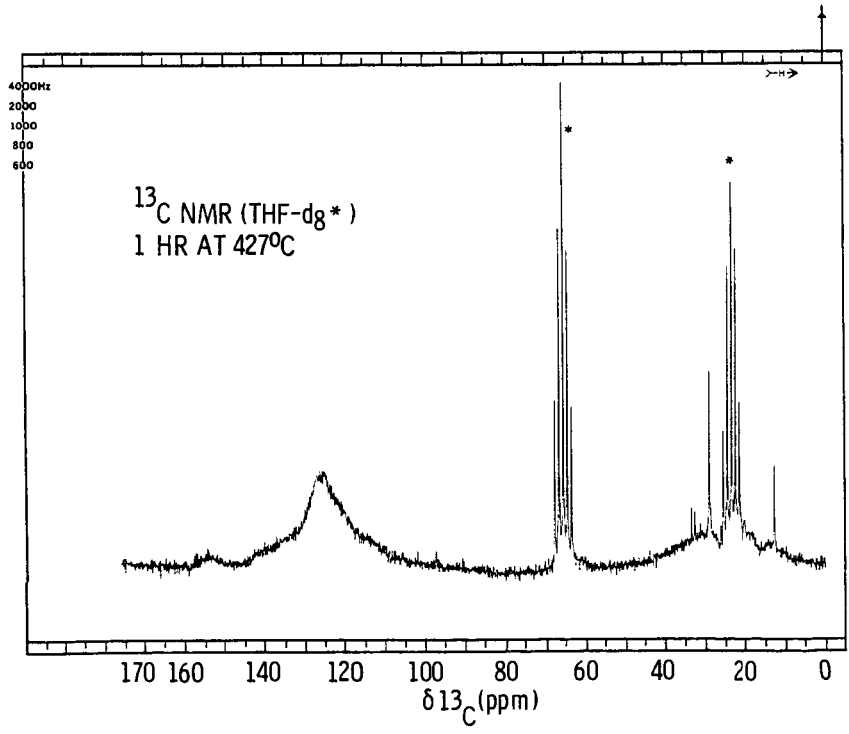

FIGURE 5. ^{13}C FTNMR Spectrum of the Pentane-Insoluble, THF-Soluble Products from the reaction of Tetralin and Coal in THF-d_8 at 427°C for 1 hr.

Effect of Hydrogen Pressure on Rate of Direct Coal Liquefaction

Minoru Morita
Shimio Sato
Takao Hashimoto

Department of Chemical Engineering
Yamagata University
Yonezawa, Japan 992

Introduction

There have been numbers of studies for direct coal liquefaction. Many of them have been carried out with batch autoclaves, which are heated up to a designed temperature (hereinafter called nominal reaction temperature), followed by holding at that temperature for a desired time (hereinafter called nominal reaction time) and cooling down. Then total pressure inside the autoclaves changes with the temperature varying and consuming of hydrogen by the reaction. Thus the hydrogenation of coal is non-isothermal and non-isobaric. Workers, however, have analysed kinetics conventionaly considering experimental results by the autoclave as those under isothermal and isobaric conditions at a reaction time according to a nominal reaction time (NRT) (1~6)

The authors pointed out that the conventional analysis (hereinafter called isothermal analysis) was unsuitable for not only investigation of reaction kinetics represented by a scheme including a unobservable species but also calculation of the real value of rate parameters (7). Effect of hydrogen pressure on a rate of the reaction has been investigated by some workers (1~3). They examined dependence of initial hydrogen pressure or average pressure during period of NRT on rate constants which are calculated by the isothermal analysis using date obtained under different initial pressures at same nominal reaction temperature (NRTM). From the same reason as above mentioned, however, it may be doutful for these studies to be calculated a accurate value of rate paramaters.

In this report, hydrogen pressure effect on the rate and rate parameters values was estimated by non-isothermal analysis, in which experimental results with a batch autoclave were allowed to remain non-isothermal and non-isobaric.

Apparatus and Procedure

The experiments were carried out with a shaking type 0.5-liter autoclave. The apparatus and procedure were identical with those previousley described (7). Experiments were made under the following conditions: from 350°C to 440°C NRTM, from 2-minutes to about 2-hours NRT and from 50 atm to 110 atm initial hydrogen pressure. 12 grms of powdered coal and 28 grms hydrogenated and decristalized anthracene oil as vehicle were used. A catalyst, consisting powdered sulpher, feric hydride and molibdenic oxide in 1:1:1 at weight ratio, was prepared in this laboratory. Taiheiyo coal (Japanese) and Morwell coal (Australian) were studied. Ultimate analysis, on a moisture-free basis, showed that Taiheiyo coal had a higher carbon-to-hydrogen ratio of 1.17 (79.8%C and 5.7%H) than that of 1.05 (65.3%C and 5.2%H) in

Morwell coal. Proximate analysis showed that moisture, fixed carbon and volatile materials contents (%) were 12.6,52.4 and 34.2 for Morwell coal, and being 4.9, 27.7 and 47.0% for Taiheiyo coal, respectively.

Extents of reaction were determined by measuring product solubility in two solvents, benzene and n-hexane. Then organic benzene insolubles (OBIS), in which unconverted coal and cokes produced by side reactions were contained, asphaltene and oil were separated and weighed by the general procedure (6)

Experimental Results and Discussions

Examples of process time- temperature and process time-pressure curves, at different NRT's, are given in Fig. 1. The changes in pressure indicates that the absorption of hydrogen apparently is initiated about 250°C, and after the temperature has been reached at the NRTM of 440°C, the pressure begins to decrease at almost constant rate by consuming of hydrogen with the hydrogenation, follows by rapid decreasing as the temperature decreases. Fig. 2 and 3 represent the experimental results of Morwell coal liquefaction under various initial hydrogen pressures at 350°C of NRTM. Those represent that dependence of reaction course and the rate on the initial hydrogen pressure is not very sharp: under any pressure the courses show similar trends-i.e., an increased NRT increases oil formation from coal, while it has less influence on asphaltene production. Compared with the reaction extent at zero NRT (that during pre-heating and quenching period), the extent for NRT period is little. Liquefaction, moreover, progresses to fair degree in spite of low NRTM of 350°C. These hydrogenation characteristics may be explained from Morwell coal's properties: pyrolysis accompanying deoxygenation from groups containing oxygene will precedes hydrogenation, because Morwell coal have much oxygene contents of 30 % (by difference) as indicated from the ultimate analysis; this coal is converted into oil and asphaltene to appreciable degree by the pyrolysis through the pre-heating and quenching period, and remaining unreacted coal is reacted to form oil. Fig. 4 and 5 show the experimental results for Taiheiyo coal. From those it is found that there is a tendency to increase reaction rate with increasing initial hydrogen pressure, and being a marked one at the heigher NRTM; moreever, the higher initial hydrogen pressure prevents cokes formation from occuring: under the lowest initial hydrogen pressure at NRTM of 440°C, oil yield decreases against OBIS fraction increasing with increasing NRT. This can be expressed as produced oil is degraded to make cokes, which is mesuared as OBIS. On the other hand, under heigher initial hydrogen pressures there is little influence of oil degradation.

Hydrogenation Rate Analysis

From previously reported facts(1~6) it may be considered that coal is liquefied through the following two-step process as the main reaction, coal→asphaltene→oil. Then under severe reaction conditions of heigher temperature, or under the infulence of a active catalyst, gasfication and/or cokes formation is accompanied with the main reaction simultaneously. For a case where the oil is degraded to an appreciable degree, the authors proposed the following four-step scheme taking into account cokes formation from polimerization of the oil, coal ⟶ asphaltene ⟶ oil ⟶ resin ⟶ cokes (7). With this scheme Miike coal (Japanese) liquefaction behaviors were investigated using

the non-isothermal analysis method to be well expressed. To decribe the Morwell coal liquefaction properties, however, the above mentioned scheme must be modefied by addition of another reaction process such as one step oil formation, coal→oil. Therefore, in this study a reaction scheme was derivated so as to express the experimental hydrogenolysis courses, and its kinetic parameters values including reaction order with respect to hydrogen pressure were estimated so that simulated courses might have close agreement with the experimental ones. On estimation of the rate parameters values in the derived reaction scheme, as its rate equations was so complicated that an analytical method might be unsuitable, a numerical analysis based on the non-linear least sum of squares method was used; Marqurdt method was adopted because of its good convergency. A estimation procedure is illustrated with flow chart. Its detail is as follows: experimental reaction temperatures and pressures values at ten or fifteen process times in each run were stored up; from these storage reaction temperature-and pressure-process time curves of each run were described by a spline function (9); reaction courses of each run were simulated using the rate equations; from this function and values of rate parameters, i.e., reaction orders, activation energies and frequency factors, the parameters values were optimally estimated from comparing the simulated courses with experimental ones. To remove interference with the optimum estimation by compensation effect between frequency factor and activation energy, variables were transformed (10). A detail of investigated results will be presented in the meeting.

Conclusions

Effect of hydrogen pressure on coal hydrogenation properties was investigated. It was found that for liquefaction of Morwell coal in which oxygene contents appears to be considerable, hydrogen pressure little effect. In the case of Taiheiyo coal liquefaction hydrogen pressure had effects: higher pressure gave higher oil yield and prevented cokes formation from occuring.

A reaction scheme was derived so as to express the experimental liquefaction courses, and kinetics was analysed by the proposed non-isothermal method using the batch autoclave data which is non-isothermal and non-isobaric ones.

Refference

1. Weller S., M. G. Pelipetz and S. Friedman, "Kinetics of Coal Hydrogenation (Conversion of Asphaltene)" Ind. Eng. Chem., 43,1572(1951)
2 Pelipetz M. G., J. R. Salmon, J. Bayer and E. L. Clark, "Catalyst-Pressure Relationship in Hydrogenolysis of Coal" Ind. Eng. Chem., 45, 806(1953)
3. Maekawa Y., T. Ishii and G. Yakeya, "The Effect of Hydrogen Pressure on the Hydrogen Reaction of Coal" J. Chem. Eng. Japan, 10, 101(1977)
4 Pelipetz M. G., E. M. Kuhn, S. Friedman and H. H. Storch, "Effect of Catalysts on the Hydrogenolysis of Coal" Ind. Eng. Chem., 40, 1259(1948)
5. John A. Ruether, "Kinetics of Heterogeneously Catalyzed Coal Hydroliquefaction" Ind. Eng. Chem., Process Des. Dev., 16, 249(1977)
6. Falkum E. and R. A. Glenn, "Coal Hydrogenation Process Studies (Effects of Time on Restricted Hydrogenolysis of Spitzbergen Coal with Adkins Catalyst)" Fuel, 31, 133(1951)
7. Morita M., S. Sato and T. Hashimoto, "Rate Analysis of Direct Coal Liquefaction under Non-isothermal Conditions" Preprint of the 14th Congress for Coal Science , Japan, Tokyo Nov. 2 (1978)
8. Marquardt, D. W., "An Algorithm for Least-Sum-Squars Estimation of Nonlinear Parameters" J. Soc. Ind. Appl. Math., 11, 431 (1963)
9. Greville T. N. E., "Introduction to Spline Functions" pl, Academic Press,(1969)
10. Himmelbrau D. M., "Process Analysis by Statistical Method" pl94, John Wiley & Sons, Inc.,(1968)

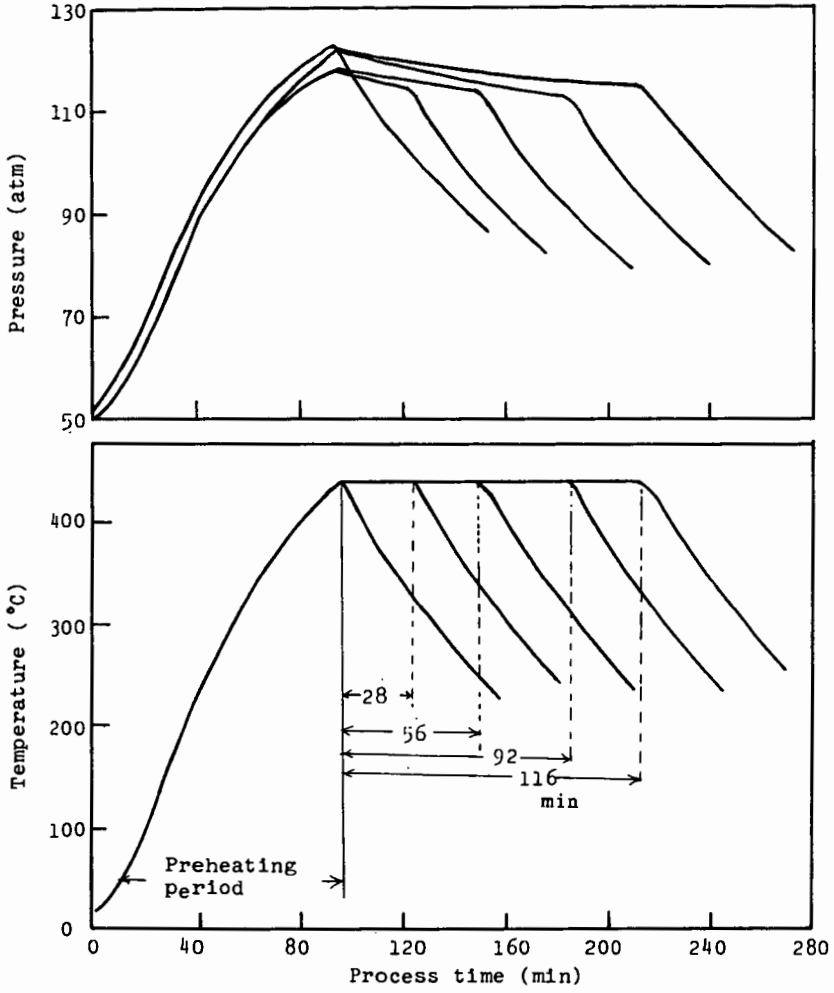

Fig. 1 Examples of the experimental pressure- and temperature-curves at the nominal reaction temperature (NRTM) of 440 °C under several nominal reaction times (NRT)

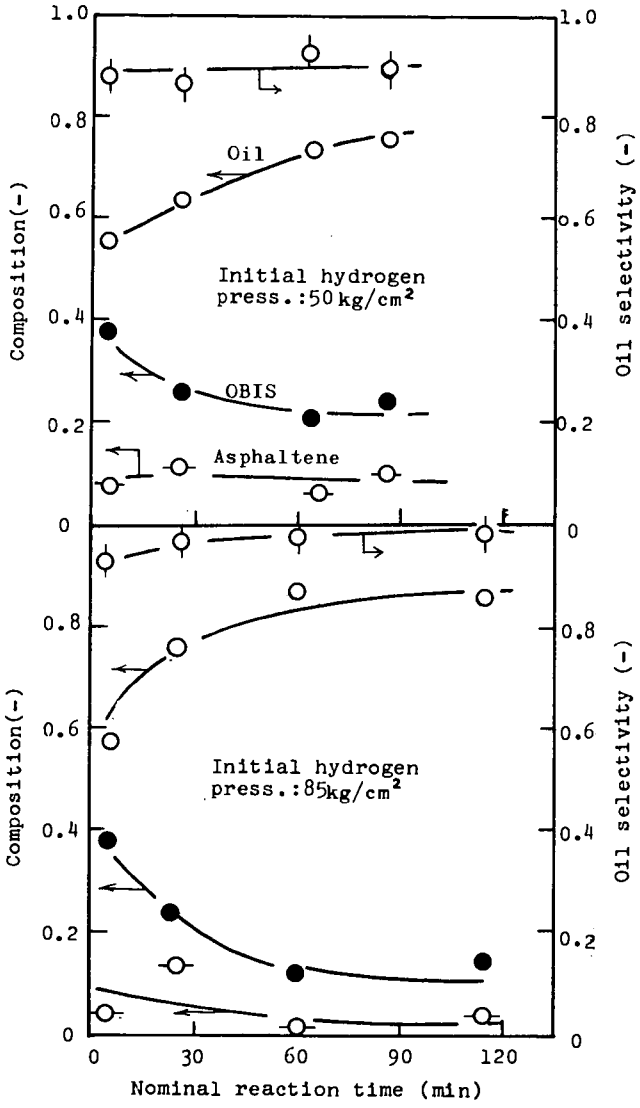

Fig. 2 Liquefaction course of Morwell coal under lower initial hydrogen pressure at NRTM of 350°C

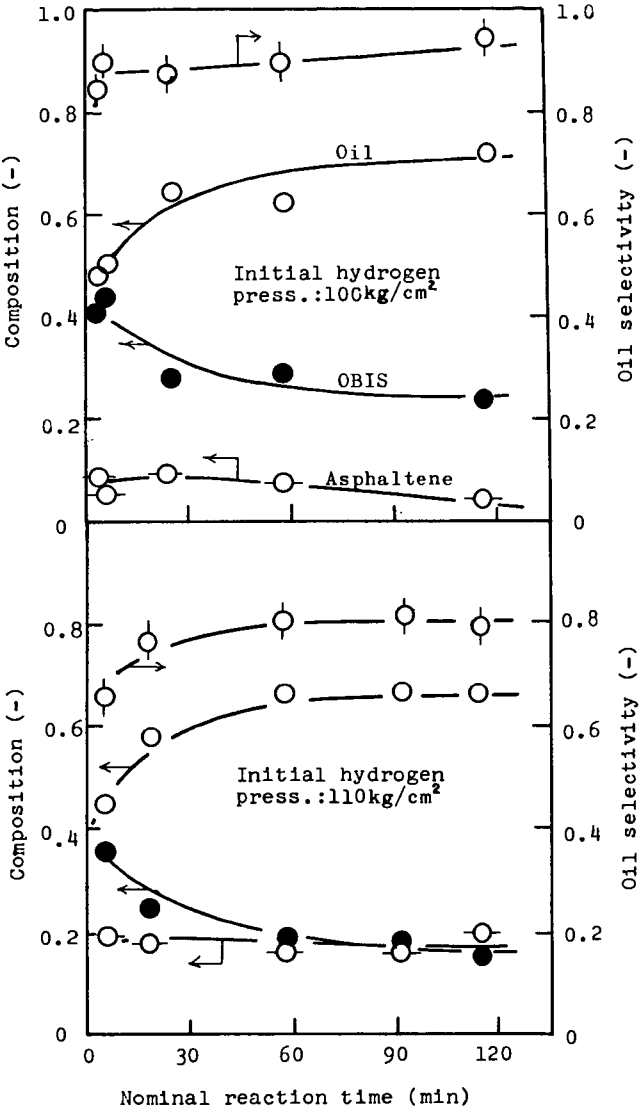

Fig. 3 Liquefaction course of Morwell coal under higher initial hydrogen pressure at NRTM of 350°C

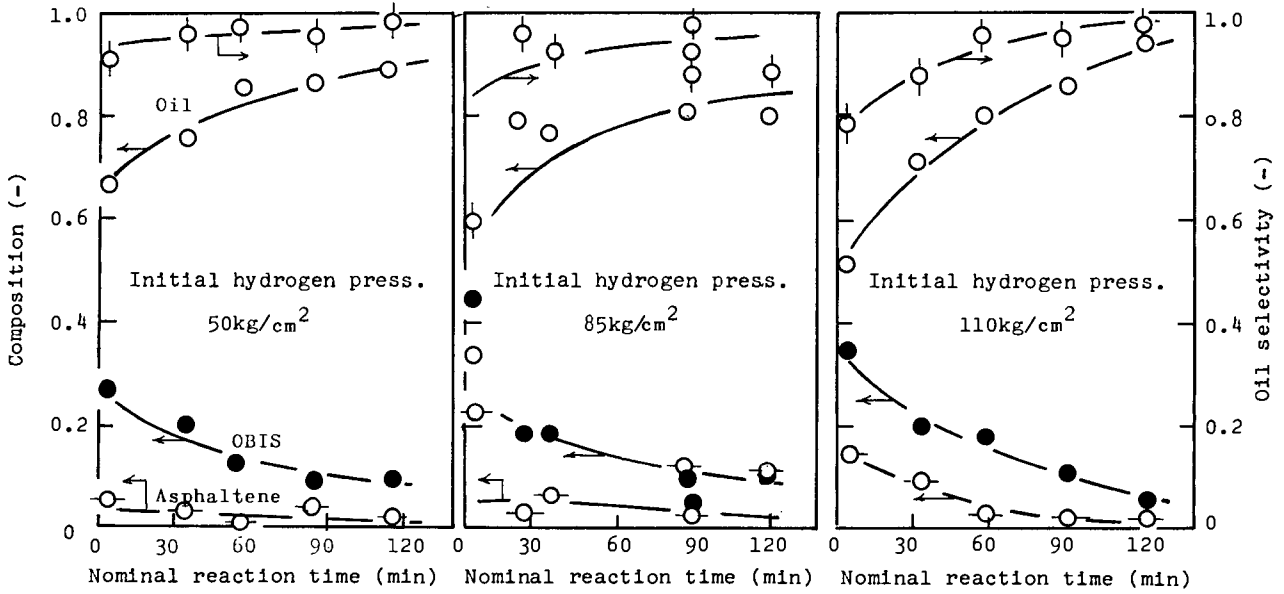

Fig. 4 Dependence of initial hydrogen pressure on liquefaction course of Taiheiyo coal at lower NRTM of 380°C

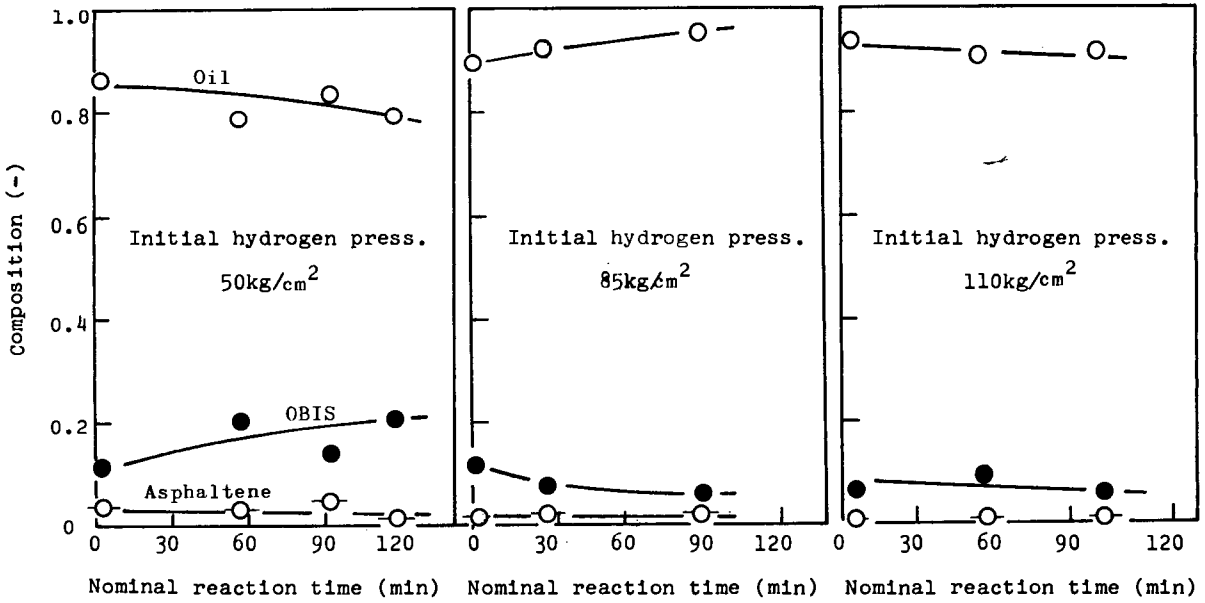

Fig. 5 Dependency of initial hydrogen pressure on liquefaction course of Taiheiyo coal at higher NRTM of 440°C

Flow chart

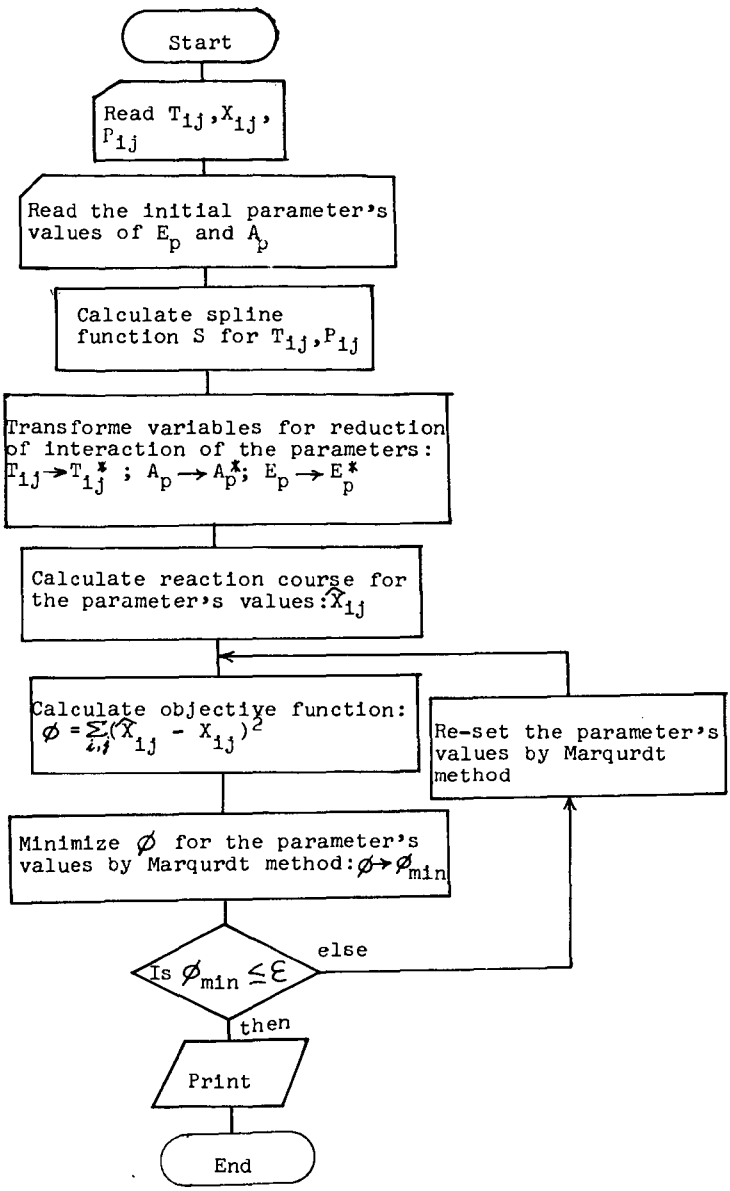
Start
Read T_{ij}, X_{ij}, P_{ij}
Read the initial parameter's values of E_p and A_p
Calculate spline function S for T_{ij}, P_{ij}
Transforme variables for reduction of interaction of the parameters: $T_{ij} \rightarrow T_{ij}^*$; $A_p \rightarrow A_p^*$; $E_p \rightarrow E_p^*$
Calculate reaction course for the parameter's values: $\hat{X}_{ij}$
Calculate objective function: $\phi = \sum_{i,j} (\hat{X}_{ij} - X_{ij})^2$
Re-set the parameter's values by Marqurdt method
Minimize ϕ for the parameter's values by Marqurdt method: $\phi \rightarrow \phi_{min}$
Is $\phi_{min} \leq \varepsilon$
else
then
Print
End

HYDROGENATION OF COAL LIQUIDS IN THE PRESENCE OF SULFIDED Ni-Mo/Al_2O_3

L. Veluswamy*, J. Shabtai+ and A. G. Oblad

Department of Mining and Fuels Engineering
University of Utah, Salt Lake City, Utah 84112

INTRODUCTION

Hydrogenation is one of the most important catalytic processing techniques applied to the petroleum industry. Although considerable work has been done on the hydrotreating of petroleum feedstocks(1,2) and model compounds(3), relatively few studies have been reported on hydrogenation of coal-derived liquids(4-9). Coal liquids contain much less hydrogen (6-8% b. wt.) and considerably more nitrogen (1-2%) and oxygen (4-5%) as compared to petroleum crudes and residua (hydrogen, 11%; nitrogen, <1%)(10). Coal liquids have much higher concentration of asphaltenes than petroleum residua (25-35% b. wt. vs 5-6% b. wt.), as well as higher overall aromaticity than the latter (60-75%) b. wt. vs 20-35% b. wt. of aromatic carbon). This high concentration of condensed aromatic ring structures in coal liquids causes coke formation to a large extent in refining processes such as catalytic cracking. The heteroatoms, particularly nitrogen and sulfur, are severe poisons for many of the catalysts employed in petroleum refining. Hence, hydrotreatment of such liquids may be necessary to upgrade their quality and make them suitable for further refining processes. In this study, the hydrogenation of Synthoil and fractions derived from it, in the presence of sulfided Ni-Mo/Al_2O_3 and Ni-W/Al_2O_3 systems, was systematically investigated as a function of experimental conditions, such as, reaction temperature, pressure and process time. Results obtained with model compounds (11-13) were correlated with results of this study to elucidate the hydrogenation behavior of syncrudes.

EXPERIMENTAL

Feedstock

The Synthoil (from West Virginia coal) used in this study was supplied by the Pittsburgh Energy Research Center. The cyclohexane soluble fraction (maltene) and cyclohexane insoluble fraction (A-P) of Synthoil were prepared according to the following procedure. Synthoil was mixed with cyclohexane in a ratio of 1:40 and the mixture was heated to near the boiling point of cyclohexane with magnetic stirring for about 40 minutes. The mixture was cooled to room temperature and kept overnight with continued stirring. The maltene fraction with cyclohexane was separated from A-P by vacuum filtration. The maltene fraction of Synthoil was separated from cyclohexane by evaporating cyclohexane under slight vacuum. The A-P fraction was dried in an oven kept at 80°C. Data on properties of the Synthoil and fractions derived from it are given in Table 1.

---

*Presently with Exxon Research and Engineering Company, Baytown, Texas

+Weizmann Institute of Science, Rehovot, Israel

Table 1

Analysis and some Properties of Synthoil and Synthoil Fractions

Material	C	H	N	S	O	H-aromaticity %
Synthoil[a]	86.4	7.2	1.3	0.7	4.4	30.7
Cyclohexane-soluble fr.[b]	88.3	7.5	1.2	0.6	2.4	28.1
Cyclohexane-insoluble fr. (Asphaltene[c]-Preasphaltene[d])	88.1	6.1	1.9	0.3	3.6	36.4

(a) Specific gravity, 1.14; viscosity SSF @ 82°C, 104; ash 1.6% b. wt.
(b) Represents 64.7% b. wt. of the total Synthoil; (c) Represents 28.1% b. wt. of the total Synthoil; (d) Represents 7.2% b. wt. of the total Synthoil

Catalyst

The catalysts used in this study were (i) HT100E, manufactured by Harshaw Chemical Company and (ii) Sphericat 550, manufactured by Nalco Chemical Company. The 1/16 inch HT100E extrudates contain 3.0% NiO and 15.0% MoO_3 on alumina. The 1/16 inch Sphericat 550 spheres contain 5.1% NiO and 20.2% WO_3 on alumina. These catalysts were chosen from several commercial catalysts for our study because of their high hydrogenation activity and low cracking characteristics in the hydrogenation of model compounds(11). Both catalysts were sulfided before use.

Hydrogenation Technique

All the experiments on hydrogenation of Synthoil were carried out in a fixed bed flow reactor (36" L. x 1.25" I.D. x 0.5" W.T.) system. An autoclave (11) of 300cc capacity was used in all the experiments on hydrogenation of maltene and A-P fractions of Synthoil.

The fixed-bed hydrotreating unit (11) was flushed with hydrogen to remove air, and the system was brought to reaction temperature and pressure. Synthoil was heated to about 80°C and pumped at a rate of 30 cc/hr. to maintain a LHSV of 0.5 hr^{-1} (catalyst:60cc) in each experiment. A hydrogen flow rate of 2 litres/min. was used. The product was cooled in the condenser and the liquid product was collected from the low pressure separator. The gaseous product was passed through a series of scrubbers (to remove H_2S and NH_3) and wet test meter. The liquid product was dissolved in $CDCl_3$, filtered and analyzed.

The hydrogenation procedure in the autoclave unit is as follows. After placing known amounts of Synthoil fraction and catalyst in the autoclave, the autoclave was purged with H_2 and then pressurized with H_2 to half the reaction pressure. The reactor was heated to the reaction temperature and the pressure was adjusted to the experimental pressure. The total pressure in the system was maintained constant throughout the reaction period by the automatic addition of hydrogen whenever necessary from the cylinder through the regulator and check valve. At the end of each experiment, the reactor was cooled rapidly, and the pressure was released. The product was mixed with $CDCl_3$, filtered to remove the catalyst and analyzed.

Due to the complex nature of coal-derived liquids and their products of hydrogenation, no attempt of structural analysis of the liquid products was made. Elemental analysis was done for all samples. A simple analytical method, using PMR (Proton Magnetic Resonance), was developed(11) to determine the overall aromatic saturation. The extent of saturation was estimated as

$$\% \text{ decrease in H-aromaticity} = \frac{(\text{H-aromaticity})_{\text{feed}} - (\text{H-aromaticity})_{\text{product}}}{(\text{H-aromaticity})_{\text{feed}}} \times 100$$

RESULTS AND DISCUSSION

Effect of Experimental Conditions upon the Hydrogenation of Synthoil

Coal derived liquids consist of condensed polycyclic aromatic hydrocarbons (mainly 3 to 5 rings), as well as aromatic-naphthenic, aromatic-heterocyclic and aromatic-naphthenic heterocyclic systems. The extent of hydrogenation and heteroatom removal depend on several factors, e.g., (a) reaction temperature, (b) reaction pressure, (c) hydrogen/substrate ratio, (d) liquid hourly space velocity (LHSV), (e) catalyst structure and type, and (f) composition of the feedstock (structural characteristics of the starting substrate components and of partially hydrogenated intermediates). The effect of some of these variables upon hydrogenation of Synthoil over Ni-Mo/Al_2O_3 was studied in a fixed bed reactor, using a hydrogen flow rate of 2 litres/ min., and a LHSV of 0.5 hr^{-1}.

Effect of Process Time

Figure 1 summarizes the observed hydrogen uptake, viz. the % decrease in H-aromaticity, in the product from hydrogenation of Synthoil as a function of process time (between 60-260 min.). Initially (process time, 60-140 min.), a rapid decrease in hydrogen uptake, is observed. However, as the process time is extended (140-300 min.), the % decrease in H-aromaticity and the hydrogen uptake reach a plateau. This indicates that the catalyst deactivates appreciably at the beginning of the experiment, but subsequently its activity is stabilized. Product analysis shows a hydrogen content of ca 10% b.wt., and a 55-60% decrease in H-aromaticity under steady state conditions (Figure 1).

Effect of Temperature

Figure 2 shows the observed change in hydrogen content and in H-aromaticity of the product from hydrogenation of Synthoil as a function of temperature (between 300-400°C at 2900 psig). As seen, the hydrogen uptake increases with increase in temperature up to ca 370°C (maximal % decrease in H-aromaticity, 62.4%; and maximal hydrogen content, ca 10%). Above 370°C, there is apparently a tendency of decrease in the hydrogen uptake. Experimental and calculated data (14,15) on hydrogenation equilibria of polycyclic aromatics indicate that at high hydrogen pressures, e.g., above 2000 psig and temperatures below 390°C, the equilibrium is displaced almost entirely in the direction of hydrogenation. On the other hand, at temperatures above 390°C (this temperature may vary depending upon the type of aromatics), there should be some of the free aromatic reactant at equilibrium. The concentration of this aromatic component increases with increase in temperature. For example, upon hydrogenation of phenanthrene, the concentration of the latter at equilibrium decreases with increase in temperature up to 375°C, but then increases with further increase in temperature (14). Hence, this provides a plausible explanation for the observed hydrogenation behavior of Synthoil. The observed increase in aromatic content of the product from hydrogenation of Synthoil at temperatures above 370°C may be also due to some increase in the extent of cracking reactions.

Figure 3 shows the change in nitrogen and sulfur content of the product from hydrogenation of Synthoil as a function of temperature (between 300-400°C). As expected, the extent of N and S removal increases with increase in temperature,

since the equilibrium data indicate that heteroatom removal proceeds irreversibly and is, therefore, not equilibrium controlled. Nitrogen removal ranges from 18% to 70% whereas the S removal ranges from 45% to 86%. This indicates that the former process is generally a slower one. The observed incomplete removal of heteroatoms may be due to the stereochemical characteristics of some more complex nitrogen-and sulfur-containing heterocyclics, and of partially hydrogenated intermediates (11,13). Another reason for incomplete saturation of polyaromatics and incomplete removal of heteroatoms in feedstocks such as Synthoil and their fractions may be due to diffusion effects (1,16).

Effect of Pressure

Figure 4 shows the observed change in H-aromaticity of the product from hydrogenation of Synthoil as a function of pressure (between 2500-2900 psig). As seen, the saturation of aromatics increases with increase in pressure. It is indicated(11) that nitrogen removal increases with increase in pressure (51% at 2500 psig and 70% at 2900 psig), but the extent of S removal changes only to a small extent (83 to 89%) with increase in pressure (between 2500-2900 psig). A similar behavior was observed in the Texaco work on hydrodesulfurization of heavier intermediate cracked gas oil(1).

Hydrogenation of Maltene (Cyclohexane-Soluble) and Asphaltene-Preasphaltene (Cyclohexane-Insoluble) Fractions of Synthoil

A Synthoil sample was separated into a maltene (cyclohexane-soluble) fraction and an asphaltene-preasphaltene (cyclohexane-insoluble) fraction as described in experimental section. These fractions derived from Synthoil were hydrogenated in an autoclave under severe conditions (pressure, 2900 psig; temperature, 288-377°C; reaction time, 7 hr.) using sulfided Ni-W/Al_2O_3 catalyst and the results are summarized in Table 2. As seen from experiment 1, the cyclohexane-soluble fraction is readily hydrogenated (% decrease in H-aromaticity=71.2%, corresponding to a residual H-aromaticity of only 8.1%). On the other hand, hydrogenation of the cyclohexane insoluble fraction (asphaltenes plus preasphaltenes), under the same set of conditions, (expt. 3) is very limited (% decrease in H-aromaticity of 23.6% corresponding to a residual H-atomaticity of 27.8%). Table 2 also shows that the saturation of the cyclohexane-insoluble fraction increases with increase in temperature.

Table 2

Change of Quality in the Product from Hydrogenation of Synthoil Fractions[a-c]

	Cyclohexane soluble fr.[d]	Cyclohexaneinsoluble fr.[e] (asphaltenes-preasphaltenes)		
Expt. No.	1	2	3	4
Reaction temperature, °C	341	288	341	377
H-aromaticity, %				
in feed	28.1	36.4	36.4	36.4
in product	8.1	34.5	27.8	25.3
% decrease in H-aromaticity	71.2	5.6	23.6	30.5
% heteroatom removed				
N	86.1	8.5	31.9	51.6
S	62.9	--	--	62.5
O	96.7	33.1	63.6	82.4

(a) Catalyst: sulfided Ni-W/Al_2O_3; (b) Pressure: 2900 psig; (c) Reaction time: 7 hr.; (d,e) For elemental composition of reactant, see Table 1.

A probable reason for the difficulty of completely hydrogenating the maltene fraction of Synthoil is indicated by results obtained from hydrogenation of model compounds, e.g. phenanthrene and pyrene(11,12) using commercial hydrogenation catalysts ($Ni\text{-}Mo/Al_2O_3$, $Ni\text{-}W/Al_2O_3$, etc.). It was found that hydrogenation of the outer rings in phenanthrene is a fast reaction. But, once the two outer rings are saturated, the subsequent step of hydrogenating the sterically hindered inner ring is much slower. It should be expected in the case of condensed polycyclic compounds present in the maltene fraction, at least a part of the inner rings become sterically hindered by adjacent hydroaromatic rings during the step-wise hydrogenation process. This would be more probable in tetracyclic and pentacyclic systems, e.g., triphenylene. In the latter compound, for instance, there is one inner ring which is fully substituted by three terminal benzene rings which upon hydrogenation form a steric barrier around the residual inner benzene ring. Examination of molecular models show that flatwise adsorption of this inner benzene ring on the catalyst surface is very difficult while edgewise adsorption is excluded. The residual 8.1% of H-aromaticity in the hydrogenated maltene fraction corresponds roughly to 15-20% of residual non-hydrogenated aromatic rings, viz. approximately one residual aromatic ring per 5-6 hydroatomatic rings, in line with the above suggested model. The relatively higher resistance to hydrogenation shown by the asphaltene-preasphaltene fraction (Table 2; expt. 2, 3, and 4) may be due to the higher complexity and proportionally higher concentration of sterically hindered inner rings in the polycyclic systems present in this fraction. For instance, in 1,2,3,4, 5,6,7,8-tetrabenzonaphthalene which is a hexacyclic system, the completely substituted rings represent 33% (one out of three) of the condensed system.

The products of hydrogenation of the asphaltene-preasphaltene fraction (expts. 2,3, and 4) were analyzed for cyclohexane solubility. Results obtained are plotted in Figure 5. As seen, solubility increases sharply with gradual decrease in the H-aromaticity of the asphaltene fraction, reaching a level of about 85% at a point of 31% decrease in H-aromaticity. This important result can be rationalized by considering three possible factors affecting solubility: (a) polar compounds such as O, S, and N-containing compounds undergo heteroatom removal (Table 2) making the product less polar, viz., more soluble in a non-polar solvent, e.g., cyclohexane, (b) decrease in the complexity and molecular weight of the asphaltene molecules resulting from splitting reactions, (c) the partial hydrogenation of the polycyclic aromatic system could also contribute to the observed increase in solubility.

CONCLUSIONS

Results obtained from this study of hydrogenation of Synthoil and its fractions indicate the following:

(i) Even under severe hydrogenation conditions where the aromatic saturation equilibria favor in the direction of complete saturation, coal-derived liquids show marked resistance to complete hydrogenation. It is concluded, in line with the results obtained with model compounds, that the resistance to complete hydrogenation may be due to sterically hindered aromatic rings.

(ii) Hydrodenitrogenation is relatively more difficult when compared to hydrodesulfurization in coal-derived liquids.

(iii) The rate and depth of hydrodenitrogenation and hydrodesulfurization of coal-derived liquids may strongly depend on the steric characteristics of condensed N and S heterocyclic aromatic feed components, or of partially hydrogenated intermediates.

(iv) The asphaltene-preasphaltene fraction of Synthoil shows higher resistance to hydrogenation than the maltene fraction of Synthoil.

(v) The solubility of the hydrogenated product of asphaltene-preasphaltene fraction of Synthoil in cyclohexane increases with decrease in H-aromaticity and heteroatom content.

REFERENCES

1. Gully, A. J. and Ballard, W. P., Advances in Petroleum Chemistry and Refining, Interscience Publishers, Wiley, N.Y., 1960, 7, Chapter 4.
2. Horne, W. A. and McAfee, J., Advances in Petroleum Chemistry and Refining, Interscience Publishers, Wiley, N.Y., 1960, 2, Chapter 5.
3. Weisser, O. and Landa, S., "Sulfide Catalysts, their properties and application", Pergamon Press, Oxford, N.Y., 1973.
4. White, P. J., Jones, J. F., and Eddinger, R. T., Hydrocarbon Processing, 1968, 47, No. 12, p. 97.
5. Jacobs, H. E., Jones, J. F., and Eddinger, R. T., Ind. Eng. Chem. Process Des. Devel., 1971, 10, No. 4, p. 558.
6. Catalytic Hydrotreating of Coal Derived Liquids - Project Seacoke, Phase II, Final report to OCR, ARCO Chemical Co., Aug., 1963-Dec., 1966.
7. John, J. J., Jones, J. F. and McMunn, B. D., Am. Chem. Soc,. Div. Fuel Chem., Prepr., 1972, 16, No. 1, p. 216.
8. Heck, R. H. and Stein, T. R., ACS, Div. Petr. Chem., Pepr., 1977, 22, No.3, p. 948.
9. de Rosset, A. J., Tan, G. and Gatsis, J. G., ACS, Div. Petr. Chem., Prepr., 1977, 22, No. 3, p. 962.
10. Stein, T. R., Voltz, S. E. and Callen, R. B., Ind. Eng. Chem. Prod. Res. Dev., 1977, 16, No. 1, p. 61.
11. Veluswamy, L. R., "Catalytic Hydrogenation of Coal-Derived Liquids and Related Polycyclic Aromatic and Heterocyclic Compounds," Ph.D. thesis, University of Utah, 1977.
12. Shabtai, J., Veluswamy, L. and Oblad, A. G., ACS, Div. Fuel Chem. Prepr., 1978, 23, No. 1, p. 107.
13. Shabtai, J.,Veluswamy, L. and Oblad, A. G., ACS Div. Fuel Chem. Prepr., 1978, 23, No. 1, p. 114.
14. Frye, C. G., ACS, Div. Petr. Chem. Prepr., 1961, 6, B157.
15. Bondi, A., Petr. Refiner, 1959, 38, No. 2, p. 161.
16. Smith, J. M., "Chemical Engineering Kinetics", Second Edition, McGraw Hill Book Company, N.Y., 1970, p. 365.

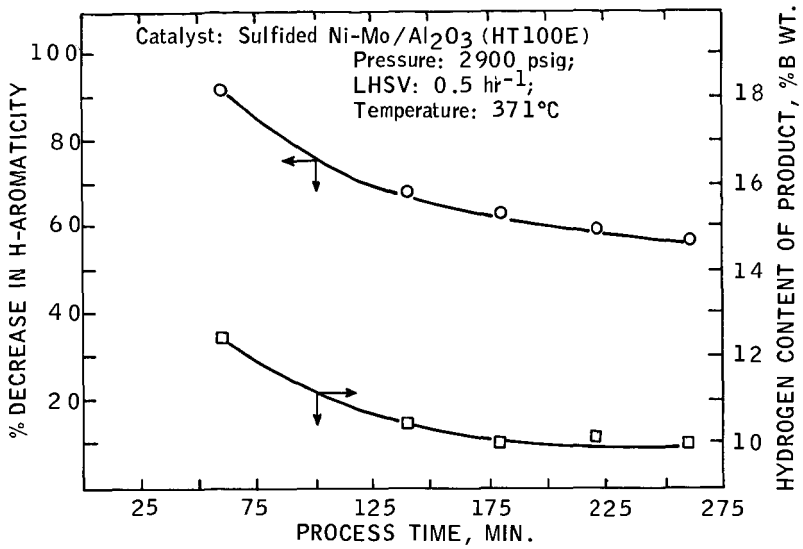

Fig. 1. Change in hydrogen content and H-aromaticity of the product from hydrogenation of Synthoil as a function of process time.

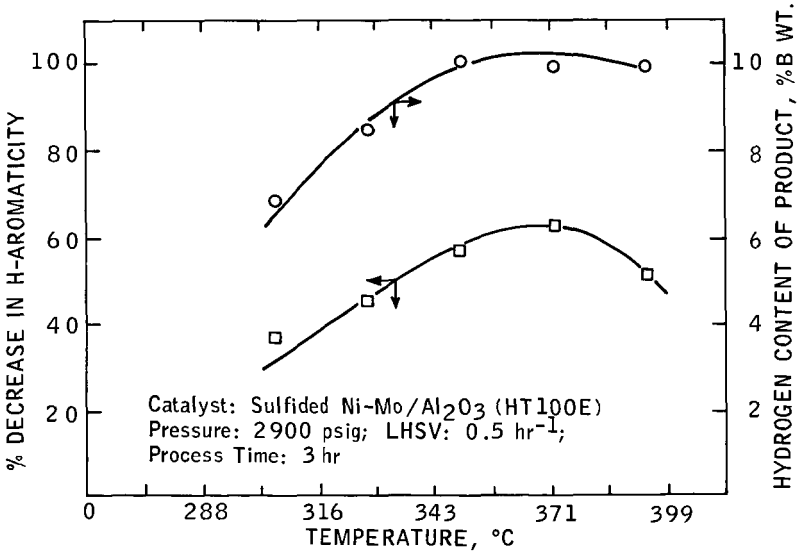

Fig. 2. Change in hydrogen content and H-aromaticity of the products from hydrogenation of Synthoil as a function of temperature.

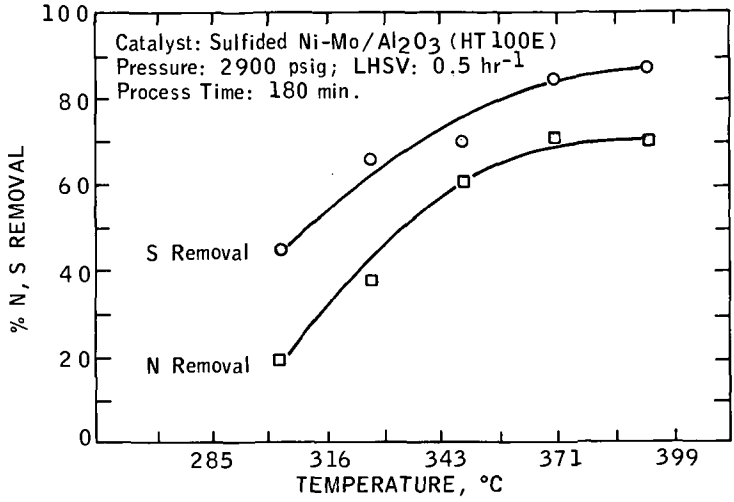

Fig. 3. Change in nitrogen and sulfur content of the product from hydrogenation of Synthoil as a function of temperature.

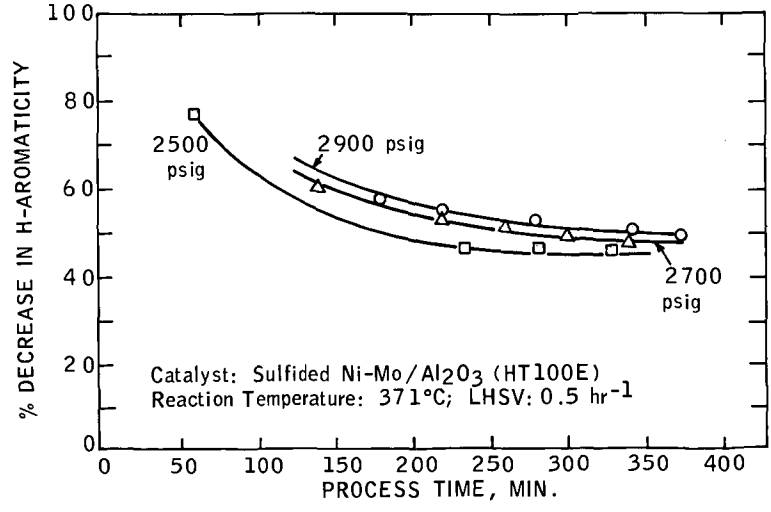

Fig. 4. Change in H-aromaticity of the product from hydrogenation of Synthoil as a function of pressure.

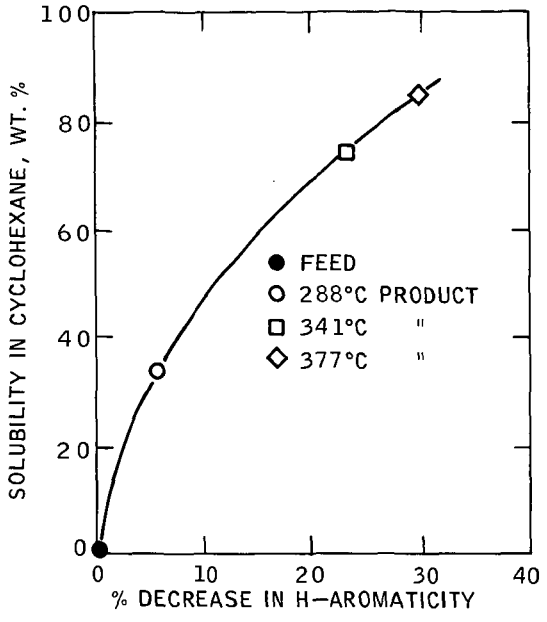

Fig. 5. Change in solubility of asphaltene fraction in cyclohexane as a function of decrease in H-aromaticity.

Pressure: 2900 psig
Reaction time in each run, 7 hr.
Catalyst: Sulfided Ni-W/Al_2O_3

Studies on Coal Hydrogenation Reaction Using High Pressure Differential Thermal Analysis

S. Yokoyama*, S. Ueda*, Y. Maekawa* and M. Shibaoka**

*Government Indistrial Development Laboratory, Hokkaido
41-2, Higashi-Tsukisamu, Toyohiraku,
Sapporo, 061-01, Japan

**CSIRO, Fuel Geoscience Unit, P.O.Box 136, North Ryde,
N. S. W. Australia 2113

Introduction

High pressure hydrogenation reaction of coal is an exothermic reaction accompanied by heat generation and hydrogen consumption. As compared against autoclave experiments, when high pressure DTA is applied it is possible to conduct a rapid and simple follow up of the course of reaction over a wide thermal range, and the results obtained are of considerable interest.

Up till the present, utilizing a 2 cell high pressure DTA apparatus developed by the present workers[1], we have conducted measurements of the heat of coal hydrogenation[2] and desulfurization reaction of heavy oil[3]. Following the above we have carried out comparative studies of catalytic activity and reactivity with regard to hydrogenation of aromatic compounds and coals[4]-[6].

In the present paper, first we will describe a newly developed single cell DTA apparatus. This single cell apparatus, as compared against the conventional 2 cell DTA apparatus, was designed in such a way as to have a simpler heating rate control and a higher measurement sensitivity.

Next, in the hydrogenation reaction of coal, generally it is not quite so easy to maintain or obtain a contact of hydrogen and the coal sample. Thus, in the present work we did not use stirring, but instead we made an even mixture of the unreacted solid, namely α-Al_2O_3 was mixed at various rates with the coal sample, and by gradually chenging the hydrogen availability, we investigated the relationship of mesophase fromation and hydrogenation.

Next, under the condition of a sufficient hydrogen availability necessary for the coal hydrogenation reaction, the exothermic peaks were measured and the reaction course of coal hydrogenation was investigated.

Experimental

Sample

The present work was undertaken as part of a series of studies on hydrogenation of the petrographic composition of coal, in the study vitrinite concentrate hand-picked from Bayswater and Liddell seam coal (N.S.W., Australia) with a high volatile bitumous rank were used. The particle size was under 100 mesh. The petrographic and chemical analysis of the hand-picked samples are given in Table 1.

Apparatus

The essentcal part of the single-cell DTA apparatus comprises two sheath thermoconples (1.6 mm diameter) and a heat-sink, which are placed in an ordinary autoclave (25 mm i.d., 50 ml capacity). One thermocouple is inserted into a hole

in the heat-sink and the other into the sample. Exothermic or endothermic reactions can be detected by measuring the temperature difference between the heat-sink and the sample. This temperature difference can be recorded on a chart as a DTA curve. The pressure change can also be recorded on a chart simultaneously by using a pressure transducer and an amplifier.

Experimental conditions

The sample coal was impregnated with accurate 10% $ZnCl_2$ using an ethanol solution and was subsequently evaporated to dryness in a vacuum dryer. 5.5 g of this sample was used for each high pressure DTA experiment. In order to vary the hydrogen availability, to each sample 0~5.5 g of unreacted solid namely α-Al_2O_3 of 80 mesh was mixed in evenly. Hydrogen initial pressure 100 kg/cm^2 was charged into the autoclave, and at a heating rate of 3°C/min, the temperature was raised to a given point and the DTA and pressure change curve was measured. After reaching a given temperature, the autoclave was immediately removed from the furnace and allowed to cool in air and the temperature was lowered at a rate of 35°C/min. After cooling down to room temperature, the reaction products were analysed using a Soxhlet extractor and a gaschromatography. Oil is defined here as a hexane-soluble fraction and asphaltene as benzene-soluble, hexane-insoluble fraction. The solid residues were examined under a reflected light microscope.

Results and discussion

1. The effect of hydrogen availability on coal hydrogenation and DTA

Previous work[7] by the present author showed that the formation of the mesophase during coal hydrogenation was controlled not only by temperature and time but also by hydrogen availability.

In the cases where coal hydrogenation was carried without the use of vehicle oil, since stirring is difficult, in the present case a new technic was attempted, namely by mixing unreacted solid, α-Al_2O_3, evenly into the sample under various ratios, the hydrogen availability was gradually changed. In Fig. 1, the DTA curve and pressure change curve obtained by mixing in 0~5.5g of α-Al_2O_3, and raising the temperature to 450°C, are shown. Fig. 2 showns the results of analyses of the reaction products after cooling down to room temperature. From microscopic observations of the extraction residues, in the case where less than 2.5 g of α-Al_2O_3 is mixed in, it was shown that while the mesophase formed, when the addition of α-Al_2O_3 was increased over 3.3 g the mesophase was not formed. In the former, from microscopic observations during the exothermic peak formation, it was considered that the reaction proceeds in the following manner. In the former half of the exothermic peak on the lower temperature side, the coal particles are independent of each other, and since the contact with hydrogen is good, the hydrogenation reaction proceeds rapidly accompanied by heat generation and hydrogen consumption. However, on the high temperature side of the exothermic peak, because of the melting point aided by a slight liquefaction, it was noted that the coal particles melted and agglomerated. Because of this, the contact of coal and hydrogen became poor and the hydrogenation was terminated. As the temperature is raised higher, mesophese formation proceeds accompanied by dehydrogenation and the evolution of carbon dioxide. In the case where more than 3.3 g of α-Al_2O_3 is mixed in, from the results of DTA and microscopic observation together with analyses of the products, it was shown that hydrogen availability was in sufficient quantity.

2. Reaction course of coal hydrogenation

In order to investigate the reaction course of coal hydrogenation, the temperature rise was terminated at 10 points of the exothermic peak and after cooling down to room temperature, the reaction products were analysed as shown in Fig. 3. These

exothermic peaks were measured under the conditions of an adequate hydrogen availability necessary for the coal hydrogenation reaction, produced by an addition 4 g of α-Al_2O_3.

From these results, the following reaction course was derived.

$$\text{Coal} \longrightarrow (\text{Preasphaltene}) \longrightarrow \text{Asphaltene} \longrightarrow \text{Oil}$$

References

1) Takeya,G., Ishii,T., Makino,K., and Ueda,S., J. Chem. Soc. Japan, Ind. Chem. Sect., 69, 1654 (1966)
2) Itho,H., Makino,K., Umeda,N., Takeya,G., and Ueda,S., J. Fuel Soc. Japan, 50, 919 (1971)
3) Ueda,S., Yokoyama,S., Ishii,T., Makino,K., and Takeya,G., Ind. Eng. Chem., Process Des. Dev., 14, 493 (1975)
4) Ishii,T., Sanada,U., and Takeya,G., J. Chem. Soc. Japan, Ind. Chem. Sect., 71, 1783 (1968)
5) Ueda,S., Yokoyama,S., Ishii,T., and Takeya,G., ibid, 74, 1377 (1971)
6) Ueda,S., Yokoyama,S., Nakata,Y., Hasegawa,Y., Maekawa,Y., Yoshida,Y., and Takeya,G., J. Fuel Soc. Japan, 53, 977 (1974)
7) Shibaoka,M., and Ueda,S., Fuel in Press

Table 1 Petrographic, Proximate and Ultimate Analyses of Sample Coals

Sample	Maceral analysis (%)					Proximate analysis (%)				Ultimate analysis (%, d.a.f.)				
	Vitrinite	Exinite	Miorinite	Semi-fusinite	Fusinite	Moisture	Ash	Volatile matter	Fixed carbon	C	H	N	S	O
Bayswater, Vitrinite concentrate	99	0.5	0.5	tr	tr	3.4	1.6	32.9	62.1	83.0	5.3	2.0	0.5	9.2
Liddell, Vitrinite concentrate	99	0.5	tr	0.5	tr	7.3	0.7	31.6	60.4	84.0	5.3	1.8	0.6	8.3

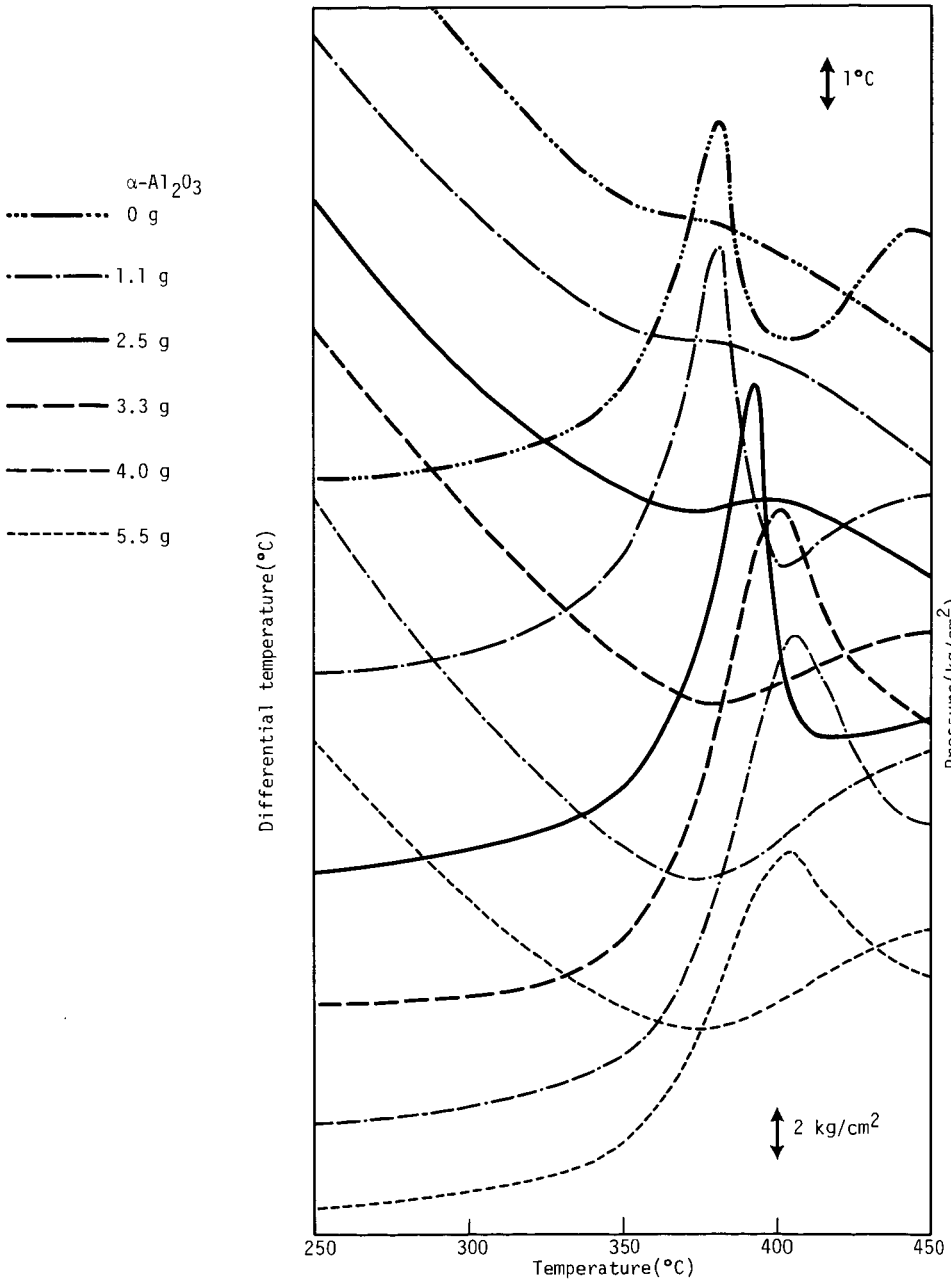

Fig. 1 DTA and pressure change curues in hydrogenation reaction of Bayswater seam coal

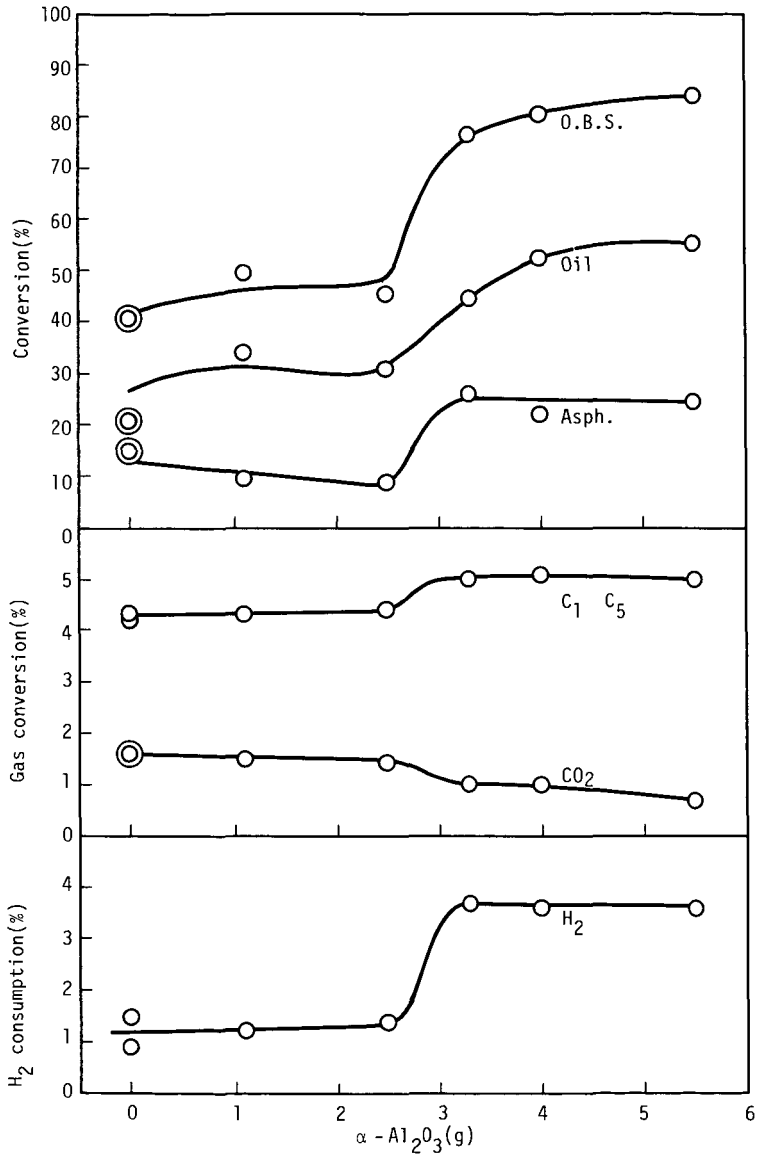

Fig. 2 Relationship between hydrogenation products and mixed α-Al_2O_3 for Bayswater seam coal

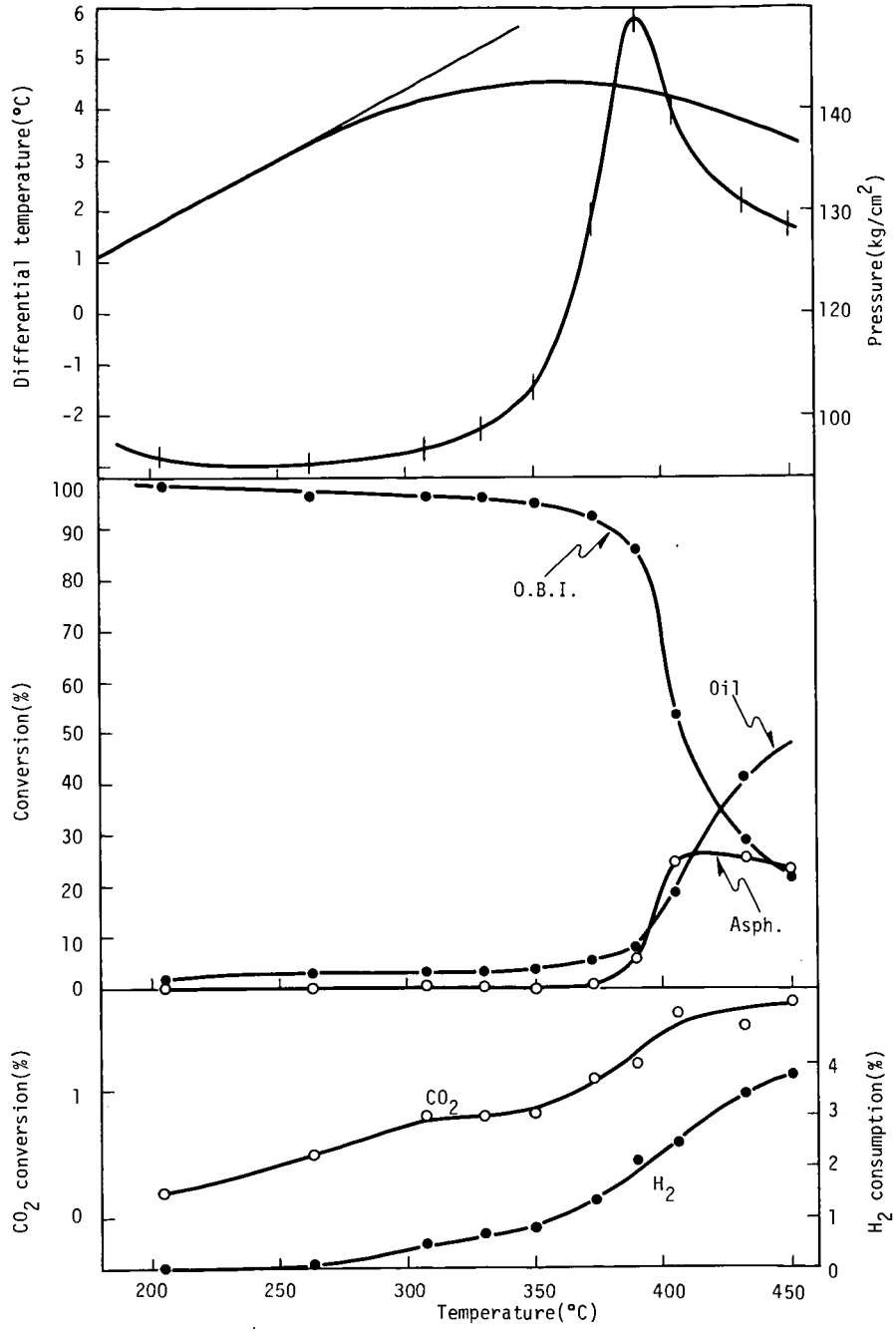

Fig. 3 DTA curue and products in hydrogenation reaction of Liddell seam coal

EFFECT OF HYDROGEN PRESSURE ON THE REACTION OF NaOH-ALCOHOL-COAL.

Masataka Makabe and Koji Ouchi.

Faculty of Engineering,Hokkaido University,Kita 13,Nishi 8, Sapporo,Japan,060.

The reaction of coals with-alcohol-NaOH has been studied in detail[1)2)] and the younger coals with less than 82%C could be dissolved nearly completely in pyridine after the reaction at 300°C for 1 hour. Even a coal of 87%C could be nearly completely dissolved by the reaction at 350°C for 1 hour. Other reaction conditions, temperature,time and the concentration of NaOH,were also examined in detail. The species of alkalis was examined,which revealed that NaOH and LiOH were most effective[3)]. Reaction mechanism was pursured by the structural analysis for the pyridine extracts of which yield were more than 90%[4)]. The results show that the main reaction is the hydrolysis and partly associated with hydrogenation by the hydrogen produced from the reaction between alcohol and NaOH as follows,[1)2)]

$$C_2H_5OH+NaOH \longrightarrow CH_3COONa+2H_2$$

The structural analysis of pyridine extracts which represent the almost all the reaction products,that is to say the original coals themselves,revealed that the aromatic ring numbers in the structural unit (cluster unit)of the younger coals consist of 1 with 0.5 naphthenic ring and the bituminous coals have the aromatic ring number of 4 with 1 naphthenic rings. The younger coals have more of ether linkages and constitute higher molecular weight structure.

As the nascent hydrogen atoms can contribute to the hydrogenation of coal molecules,probably the atmospheric pressure affects the reaction degree and the hydrogen pressure will give more effects. This report treats the effect of hydrogen pressure on this reaction.

Experiments

Coal sample is the vitrinit of Taiheiyo coal(C:77.5%,H:6.3%, N:1.1%,S:0.2%,O_{diff}:14.5%)prepared by the float-and-sink method. The crushed coal of 1g,NaOH of 1g and 10ml of alcohol were placed in an autoclave of 38ml with the magnetic stirrer and the atmosphere was replaced with pressurized nitrogen or hydrogen.Then they were reacted at 300~430°C,for 1 hour. After reaction the gas was analyzed with GC and the product was acidified with 2N HCl. The precipitate was centrifuged,filtered,washed and dried. The extraction was carried out by shaking the product with pyridine,alcohol or benzene for 10 hours at room temperature.

At the higher reaction temperature than 400°C,the product becomes oily. Therefore benzene was added to the product and small amount of water was also added to dissolve the block of sodium acetate. The mixture of two phase solution with the unreacted powder was filtered to eliminate the unreacted part and the benzene phase was separated from aqueous phase.The benzene solution was washed well with water and dried with sodium sulfate,then benzene was recovered by distillation.The residue was extracted with benzene by shaking at room temperature as above.

IR spectra were recorded by KBr pellet with the special care to

eliminate the humidity.

Results and discussion

The reaction condition,products yield and solvent extraction yield are listed in Table 1~2 and Fig 1~2. Under the nitrogen pressure the yield of ethanol extraction increases with the pressure. The main reaction of NaOH-alcohol-coal system is the hydrolysis which results the splitting of ether linkages and contributes the reduction of molecular weight[1)3)4)]. But as pointed out in the previous papers a slight hydrogenation takes place with the hydrogen produced from the reaction of alcohol with NaOH. This hydrogen is expected to act as a nascent hydrogen and under the pressure it may be confined in the solution,which contributes to the rise of reactivity.

The yield of extraction with ethanol for the products under hydrogen pressure has the higher values than those under nitrogen. The dissolution of atmospheric hydrogen into the solution may contribute to the hydrogenation.

The rise of temperature also increases the extraction yield. The yield of extraction with ethanol under hydrogen pressure always has the higher values than those under nitrogen pressure. The yield of extraction with benzene under nitrogen has the higher values than those under hydrogen at the lower temperature,but at the higher temperature the yield of extraction under hydrogen becomes higher. This can not be explained well. The possibility is that under hydrogen ether linkages split more than under nitrogen and the product contains more of OH groups,which favors the solubility into ethanol and limits the solubility into benzene.

(references)
1)K.Ouchi,M.Makabe,Nenryokyokaishi(J.Fuel Soc Hapan),57,249(1978)
2)M.Makabe,K.Ouchi,Fuel,57,289.(1978)
3)M.Makabe,K.Ouchi,Fuel,in press.
4)M.Makabe,K.Ouchi,Fuel Proc,Tech in press.
5)M.Makabe,K.Ouchi,Fuel,in press.

Table 1. Reaction conditions,product yield and solvent extraction yield at 300°C

Initial pressure,MPa	Species* of gas	Product yield %	Solvent extraction yield%	
			Pyridine	Ethanol
0.1	N	84.1	98.1	47.7
	H	87.0	95.6	83.5
2	N	89.1	93.7	68.4
	H	89.7	95.6	86.8
5	N	87.9	91.9	69.3
	H	86.4	97.0	91.0
8	N	87.9	95.9	74.5
	H	88.5	95.0	88.1

* N:nitrogen, H:hydrogen

Table 2. Reaction conditions,product yield and solvent extraction yield.

Reaction temperature °C	Species of gas	Product yield%	Solvent extraction yield%		
			Pyridine	Ethanol	Benzene
300	N	87.4	98.1	47.7	35.7
	H	89.7	95.6	86.8	18.4
350	N	89.2	97.5	51.1	42.9
	H	91.0	98.6	72.2	38.4
400	N	93.0	98.4	72.9	74.7
	H	–	–	85.5	85.0
430	H	–	–	–	70.8

* N:nitrogen 0.1MPa, H:hydrogen 2MPa(initial pressure)

FIG I. PRESSURE DEPENDENCY OF SOLVENT EXTRACTION YIELD

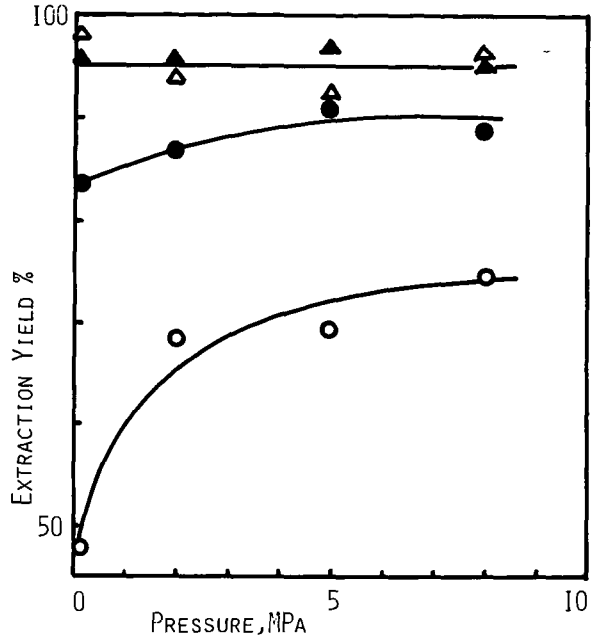

FIG 2. TEMPERATURE DEPENDENCY OF SOLVENT EXTRACTION YIELD

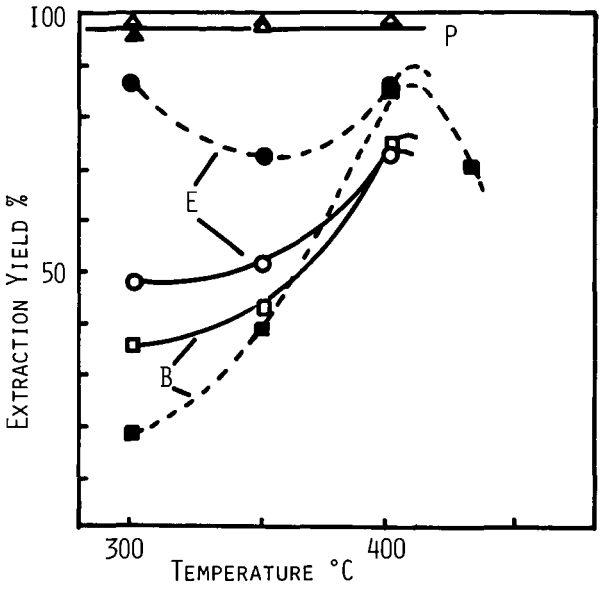

△ □ ○ N_2, 0.1MPA

▲ ■ ● H_2, 2MPA

P:PYRIDINE
B:BENZENE
E:ETHANOL

Characterization of Organic Functional Groups in Model Systems for Coaly Matter Employing ^{19}F NMR

H. C. Dorn, P. S. Sleevi, K. Koller and T. Glass

Dept. of Chemistry, Virginia Polytechnic Institute and State University
Blacksburg, Virginia 24061

INTRODUCTION

The characterization of complex organic mixtures has been explored using ^{19}F NMR to introduce a fluorine "tag" into molecules containing hetero atom functional groups. The ^{19}F NMR approach was suggested because it is nearly as sensitive as ^{1}H NMR and has a much wider range of chemical shifts (~375 ppm vs. ~15 ppm for ^{1}H). This range indicates that fluorine chemical shifts are more sensitive to subtle changes in molecular structure when compared to ^{1}H. An added advantage of ^{19}F NMR is that most analytical samples of interest (e.g., coal products) contain no fluorine alleviating the inherent background problem when compared with ^{1}H and ^{13}C NMR techniques.

The use of ^{19}F nmr to characterize organic functional groups was first suggested by Manatt (1), who used trifluoroacetic anhydride as the reagent for the introduction of a "fluorine tag" into the molecules of interest. Manatt examined various trifluoroacetic acid esters formed from various alcohols which have characteristic ^{19}F nmr chemical shifts dependent upon whether the substrate was a primary, secondary or tertiary alcohol. The general reaction for this reagent is indicated below.

$$(CF_3-\overset{O}{\overset{\|}{C}})_2O + RXH \rightarrow R\text{-}X\text{-}\overset{O}{\overset{\|}{C}}\text{-}CF_3 + CF_3\text{-}\overset{O}{\overset{\|}{C}}\text{-}O\text{-}H \quad \text{where X = O, S or N} \qquad 1)$$

Later, other studies extended the trifluoroacetic anhydride approach to other organic functional groups including phenols (2), steroids (3), and hydroxy groups in poly(propylene oxides) (4).

Another ^{19}F reagent, hexafluoroacetone, was suggested by Leader (5) for the characterization of various functional groups. The adduct (formation of hexafluoroacetone with active hydrogen compounds) is indicated below.

$$CF_3\text{-}\overset{O}{\overset{\|}{C}}\text{-}CF_3 + RXH_n \rightleftarrows CF_3\text{-}\underset{OH}{\overset{RXH_{n-1}}{C}}\text{-}CF_3 \quad \text{where X = O, S or N} \qquad 2)$$

This reagent has been utilized for characterization of alcohols, amines, mercaptans and other active hydrogen containing compounds (5-9). Preparation of the adducts is easily accomplished *in situ* by bubbling the reagent gas (hexafluoroacetone) into a solution of the sample and solvent. Although the equilibrium indicated in equation 2 strongly favors the adduct product on the right for most primary alcohols and many other simple systems, the equilibrium tends to shift to the left for more complex and/or sterically hindered active hydrogen containing functional groups (10). Obviously, this feature limits the scope of this reagent if quantitative data is desired.

By comparison, it should be mentioned that ^{1}H nmr reagents (i.e. hexamethyldisilazane (11), acetic anhydride (12), dichloroacetic anhydride (13), etc.) have also been developed for characterizing functional groups. Unfortunately, most of

these reagents typically yield ^{1}H nmr spectra with relatively small chemical shift ranges (0.1 - 0.4 ppm). That is, for even partial characterization of the various possible functional groups encountered in coal product samples (e.g., phenols, carboxylic acids, alcohols, etc.), the highest available nmr field strengths (super-conducting magnets) are normally employed (14) with the ^{1}H nmr reagents presently available. In contrast, the range of ^{19}F chemical shifts for numerous model systems observed for the hexafluoroacetone adducts and trifluoroacetyl derivatives are ~10 ppm and ~1-2 ppm, respectively. These results reinforce the basic premise that ^{19}F nmr chemical shifts are usually more sensitive than ^{1}H shifts to subtle changes in molecular structure.

RESULTS AND DISCUSSION

In the present study, preliminary nmr examination of the reaction products of the trifluoroacetic anhydride (^{19}F nmr), hexafluoroacetone (^{19}F nmr), and hexamethyldisilazane (^{1}H and ^{13}C nmr) reagents discussed in the Introduction with typical model compounds and actual solvent refined coal fractions indicate a number of limitations with these reagents. This point is particularly true in utilizing these reagents for relatively complex coal product samples. Based on these initial findings, it was deemed appropriate to establish certain criteria necessary for an "ideal" nmr reagent for general characterization of a wide range of different functional groups. These criteria are listed below.

1) The ideal nmr reagent should not require harsh preparation conditions and only very limited manipulations should be involved in the preparation procedure.
2) The nmr reagent should react quantitatively and side reactions should be kept to a minimum.
3) The scope of the nmr reagent would be enhanced if derivative preparation could be accomplished in various solvents.
4) The nmr "probe nuclei" for the reagent should be very sensitive to subtle changes in molecular structure.
5) Ideally, a complimentary feature of item 4 would be the availability of selective nmr reagents. That is, reagents which would only detect the presence of certain specific functional groups.

With these criteria in mind, new ^{19}F nmr reagents have been examined. The first of these is trifluoroacetyl chloride which yields the same derivatives as the trifluoroacetic anhydride reagent (1-4) (Equation 3).

$$CF_3\text{-}\overset{O}{\overset{\|}{C}}\text{-Cl} + \text{R-X-H} \rightarrow CF_3\text{-}\overset{O}{\overset{\|}{C}}\text{-X-R} + \text{HCl} \quad \text{where X = O, S or N} \qquad 3)$$

This reagent is a gas (b.p. -18°C) and derivatives are easily prepared *in situ* by bubbling the reagent into a solution consisting of the sample and solvent at temperatures from ~-50°C to ~-10°C. Various solvents have been utilized including chloroform or chloroform-d, tetrahydrofuran, and methylene chloride. The entire preparation procedure can be carried out in the sample nmr tube. This represents a distinct advantage in the derivative preparation when compared with the trifluoroacetic anhydride reagent. In addition, the by-product of this reaction is HCl compared with CF_3CO_2H, the by-product formed with the trifluoroacetic anhydride reagent, which in many cases causes a large interferring peak in the ^{19}F spectra of these derivatives. It should be noted, however, that if water is present in the sample, the trifluoroacetic acid peak also appears in the ^{19}F nmr spectrum when trifluoroacetyl chloride is the reagent.

The initial phase of the trifluoroacetyl chloride study was an examination of suitable trifluoroacetyl derivative preparation procedures, the range of ^{19}F chemical shifts for model systems, and typical yield data for this reagent. A typical ^{19}F spectrum for the trifluoroacetyl derivative obtained from benzyl alcohol is indicated in Figure 1. The reference at 0.0 ppm in these spectra is 1,2-difluorotetrachloroethane ($CFCl_2CFCl_2$) and was the ^{19}F reference employed in most of this work. The trifluoroacetyl chloride reagent reacts with primary, secondary, tertiary alcohols, benzyl alcohols, amines, phenols and thiols. The by-product of the reaction, HCl, does not interfere in the ^{19}F NMR spectrum.

Certain reactions, particularly those of phenols and amines were quite slow. A study was conducted to see if using a nucleophilic base would improve the reactions. Those bases which were tried were pyridine, triethyl amine, 2,6-lutidine, and 4-dimethylaminopyridine (DMAP). Based on reaction yields, 2,6-lutidine and DMAP appear to be the best catalysts. It has been shown previously that DMAP is an excellent acylation catalyst (17).

A side reaction which can occur using this reagent is the formation of trifluoroacetic acid. This interference, however, can easily be removed by allowing the reaction mixture to stand over a small amount of K_2CO_3. The acid peak is entirely removed from the spectrum. The peak which occurs from excess trifluoroacetyl chloride is also readily removed by degassing the sample with N_2.

It appears that the derivatives formed using trifluoroacetyl chloride are well-resolved in the ^{19}F NMR spectra as indicated by figure 2 with only a couple of regions of overlap. The overall chemical shift range is about 2 ppm. It appears that this reagent will be useful as an analytical tool for characterization of functional groups. All interferences in the spectrum can be removed and the reactions occur in high yield with the proper choice of catalyst.

A second and entirely new class of ^{19}F nmr reagents under examination is fluorinated diazoalkanes. Diazomethane with and without a Lewis acid catalyst has been extensively used in organic chemistry for preparation of methyl ester and methyl ether derivatives (15). An obvious extension of this approach would be the use of a fluorine containing diazo reagent.

The first fluorinated diazoalkane examined in this study was trifluorodiazoethane (16). We have found that this reagent reacts smoothly with alcohols, phenols and carboxylic acids at room temperature to -10°C in the presence of a catalyst (typically HBF_4) to yield fluorinated ethers and esters according to equations 4 and 5.

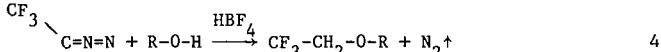

$$CF_3(H)C{=}N{=}N + R\text{-}O\text{-}H \xrightarrow{HBF_4} CF_3\text{-}CH_2\text{-}O\text{-}R + N_2\uparrow \qquad 4)$$

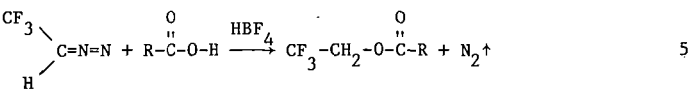

$$CF_3(H)C{=}N{=}N + R\text{-}C(=O)\text{-}O\text{-}H \xrightarrow{HBF_4} CF_3\text{-}CH_2\text{-}O\text{-}C(=O)\text{-}R + N_2\uparrow \qquad 5)$$

One of the disadvantages of this reagent using our present reaction conditions is the water present in the added catalyst (50% water solution of HBF_4). The trifluorodiazoethane reacts with the water to yield 1,1,1-trifluoroethanol and bis (1,1,1-trifluoroethyl)ether.

The ^{19}F spectra for these derivatives appear as triplets (^{19}F-^{1}H coupling to methylene protons). However, singlet spectra can be obtained by ^{1}H decoupling.

Figures 2 and 3 indicate the range of ^{19}F chemical shifts observed for a number of model compounds using the trifluoroacetyl chloride and trifluorodiazoethane reagent, respectively. In general, the yields are somewhat higher for the trifluorodiazoethane reagent. The chemical shift range, however, appears to be slightly larger for the trifluoroacetyl derivatives. Nevertheless, both of these reagents have potential advantages over other reagents previously employed.

Figure 4 is the first spectrum obtained from the acid fraction of an Amax solvent refined coal (SRC) sample using the trifluoroacetyl chloride reagent. The large peak at ~8.5 ppm is trifluoroacetic acid. The peak centered at ~7.6 ppm with fine structure is undoubtedly due to phenols and perhaps benzyl alcohols. The peaks between 7.7 ppm and 8.4 ppm indicate limited presence of aliphatic alcohols. The broad peak centered at ~7.4 ppm has not been assigned at the present time. Although these are only the first results obtained from the ^{19}F nmr reagents, the number of resolved lines in several SRC fractions indicate that the ^{19}F nmr approach is indeed a promising technique. Results applying the ^{19}F nmr approach to additional coal products will be discussed in this presentation.

REFERENCES

1. Manatt, S.L., J. Amer. Chem. Soc., 88, 1323 (1966).

2. Konishi, K., Y. Mori and N. Taniguchi, Analyst, 94, 1002 (1969).

3a. Jung, G., W. Voleter, E. Brietmaier and E. Bayer, Anal. Chem. Acta, 52, 382, (1970);
b. Voelter, W., W. Brietmaier, G. Jung and E. Bayer, Org. Mag. Res., 2, 251, (1970).

4. Manatt, S.L., D.D. Lawson, J.D. Ingham, J.D. Rapp and J.D. Hardy, Anal. Chem., 38, 1036 (1966).

5. Leader, G.R., Anal. Chem., 42, 16 (1970).

6. Leader, G.R., Anal. Chem., 45, 1700 (1973).

7. Ho, F.F.-L, Anal. Chem., 45, 603 (1973).

8. Ho, F.F.-L, Anal. Chem., 46, 496 (1974).

9. Ho, F.F.-L and R.R. Kohler, Anal. Chem., 46, 1302 (1974).

10. Leader, G.R., Appl. Spect. Reviews, 11, 287 (1976).

11. Friedman, S., M.L. Kaufman, W.A. Steiner and I. Wender, Fuel, 40, 33 (1961).

12. Mathias, I.A., Anal. Chem. Acta, 31, 598 (1964).

13. Vickers, G.D., Anal. Chem., 40, 610 (1968).

14. Schweighardt, F.K., H.L. Retcofsky, S. Friedman and M. Hough, Anal. Chem., 50, 368 (1978).

15. M.C. Casserio, J.D. Roberts, M. Neeman, and J.S. Johnson, J. Amer. Chem. Soc., 80, 2584 (1958); M. Neeman, M.C. Casserio, J.D. Roberts, and W.S. Johnson, Tetrahedran, 6, 36 (1959).

16. Preparation of trifluorodiazoethane was by a procedure described by, R. Fields and R.N. Hazeldine, J. Chem. Soc., 1881 (1964).

17. G. Hofle, W. Steglich, H. Vorbrüggen, Angew. Chem. Int. Ed. (Eng.), 17, 569 (1978).

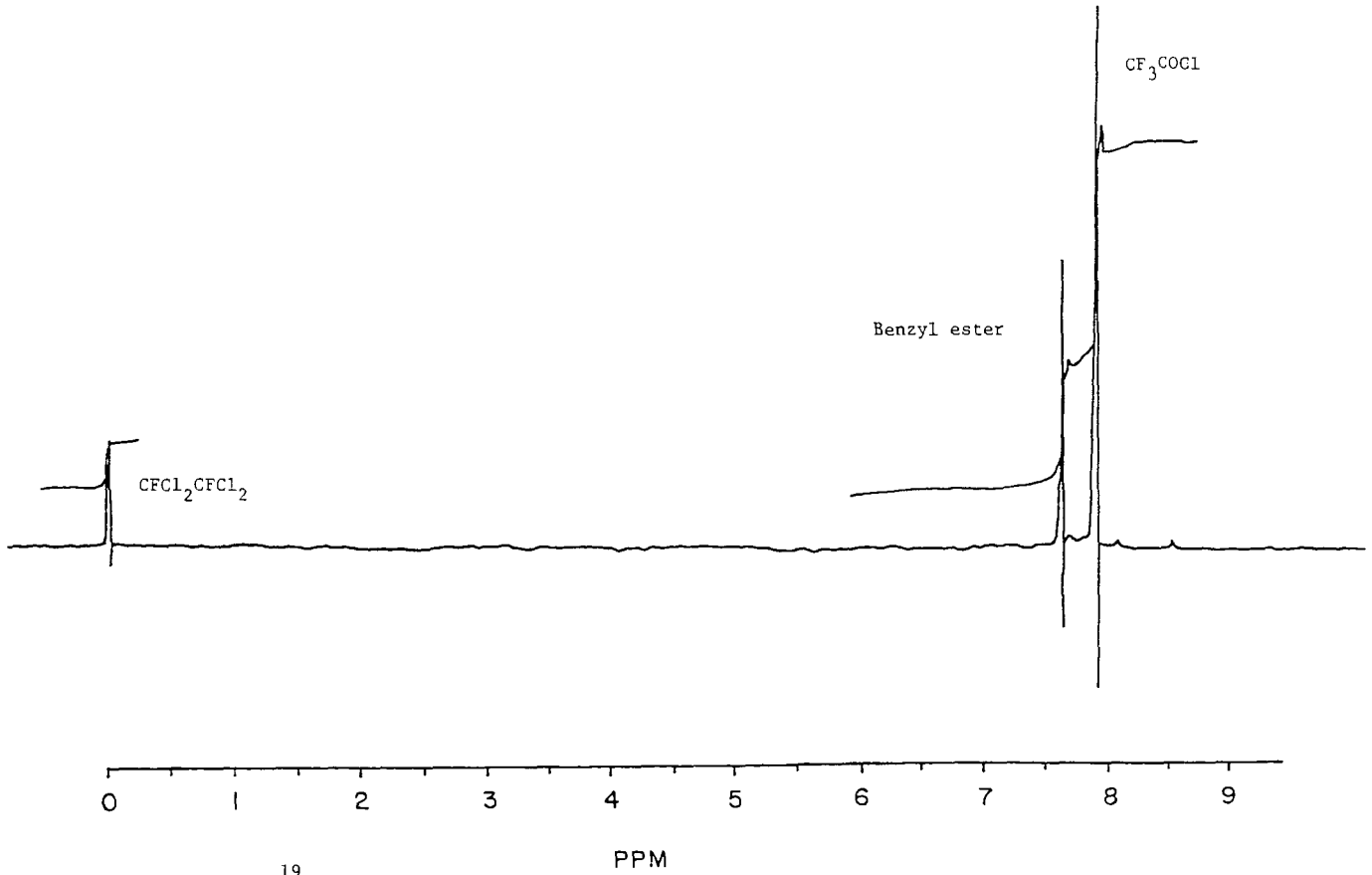

Fig. 1. ^{19}F nmr spectrum of solution prepared by reacting benzyl alcohol with trifluoroacetyl chloride, solvent is chloroform-d with 1,2-difluorotetrachloroethane used as the reference.

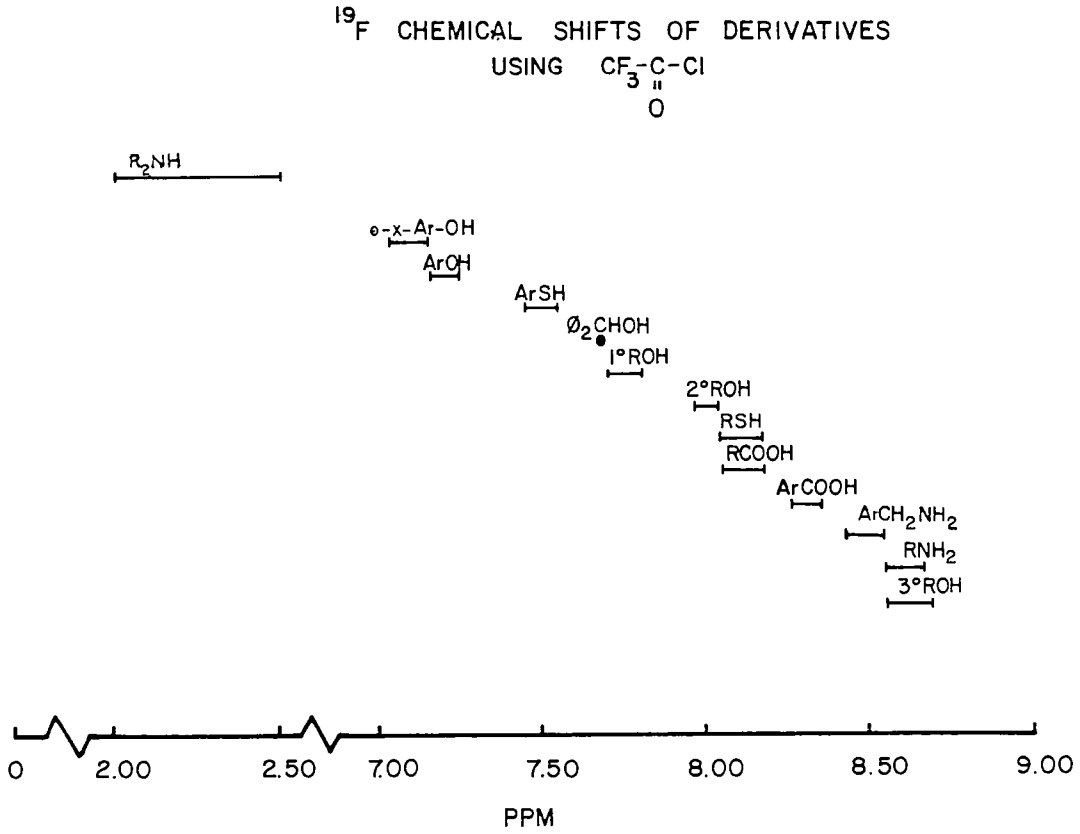

Fig. 2. Range of ^{19}F nmr chemical shifts observed for trifluoroacetyl derivatives of model compounds with 1,2-difluorotetraethane used as the reference.

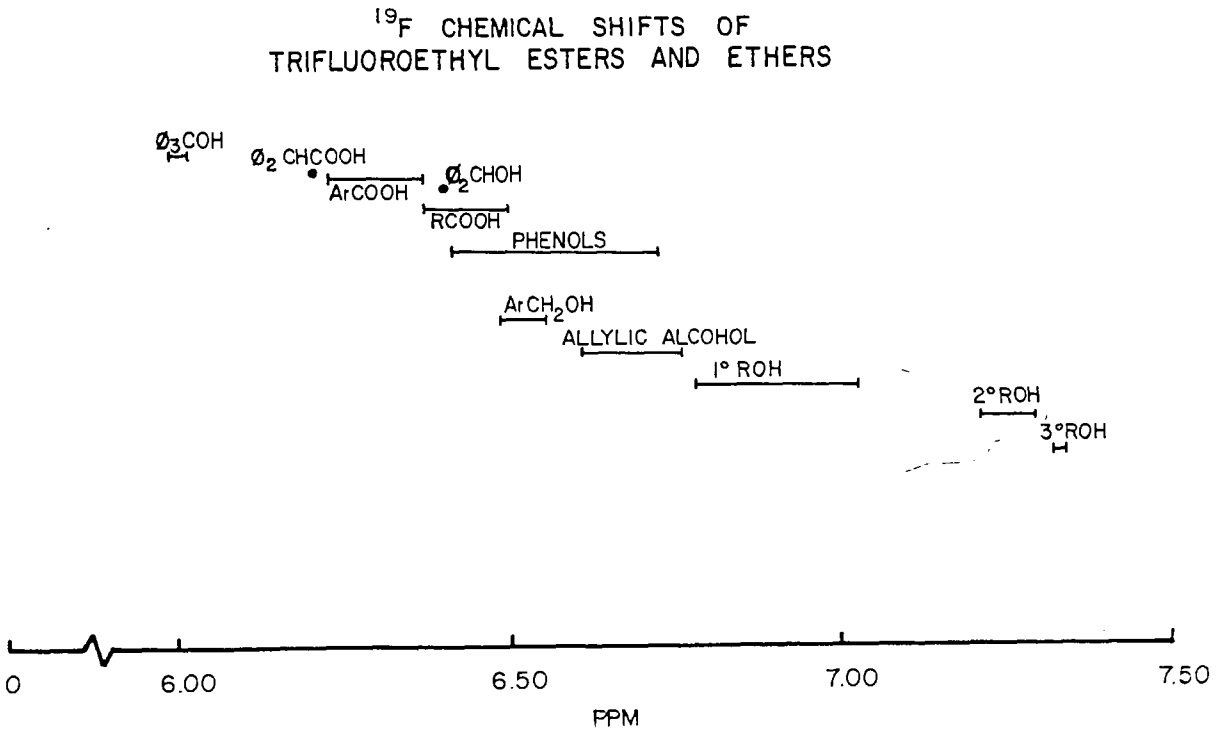

Fig. 3. Range of ^{19}F nmr chemical shifts observed for trifluorodiazoethane derivatives of model compounds with 1,2-difluoroethane used as the reference.

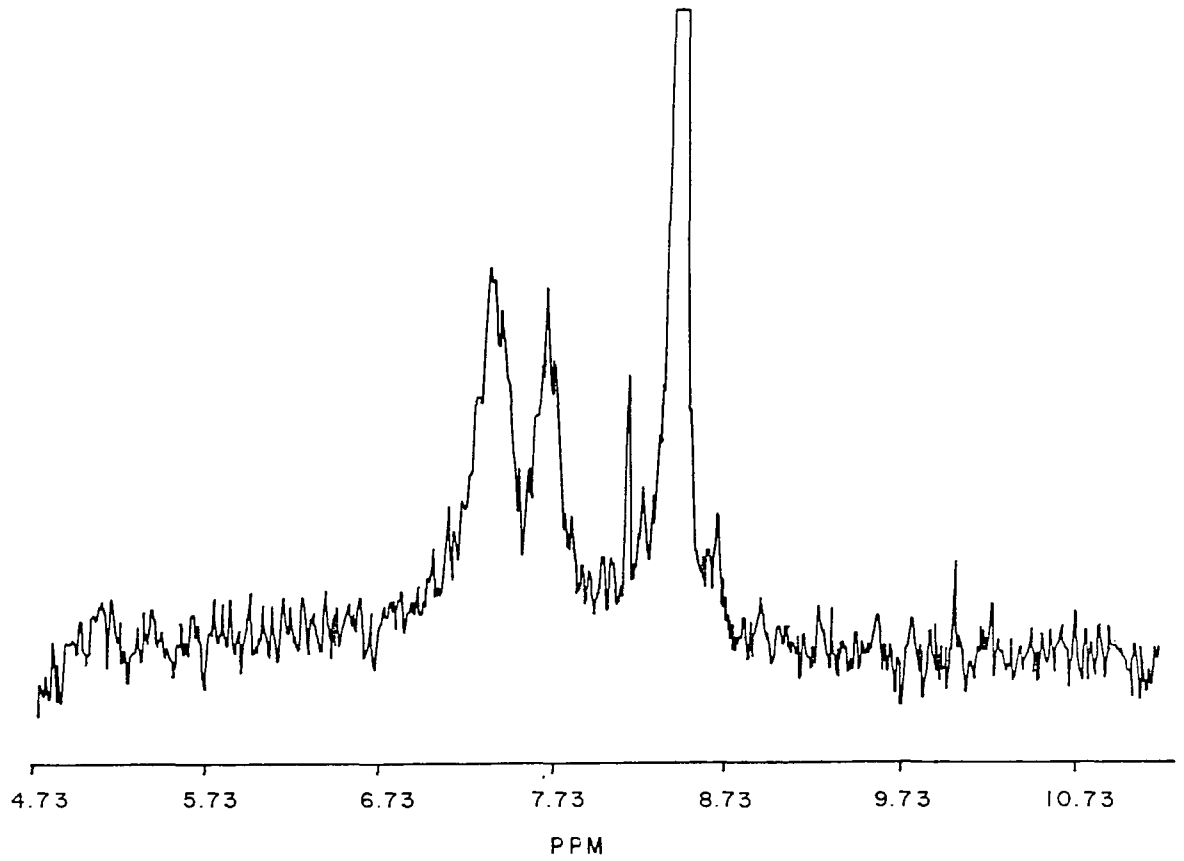

Fig. 4. ^{19}F FT nmr spectrum of reaction mixture of trifluoroacetyl chloride and Amax SRC acids fraction, solvent is chloroform-d with 1,2-difluoroethane used as the reference.

The Use of Acetylation to Quantitate Acid Groups in Coal Derived Liquids

R. J. Baltisberger, K. M. Patel,
V. I. Stenberg, and N. F. Woolsey

Department of Chemistry
University of North Dakota
Grand Forks, North Dakota 58202

The determination of types of nitrogen and oxygen species in coal derived products is an important problem to be solved in liquefaction research. Methods are needed which can rapidly isolate or characterize the nitrogen and oxygen heteromolecules in complex mixtures. Two major types of problems need to be solved. First, the types of functional groups can be identified by specific chemical reactions, but such reactions must be quantitative to be of use. Secondly, a large portion of coal derived products formed in the early stages of a liquefaction process are preasphaltenes, which limit any subsequent chromatographic procedures used to isolate compound types or molecular fractions. In this paper we shall describe the use of acetylation as a means of measuring quantitatively the fraction of acidic protons in coal derived products.

The similarity of the fractions of acidic protons measured by acetylation techniques with those of acid-base titration data suggest that no alcoholic groups are present in the SRL and SRC samples selected for this study. In addition, the acetylation process greatly increased the dissolubility of the coal derived substances in benzene and chloroform. Such dissolubility would give the opportunity for studies not accessible in pyridine. For example, the use of NMR shift reagents in chloroform could be employed in structural analysis.

Experimental

Materials

Three solvent refined lignite (M11-A, M34-A and M39-A) and two solvent refined coal (AMAX and Tacoma) samples were obtained and ground to about 40 mesh for this study (1). Elemental analysis of the samples was performed by Spang Micro-Analytical Laboratory.

NMR Spectra

Proton NMR spectra were obtained using a Varian EM-390 spectrometer. Samples were dissolved in pyridine-d_5 containing a calibrated amount of s-trioxane as standard. Correction for pyridine was based on a standard versus residual pyridine integration. Generally, seven integrations were run and averaged. Carbon 13 PFT-NMR were measured in a JOEL JNM-FX60 spectrometer. Chloroform-d_1 was used as the solvent with TMS as an internal standard.

Non Aqueous Titration

Non-aqueous potentiometric titration of the acidic groups was carried out in pyridine using 0.05 M of tetra-n-butylammonium hydroxide in benzene as the titrant (2). The emf was measured by a Beckman Zeromatic -pH meter with a glass electrode and a simple side arm column reference electrode connected by a salt bridge of KCl-dry methanol through a medium porosity filter to the titration solution (3).

Acetylation

Samples of SRL or SRC (1.0 g) were acetylated by refluxing for 24 h with 15 ml acetic anhydride-pyridine mixture (1:3) under an inert atmosphere of argon. Subsequently, the reaction mixture was concentrated by rotovap to about 5 ml. The mixture was added to 250 ml water and the precipitated derivative filtered. The residue on the filter was washed with water until the effluent was free of acid. The acetylated sample was freeze dried with benzene to remove the last portion of residual pyridine. Finally, the sample was vacuum dried at 80° in an abderhalden apparatus.

Acidic Proton Analyses

The acetylated samples were analyzed for acidic proton content by saponification-titration, and by NMR measurement. The saponification of a dried acetylated sample was carried out with 1.5 g potassium hydroxide in 100 ml water-pyridine (3:1) by refluxing for 20 h. The mixture was then acidified (pH 3.0) with concentrated sulfuric acid. The liberated acetic acid was collected by distillation and titrated with standard sodium hydroxide.

Proton NMR measurements of the sample in pyridine-d_5 before and after acetylation were used to measure the fraction of acid groups in the sample. Prior to acetylation the acidic proton signals are located under the aromatic region. After acetylation the methyl group of the acetyl group signals are in the aliphatic region. The percentage H as acidic hydrogens can be calculated

from (equation 1),

$$\%\,H \text{ as acidic } H = \frac{R_2 - R_1}{2R_1 + 1} \times 10^2 \qquad (1)$$

where R_1 is the fraction of the aromatic protons (area) in the acetylated SRC and SRL samples and R_2 is the fraction of aromatic protons (area) in the non-acetylated samples.

Measurement of the percentages of acidic protons by C^{13} NMR was calculated from the relative area of the carbonyl carbon (169 ppm) to the total carbon atoms and from the carbon-hydrogen elemental analysis (equation 2).

$$\%\,H \text{ as acidic } H = \frac{(C{=}O \text{ Area}) \times (\text{Wt } \%\ C) \times 10^2}{[\text{Total Carbon Area} - 2\ (C{=}O \text{ Area})] \times 12 \times (\text{Wt } \%\ H).} \qquad (2)$$

Results and Discussion

Dissolubility

Table I shows the chemical analysis of the SRL and SRC samples studied in this work. The increased dissolubility of the coal derived products in several solvents due to acetylation is shown in Table 2. The dissolubility in this work was not run in the necessary manner to define the percentage of pre-asphaltenes, asphaltenes and oils in the samples, but rather to demonstrate the increased dissolubility obtained through the acetylation reactions. The dissolubility was measured by mixing 1 gm of sample in 10 ml of solvent for 20 h at room temperature. The mixture was filtered through Whatman number one filter paper. The resulting filtrate and residue was dried and weighed. The total recovery varied from 97 to 99%. One immediate benefit of this increased dissolubility is that C^{13} NMR techniques could be used to measure the percentage of acetyl groups using chloroform-d_1 as the solvent. The remarkable increase in dissolubility after derivatization of the acidic groups can be attributed to the breaking of intermolecular hydrogen bonding (4,5). Gould, et.al. have recently reported the silylation of coal liquefaction bottoms which resulted in a four to seven fold decrease in viscosity and 0 to 26% increase in extrability in heptane (6).

Acid Content

Nonaqueous titration for acidity gave a range of 1.34 to 2.22 meq/gm for the corresponding to 2.5 to 4.0% protons as acidic protons. The pure com-

pounds, carbazole and phenol, can be titrated with a precision of ±3%. The actual SRL and SRC samples give a wider range of uncertainty as shown in Table 3. This is due to the presence of a wide range of weak acids which give a poor titration break.

The acetyl group content of a derivatized sample was measured by different methods. The saponification-titration procedure gave the same meq/gm as the nonaqueous titration results. The results were converted to % H as acidic H in Table 3 for comparison. The number of acetyl groups determined by proton NMR (equation 1) agreed with both types of titration data. Acetylation of model compounds (phenol, carbazole, and several hindered phenols) gave complete acetylation of the acidic groups as determined by NMR measurement of the products. The agreement between the three types of data would be consistent with the following. 1) No acylation of the aromatic carbon of the aromatic rings in coal was apparent. The acylation of an aromatic carbon seems remote under the reaction conditions, but in any case the agreement between the saponification-titration and proton NMR data eliminates that possibility. 2) The presence of alcoholic hydrogens in the samples can be ruled out because of the agreement between the acetylation and nonaqueous titration data. If alcohol acetylation had occurred a similar quantity of phenolic groups would have to remain unreacted for comparable results. That this would occur to the same extent to agree with the nonaqueous titration seems extremely remote. To check this point we are planning to measure total replaceable hydrogen content by LAH reduction in pyridine. 3) The location of the acidic protons lies under the aromatic portion of NMR spectra when the samples are dissolved in pyridine. In our study of several model compounds, the chemical shifts of OH (phenols) and NH (carbazole) hydrogens in pyridine-d_5 are generally downfield (between 9.5 to 6.3 ppm, aromatic region) depending upon the concentration (7).

Carbon-13 NMR integration data were generally lower than the other two types of acetyl analyses as shown in Table 3. The precision also is poorer as noted in Table 3. The reason for this is due to the small percentage of C=O groups relative to the total number of carbons and the inability to properly phase the baseline in the C=O region of the NMR experiment.

Acknowledgement

We acknowledge the support of the Department of Energy in this work.

References

1. Samples were obtained as follows:
   M11-A prepared by the University of North Dakota Chemical Engineering Department under Project Lignite, from North Dakota Lignite. Conditions: 2500 psi of 1:1 CO; H_2 at 479°C (max); M34-A, 2500 psi of 1:1 CO; H_2 at 426°C (max); M39-A, 2500 psi of hydrogen at 426°C (max).
   Tacoma prepared by Pittsburg and Midway Coal Co. at their Fort Lewis PDU from a blend of Kentucky No. 9 and No. 14 bituminous coals from the Colonial Mine. Conditions: 1500 psi of H_2 (85% min) at 450°C (max) using recycle solvent.
   Amax Catalytic Inc., Wilsonville, Alabama from Amax subbituminous coal from Bel Ayr Mine, Wyoming. Conditions: 2500 psi H_2 and recycle gases at 460°C (max) using recycle solvent heavy in phenols and 1, 2 and 3 ring aromatics.
2. Woolsey, N. F., Baltisberger, R. J., Klabunde, K., Stenberg, V., and Kaba, R., Am. Chem. Soc., Fuel Div. Preprints, 21 (7), 33 (1976).
3. Adams, R. N., in "Electrochemistry of Solid Electrodes", Marcel Dekkar, New York, p 288 (1969).
4. Sternberg, H. W., Raymond, R. and Schweighardt, F. K., Science, 188, 49 (1975).
5. Schweighardt, F. K., Friedel, R. A. and Retcofsky, H. L., Applied Spectroscopy, 30, 291 (1976).
6. Gould, K. A., Gorbaty, M. L., and Miller, S. D., Fuel, 57, 510 (1978).
7. See for the chemical shifts of phenols in DMSO, Chapman, O. L, and King, R. W., J. Am. Chem. Soc., 86, 1256 (1964).

Table 1

Comparison of Coal and Lignite Derived Samples

	M11-A	M34-A	M39-A	Tacoma	Amax
C%	89.31	86.74	87.47	87.31	88.29
H%	5.80	6.73	6.09	5.59	5.65
N%	1.11	1.63	1.11	2.36	1.65
S%	0.86	1.15	0.74	0.30	< 0.1
O%	2.35[a]	2.10[b]	3.57[b]	3.22[a]	3.37[a]
H% (Acid)	2.6	2.70	3.3	3.7	4.0
Ash %	< 0.1	1.7	1.0	< 0.1	< 0.1

[a] measured by neutron activation analysis [b] measured by difference

Table 2

Dissolubility in Various Solvents

	Pyridine	Benzene	Chloroform
M11-A	96.8	50 (90)[a]	60 (100)[a]
Tacoma	95.4	25 (80)	40 (100)
M39-A	96.5	48 (85)	62 (99)

[a] The number in parenthesis indicates the dissolubility after acetylation.

Table 3

Acid Proton Contents of Various Samples

Samples	Acetylated Samples and ^{1}H - nmr	^{13}C nmr	Saponification/ Titration	Direct Nonaqueous Titration
M11-A	2.65 ± 0.06% [a]	2.0, 2.3 %	2.57 ± 0.05% [a]	2.6 ± 0.3% [a]
M34-A	2.7 ± 0.2	2.8	2.7 ± 0.2	2.5 ± 0.2
M39-A	3.1 ± 0.2	3.1, 3.3	3.3 ± 0.1	3.3 ± 0.1
Tacoma II	3.9 ± 0.2	3.1, 3.4, 3.5, 3.7	3.7 ± 0.2	3.7 ± 0.1
AMAX	4.1 ± 0.2	3.6, 3.9	4.0 ± 0.2	4.0 ± 0.2

[a] The uncertainty reported is the standard derivation (1σ) for four to five determinations.

DETERMINATION OF PROTONATED AND QUATERNARY CARBONS IN H-COAL LIQUIDS FROM QUATERNARY CARBON SUPPRESSED AND NONSUPPRESSED CMR SPECTRA

Joseph T. Joseph and John L. Wong*

Department of Chemistry, University of Louisville
Louisville, Kentucky 40208

INTRODUCTION

The potentially rapid and accurate measurement of the carbon distribution by structural types in a coal liquid is an attractive application of ^{13}C FT-NMR spectroscopy. Extensive CMR work has been carried out in many laboratories[1] on coal-derived liquids. As part of a continuing program to study the physicochemical properties of the H-Coal liquids to provide analytical support for the commercial development of the H-Coal process[2], we have made further application of quantitative FT-CMR technique to determine the distribution of several types of aliphatic and aromatic carbons in three H-Coal liquids. In order to confirm the interpretation of the highly complex spectra based on chemical shifts, use has been made of the difference in CMR absorptivity of protonated and quaternary carbons as a means to distinguish between them. We have demonstrated the reliability of this difference by comparing the quantitative CMR spectrum of a simulated coal liquid containing 30 peaks (15 each in the aliphatic and aromatic region) with the spectrum of the same mixture obtained with a Fourier transform parameter set wherein the quaternary carbons are suppressed. This difference CMR technique has been applied to three H-Coal liquids: atmospheric still overhead (ASO), atmospheric still bottom (ASB), and vacuum still overhead (VSO). There is no discernible amount of aliphatic quaternary carbon found in these liquids. In the aromatic region, the ring carbons are divided into six subgroups by ring substitutions. The three liquids are thus compared by structural classification and quantitation of their CMR spectra.

EXPERIMENTAL

The liquefied coal samples under investigation were received from the Institute for Mining and Minerals Research, University of Kentucky. The liquefaction was performed by the H-Coal process involving a catalyst in the "syncrude" mode with reactor temperature at 454°C, exit reactor partial pressure of hydrogen at 2245 psig. The samples were designated atmospheric still overhead (ASO), atmospheric still bottom (ASB), and vacuum still overhead (VSO). The nominal boiling ranges of these samples are ASO C_4 - 200°C, ASB 200-350°C, VSO 350-520°C[2]. Chemicals were purchased from Aldrich Chemical Co.

A Bruker WH-90DS nuclear magnetic resonance spectrometer with a 10 mm probe and a Nicolet BNC 1180 computer (16 K memory) was used in the Fourier transform mode to obtain the ^{13}C spectra at 22.63 MHz. The FIDs were accumulated on 8K memory, using an acquisition time of 0.819s. A 5000 Hz spectral width with 200 microseconds dwell time was used in all spectra. The quantitative spectra were obtained at 30° pulse width with 5s delay between the end of data acquisition and the beginning of the next pulse for $\sim$10,000 pulses. During the delay, the proton spin decoupler was gated off, but a 5.0 watt decoupling power was applied while scanning. The relaxation agent $Cr(acac)_3$ was used at 20 mg/g of sample. For the quaternary carbon-suppressed spectra, the following FT parameters were adopted: 90° pulse width, no pulse delay, broad band proton decoupling at 5.0 watt for $\sim$10,000 scans, and no paramagnetic relaxation agent added.

The H-Coal samples were prepared by adding 1.0 g of of the respective coal liquid to 1 ml of $CDCl_3$ containing 1% of tetramethylsilane. The solvent $CDCl_3$ also served the purpose of internal deuterium lock. For the simulated coal liquid, the following mixture was made up: t-butylbenzene (69.0 mg, 0.515 mmol), decalin (77.2 mg, 0.559 mmol), tetralin (77.5 mg, 0.587 mmol), 2-phenylpentane (76.4 mg, 0.516

mmol), and 2,3-dimethylnaphthalene (75.9 mg, 0.487 mmol), and $CDCl_3$ was added to make a 2 ml solution. When the spectra were calibrated for integration, a weighed amount of dioxane in a sealed capillary tube was placed along the axis of the 10 mm nmr tube with the aid of a vortex-type plug.

RESULTS AND DISCUSSION

The quaternary carbons which are devoid of protons in their immediate vicinity, hence lacking the $^{13}C - {}^{1}H$ dipole-dipole relaxation mechanism, are expected to have long spin-lattice relaxation recovery times (T_1). This makes the signal intensity very dependent on the pulse repetition rate. The presence of nuclear Overhauser enhancement (NOE) for the protonated carbons further accentuates the difference in absorptivity between these two types of carbons. Thus, in a normal broad band proton decoupled CMR spectrum, the quaternary carbons show much reduced signal intensities relative to others. We have quantitated the differences in absorptivity for carbons with various levels of proton attachment (1°, 2°, 3°, and 4°) using a simulated coal liquid (Cf. Experimental). This mixture is comprised of 25 aliphatic carbons (primary 7, secondary 14, tertiary 3, and quaternary 1) and 28 aromatic carbons (protonated 20 and quaternary 8) as shown below. The aromatic and aliphatic

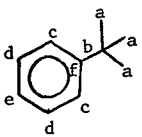

I

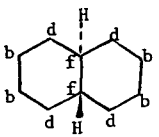

trans

II

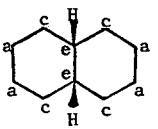

cis

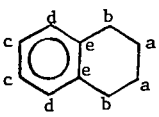

III

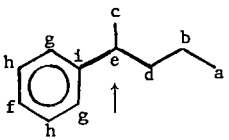

IV

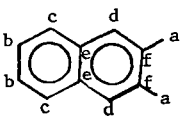

V

regions of this spectrum are shown in Figures 1A and 2A respectively. This set of FT parameters tend to equalize all signal intensities per carbon unit irrespective of their molecular environment. Thus, the one aliphatic and eight aromatic quaternary carbons were separately integrated to yield absolute value within 5% deviation from the theoretical. On the other hand, when the spectrum was taken in the absence of $Cr(acac)_3$ using broad band decoupling at 90° pulse width and no delay, vast variations of the signal intensities including suppression of the quaternary carbons were registered. The respective aromatic and aliphatic regions shown in Figures 1B and 2B reveal the differences from those in Figures 1A and 2A. In order to quantitate these changes, the height of each peak in both spectra was normalized to either the tallest peak at δ125.47 (protonated carbons IIIc and Vb) or to an internal standard of dioxane. The normalized peak height of each peak in the quantitative spectrum is expressed as a ratio to that of the same derived from the quaternary carbon suppressed spectrum to show the signal intensity changes in the latter spectrum. These reults are shown in Table I. It can be seen that the two columns of peak height ratios point to the same trend and agree to within 7% of deviation. Thus, the dioxane methylene carbons and the aromatic methine carbons IIIc and Vb exhibit similar relaxation characteristics and are both adequate as integral references. In the

nonquantitative spectrum, the eight quaternary aromatic carbons appearing in 5 peaks average a 5 fold decline. The twenty protonated carbons in ten peaks increase by ∿20% per carbon. The single aliphatic quaternary carbon is suppressed 4.7 fold, while the 14 peaks representing 3 tertiary, 14 secondary, and 7 primary aliphatic carbons average an increase of 0%, 37%, and 43% per carbon respectively. Although these peak enhancements of various protonated carbons are similar, hence not diagnostic of the extent of proton attachment, it is demonstratably clear that the quaternary carbons can be confirmed by this difference CMR method due to their pronounced peak height changes.

Thus, the H-Coal liquids ASO, ASB, and VSO were submitted to close examination by the difference CMR technique. The comparisons for the aromatic and aliphatic regions are shown in Figures 3 and 4 respectively for ASO, Figures 5 and 6 for ASB, and Figures 7 and 8 for VSO. In each figure, spectrum A is the quantitative type and B the quaternary carbon-suppressed type. Those peaks which have disappeared or declined in intensity by at least 3.8 fold for ASO and ASB and at least 2 fold for VSO are assigned to the quaternary aromatic compounds either as bridge carbons in a condensed ring system or carbons to which alkyl or aryl substituents are attached. The remainder of the aromatic resonances therefore belong to the protonated carbons. It is interesting to note that the aliphatic regions for all three liquids show no discernible difference when the two types of spectrum are compared, indicating the absence of quaternary branching in the saturated carbon skeletons.

The chemical shifts of unsubstituted carbons in mono, di, tri, and tetra aromatic ring systems fall in a narrow range of 123 - 130 ppm[3,4]. When the benzene ring bears heteroatom substituent such as OH or OR, the protonated carbons are shifted upfield considerably, e.g. to 113 ppm in m-cresol and to 106 ppm in benzofuran[5]. In the region of 130-133.8 ppm, most of the condensed-ring bridge carbons can be found[3,4]. However, in a highly condensed system such as pyrene, the interior bridge carbons resonate at 125 ppm due to the anisotropic ring current effect[3]. The 133.8 - 137.3 ppm region is appropriate for substituted carbons in tetralin and methylbenzenes[3,5]. Short chains (Et, Pr, iPr, etc.) tend to shift the substituted carbons downfield to 149 ppm[3,5]. Also, an alkyl substituent at C-8 in tetralin and particularly gem-substituted tetralins can bring the bridge carbon C-8a to the 140's[3]. Biphenyls also appear in this region[5]. Beyond 149 ppm, the aromatic carbons carrying a heteroatom group such as OH or OR appear[1c,5]. Such chemical shift analysis in combination with the difference CMR method to determine the quaternary and protonated carbons permit a reasonable interpretation of the aromatic resonances in the H-Coal liquids. In Table II, the distribution of the aromatic carbons in ASO, ASB, and VSO are shown as obtained from the integration of the chemical shift regions indicated. The one quaternary carbon detected in ASO at 127.1, at 124.4 in ASB and at 124.7 in VSO may be attributed to highly condensed interior carbon. The absence of other reduced signals in the 123 - 130 ppm region confirms the assignment of this region to the protonated carbons. The patterns of the distribution of aromatic carbons in the three liquids generally denote the more condensed ring systems with higher branchings in the VSO liquid, whereas ASO and ASB are more similar.

ACKNOWLEDGEMENT

This investigation was supported by Grant S 3688, awarded by the Institute for Mining and Minerals Research, University of Kentucky. The authors also wish to acknowledge the consultation with Professor Stanford L. Smith, Department of Chemistry, University of Kentucky on FT-CMR spectroscopy.

REFERENCES

1. (a) H. L. Retcofsky and R. A. Friedel, Fuel, 55, 363 (1976); (b) H. L. Retcofsky, Appl. Spectroscopy, 31, 116 (1977); (c) R. J. Pugmire, D. M. Grant, K. W. Zilm, L. L. Anderson, A. G. Oblad and R. E. Wood, Fuel, 56, 295 (1977); (d) R. J. Pugmire, K. W. Zilm, D. H. Bodily, D. M. Grant, H. Ito and S. Yokoyama, Am. Chem. Soc. Div. Fuel Chem., Preprints, 23, No. 2, 24 (1978); (e) D. L. Wooten, W. M. Coleman, L. T. Taylor and H. C. Dorn, Fuel, 57, 17 (1978).

2. (a) D. L. Katz, "Evaluation of Coal Conversion Processes to Provide Clean Fuels", EPRI 206-0-0 Final Report, Parts II, III, Feb. 1974; (b) R. I. Kermode, Institute for Mining and Minerals Research Annual Report, Sept. 1973.

3. K. S. Seshadri, R. G. Ruberto, D. M. Jewell and H. P. Malone, Fuel, 57, 17 (1978).

4. H. C. Dorn and D. L. Wooten, Analyt. Chem., 48, 2146 (1976).

5. (a) J. N. Shoolery and W. L. Budde, Analyt. Chem., 48, 1458 (1976); (b) The Sadtler Standard Carbon-13 NMR Spectra, Sadtler Research Laboratories, Philadelphia, PA.

Table I. Ratios of Carbon Peak Heights from Quantitative and Quaternary Carbon Suppressed CMR Spectra of the Simulated Coal Liquid[a]

A. Aromatic Region

Peak No	δ TMS = 0	Assignment[b] Notation	Carbon Type	Peak Height Ratios Internal Reference[c]	Dioxane Reference[d]
1	151.0	If	4^o	6.4	6.1
2	147.9	IVi	4^o	5.7	5.4
3	137.1	IIIe	4^o	4.5	4.2
4	135.4	Vf	4^o	4.2	3.9
5	132.5	Ve	4^o	5.4	5.1
6	129.1	IIId	3^o	1.0	1.0
7	128.3	IVh	3^o	0.8	0.7
8	128.1	Ie	3^o	1.0	1.0
9	127.4	Vd	3^o	0.8	0.7
10	127.0	IVg	3^o	0.9	0.8
11	126.9	Vc	3^o	0.8	0.8
12	125.8	IVf	3^o	0.9	0.9
13	125.5	IIIc,Vb	3^o,3^o	1.0	0.9
14	125.3	Id	3^o	1.0	1.0
15	125.0	Ic	3^o	0.8	0.8

B. Aliphatic Region

16	43.5	IIf	3^o	1.2	1.1
17	40.8	IVe	3^o	0.8	0.7
18	39.7	IVd	2^o	0.9	0.6
19	35.4	IIe	3^o	1.3	1.2
20	34.6	Ib	4^o	5.0	4.7
21	34.3	IId	2^o	0.8	0.8
22	31.3	Ia	1^o	0.7	0.7
23	29.4	IIb,IIc	2^o,2^o	0.8	0.7
24	26.8	IIb	2^o	0.9	0.8
25	24.8	IIa	2^o	0.9	0.9
26	23.3	IIIa	2^o	0.7	0.6
27	22.3	IVc	1^o	0.7	0.6
28	20.9	IVb	2^o	0.7	0.7
29	20.1	Va	1^o	1.0	0.9
30	14.2	IVa	1^o	0.7	0.6

[a] A mixture of t-butylbenzene (I), decalin (II, cis:trans 1:4) tetralin (III), 2-phenylpentane (IV) and 2,3-dimethylnaphthalene (V) was made up in mole fractions of 0.1955, 0.2105, 0.2180, 0.1955 and 0.1805 respectively.

[b] According to The Sadtler Standard Carbon-13 NMR Spectra[6b]

[c] Peak heights are normalized to the tallest peak at δ125.47 (protonated carbons, IIIc and Vb)

[d] Peak heights are normalized to the capillary dioxane peak. Refer to footnote a in Table I.

Table II. Distribution of Aromatic Carbons in H-Coal Liquids by Structural Types

Benzene Ring Carbon Types	Chemical Shift Range, ppm	% Distribution ASO	ASB	VSO
CH, OR subst.	111-123	3.4	12.0	9.7
CH, Unsubst.	123-130	53.0	49.2	46.1
CR, Condensed bridge	130-133.8	11.7	11.4	14.9
CR, Tetralin & Me Subst.	133.8-137.3	13.4	11.5	10.4
CR, Aryl & Branched Alkyl	137.3-149	18.5	15.9	18.8
C-OR	149-160	a	b	b

[a] No discernible signals are found.
[b] A few low intensity signals are observed but they are too small to integrate.

Figure 1 Aromatic Regions of the Quantitative (A) and Quaternary Carbon Supressed (B) CMR Spectra of the Simulated Coal Liquid.

Figure 2 Aliphatic Regions of the Quantitative (A) and the Quaternary Carbon Suppressed (B) CMR Spectra of the Simulated Coal Liquid.

Figure 3 Aromatic Regions of Quantitative (A) and Quaternary Carbon Suppressed (B) CMR Spectra of ASO.

Figure 4 Aliphatic Regions of Quantitative (A) and Quaternary Carbon Suppressed (B) CMR Spectra of ASO.

Figure 5 Aromatic Regions of the Quantitative (A) and Quaternary Carbon Suppressed (B) Spectra of ASB

Figure 6 Aliphatic Regions of the Quantitative (A) and Quaternary Carbon Suppressed (B) CMR Spectra of ASB

Figure 7 Aromatic Regions of the Quantitative (A) and Quaternary Carbon Suppressed (B) CMR Spectra of VSO

Figure 8 Aliphatic Regions of the Quantitative (A) and Quaternary Carbon Suppressed (B) CMR Spectra of VSO

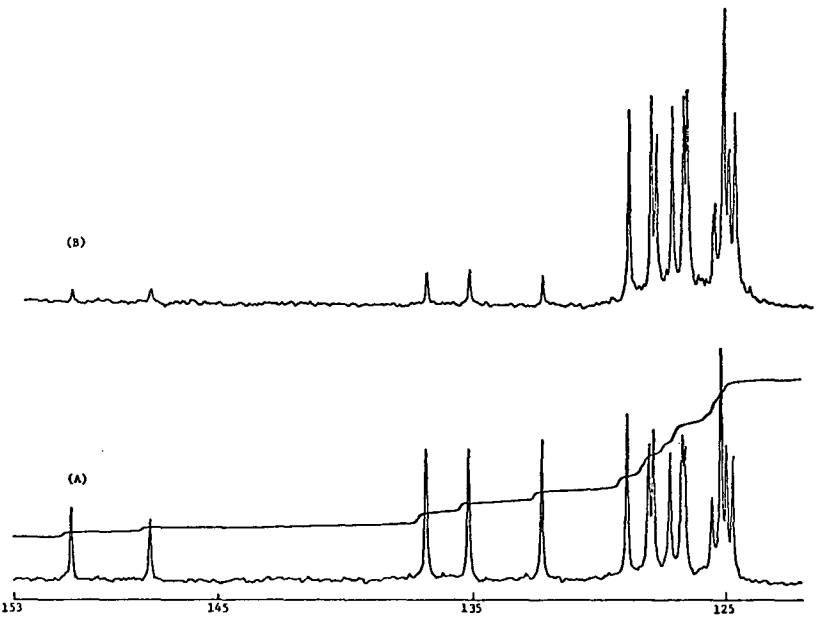

Figure 1

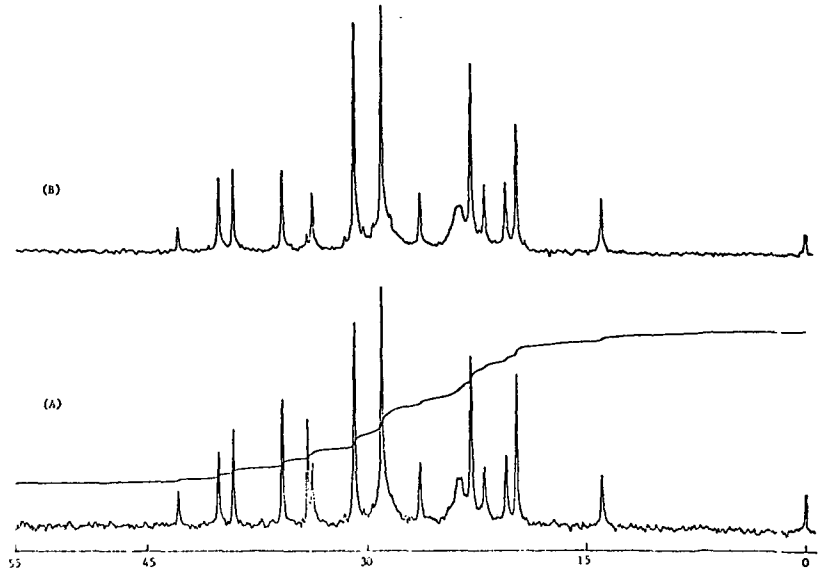

Figure 2

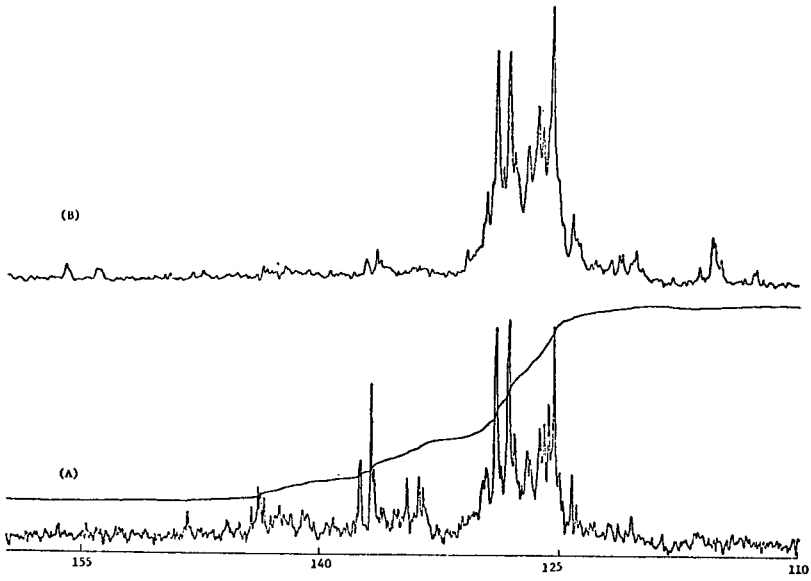

Figure 3

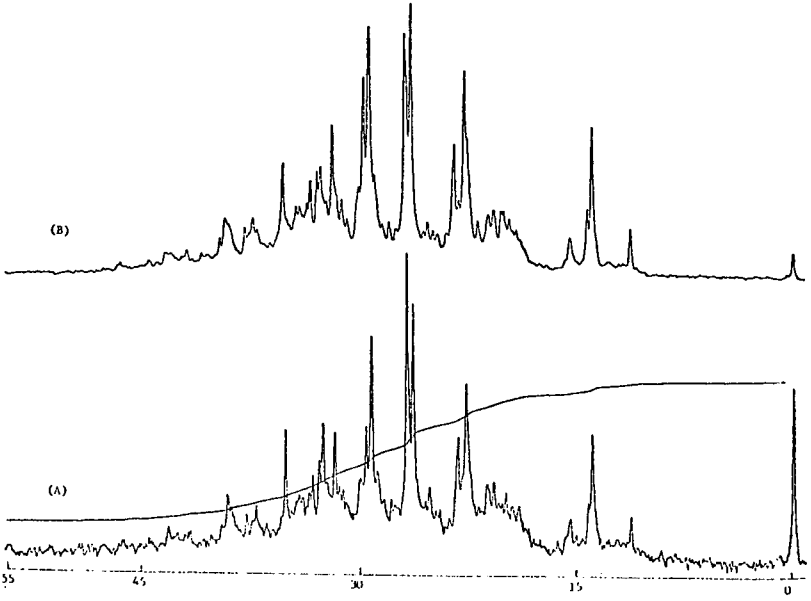

Figure 4

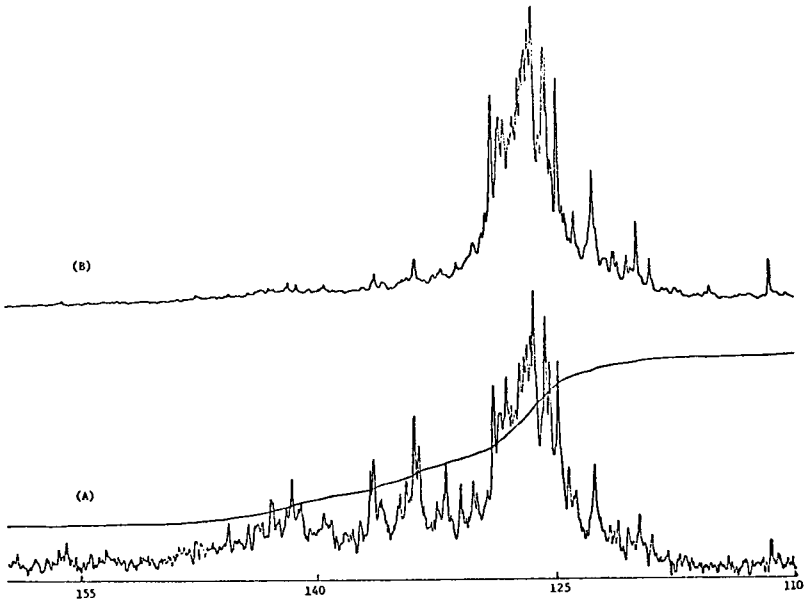

Figure 5

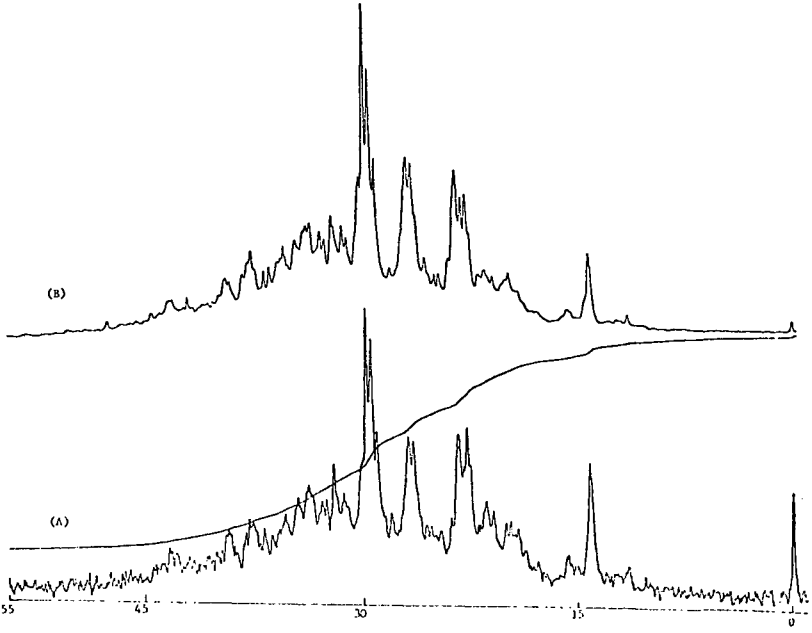

Figure 6

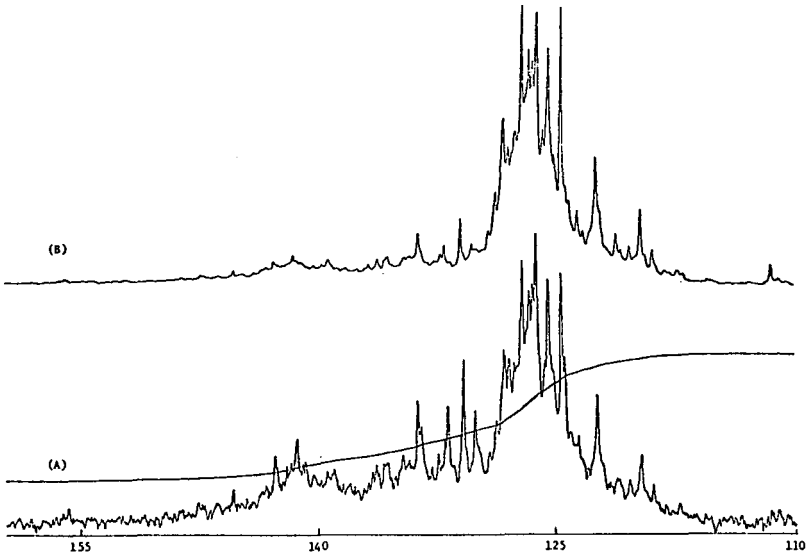

Figure 7

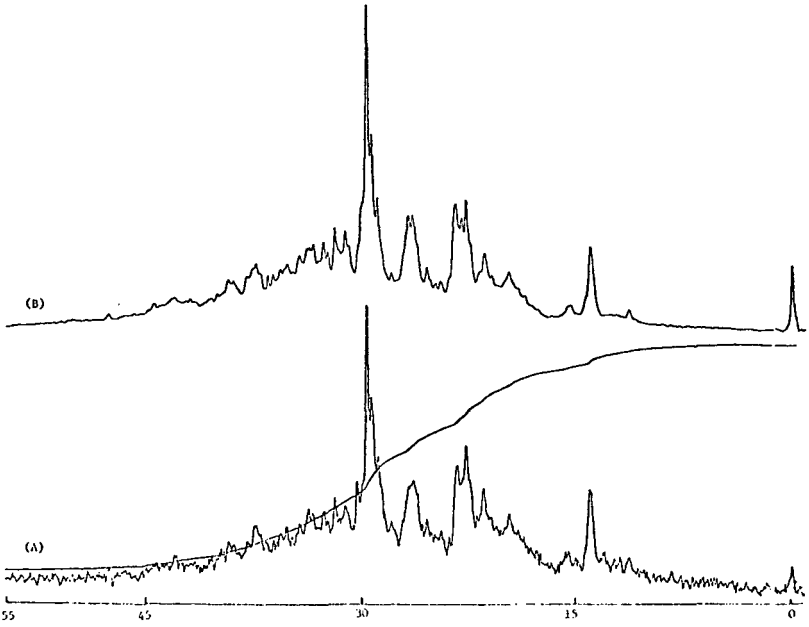

Figure 8

CARBON-13 NMR STUDIES OF COALS BY CROSS POLARIZATION AND MAGIC-ANGLE SPINNING

F. P. Miknis

U.S. Department of Energy, Laramie Energy Technology Center
P.O. Box 3395, University Station, Laramie WY 82071

and

G. E. Maciel and V. J. Bartuska

Department of Chemistry, Colorado State University
Fort Collins CO 80523

INTRODUCTION

Knowledge of the chemical structures of the organic compounds in fossil fuels is essential for a fundamental understanding of these important materials and how to utilize them most effectively. For solid fossil fuels (e.g., oil shales and coals) this kind of chemical characterization has been difficult because many of the most powerful analytical techniques for organic structure determination, including conventional nuclear magnetic resonance (NMR) have required liquid samples. However, for coals and oil shales only small fractions of the organic constituents can be dissolved under conditions for which one can be confident that the structural integrity of the organic compounds is retained.

Until recently NMR spectra of solid samples have usually consisted of featureless, broad resonances with little or no useful information available regarding molecular structure. Recently, it has been demonstrated that useful ^{13}C NMR spectra can be obtained on solid samples by using some newly developed techniques.

Standard continuous wave or pulse Fourier transform NMR approaches on powdered or amorphous samples give very broad lines of generally low intensity. The breadth of ^{13}C resonances is due to the manifold of ^{1}H-^{13}C dipole-dipole interactions and the chemical shift anisotropy resulting from random orientation of the molecules in the sample. The low signal-to-noise ratio found in such ^{13}C NMR spectra is at least partly due to the long ^{13}C spin-lattice relaxation times (T_1) characteristic of solids and the fact that repetitions of the experiment are thereby constrained to long time intervals. Pines, Gibby and Waugh[1,2] have shown how the ^{1}H-^{13}C dipole-dipole problem can be eliminated by a high-power ^{1}H decoupling method which also provides an enhancement in the ^{13}C NMR signal and effectively deals with the problem of long T_1's. This approach has previous been applied to coal samples.[3,4,5]

The remaining line broadening source one would like to remove, chemical shift anisotropy, can be eliminated by rapidly spinning the sample about an axis at an angle of 54°44',[6,7,8] the "magic-angle," with respect to the axis of the static magnetic field. A combination of cross polarization and magic-angle spinning techniques has provided promising spectra for coals[9] and oil shales.[10-13]

While anticipated improvements in the ^{13}C techniques--e.g., using larger static magnetic fields--may provide more detailed structural information, valuable information on the aromatic/aliphatic character of coals is presently obtainable using CP-MAS techniques. This paper provides information at that level on some representative coals and coal-derived materials.

EXPERIMENTAL

The coals on which ^{13}C NMR measurements were made include a Texas lignite, three Wyoming subbituminous coals (two from Hanna, one Wyodak), an Illinois bituminous, two Indiana bituminous, two eastern bituminous coals and an anthracite. In addition, the following coal-derived materials were studied: metallurgical coke; a Hanna coal that had been subjected to reverse combustion; and a solvent refined coal derived from the Wyodak coal. Each sample was studied as a powder, about 1.4 cm^3 in each case.

The ^{13}C NMR measurements were based upon the single-contact cross polarization method.[1,2] A 90° ^1H pulse is applied, followed by a 90° phase shift, after which ^1H rf power is maintained during the ^1H-^{13}C cross polarization and for ^1H decoupling during data acquisition. Radio frequency power at the ^{13}C resonance frequency is applied according to the Hartmann-Hahn condition during the contact period and then turned off during the period in which the ^{13}C resonance frequency of 15.1 MHz on a home-built spectrometer, using a 14 kgauss magnet and a commercially available ^{13}C Fourier transform data system. The H_1 field for ^1H was 10 gauss and that for ^{13}C was 40 gauss. Magic-angle spinning rates of 1.9 to 2.4 kHz were achieved with a spinner of the Andrew type,[7] using air pressure of 13 to 20 lb/in^2. All spectra obtained using magic-angle spinning resulted from data accumulated from 4000 scans.

RESULTS

Before truly quantitative results can be reported from ^{13}C NMR techniques of the type employed in this study, a great deal of calibration work will be required with standards, and the detailed dynamics of the cross polarization phenomenon will have to be characterized for each coal type. Such work is not yet completed, but was not considered a prerequisite for reporting the essence and qualitative significance of the present results. VanderHart and Retcofsky[4] and Bartuska et al.[3] have previously discussed the problems of obtaining quantitative analytical data from cross polarization experiments.

In order to choose a reasonable set of experimental parameters, which could be expected to give integrated intensities of at least semiquantitative significance, parameter variations were carried out in experiments on the Illinois bituminous sample. The contact (cross polarization) time, which must be chosen to conform with the dynamics of ^{13}C-^1H cross polarization and ^1H $T_{1\rho}$ constraints,[5] was varied over the following values: 0.5 msec, 1.0 msec, 3.0 msec, and 5.0 msec. Using a repetition time of 4.0 sec, we measured the integrated signal intensity of the "aromatic" and "nonaromatic" carbon resonances and the apparent carbon fraction found in the aromatic region, f_a (aromaticity); these values were found to be 0.75 and 0.76 for 1 msec and 3 msec, and 0.72 and 0.68 for 5 msec and 0.5 msec, respectively, for the contact time. The best signal-to-noise ratio (S/N) was found for the 1 msec contact time; S/N deteriorated badly at 5 msec. Choosing the 1 msec contact period, we repeated the experiment with a repetition time of 8.0 sec, obtaining a 0.74 value for f_a. Settling on 1 msec and 4 sec contact and repetition times, respectively, all cross polarization results reported in this paper were obtained using these parameters.

In order to check that by using the above-mentioned experimental parameters reasonable f_a values would be obtained in cross polarization experiments, we made ^{13}C NMR measurements on the Illinois bituminous sample by using the pulse Fourier transform method, with magic-angle spinning and high-power ^1H decoupling, but <u>without</u> cross polarization. Intensity data of such experiments are still subject to uncertainties associated with nuclear Overhauser effects[14] and differing relaxation times,[15] but such uncertainties are entirely different from those associated with the cross polarization approach. When pulse repetition times of 30 and 99 sec were employed, f_a values of 0.71 and 0.77, respectively, were obtained. Hence, while

there is no guarantee that the same cross polarization parameter set (1.0 msec and 4.0 sec) will serve equally well for all of the coal samples, indications are that this set leads to no major intensity distortions for the Illinois bituminous sample, and is a reasonable set to employ in the present survey.

DISCUSSION

An example of the advantages of magic-angle spinning in conjunction with cross polarization and high-power decoupling is shown in Figure 1a and b for the Hanna subbituminous coal. Clearly, the main structural distinction that can be made is between aliphatic and aromatic carbons. The spinning case shows much better resolution because the chemical shift anisotropy, which is evident in the aromatic region of Fig. 1a, has been eliminated. Aromaticity values are determined by dividing the integrated intensity of the aromatic band by the integrated intensity of the complete spectrum.

A ^{13}C spectrum of the Hanna coal which had been subjected to reverse combustion at 500°C is shown in Fig. 1c. The spectra clearly show depletion of the aliphatic carbons, relative to the aromatic carbons. Similarly, the CP-MAS spectra of a Wyodak coal (Fig. 2a) and its solvent refined product (Fig. 2b) show that the solvent refining process increases the aromaticity of subbituminous coals. These examples suggest the use of CP-MAS techniques for studies of coal combustion and processing.

^{13}C NMR spectra of a series of coals of varying rank are shown in Fig. 3a-f. This simple montage of ^{13}C spectra shows quite graphically that the aromaticity of coals increases with increasing rank. The metallurgical coke is included because it had a measured f_a of 1.00. A matter of concern regarding quantitative measurements in CP-NMR of solids is whether all the carbon types in the sample are being polarized equally, particularly aromatic carbons in condensed systems.[4] The fact that the f_a of the coke yielded a very reasonable value of 1.00 implies that all of the carbons in the coal are being observed. Recent work on oil shales also addresses this problem.[12,13]

One fuel property that would be interesting to relate to structural features is the heating value. Figure 4 shows a plot of the heating values of the coals vs. the f_a values derived from the ^{13}C spectra. That a simple correlation is not found is not surprising, as a variety of variations occur within these samples. In progressing from a lignite to a bituminous coal to an anthracite, the percent organic carbon of the material increases, which tends to increase the heating value.

An increase in f_a, by itself, would tend to decrease the heating value, as can be seen from the following heats of combustion: benzene, 782.3 kcal/mole; cyclohexane, 937.8 kcal/mole; n-hexane, 989.8 kcal/mole; phenol, 732.2 kcal/mole; cyclohexanol, 890.7 kcal/mole. In addition, within a collection of coal samples there are substantial variations in the percent oxygen, nitrogen and sulfur--i.e., in the occurrence of oxygen-, nitrogen- or sulfur-containing organics. Oxygen-containing species tends to decrease the heating value of a coal, for a given amount of carbon, as seen from the following heats of combustion: benzene, 782.3 kcal/mole; phenol, 732.2 kcal/mole; cyclohexane, 937.8 kcal/mole; cyclohexanol, 890.7 kcal/mole; toluene, 934.3 kcal/mole; benzyl alcohol, 894.3 kcal/mole; benzoic acid, 771.2 kcal/mole.

In viewing variations of heating values of coals, if one wishes to eliminate the factor due to percent organic carbon in the coal, the heating value per pound of carbon (maf) is of interest. Figure 5 shows a plot of this heating value vs. f_a. Note that, if the organic constituents of coal were strictly hydrocarbons, such a plot would be expected to show a decrease in BTU/lbC as f_a increases, reflecting the heat of combustion pattern stated above. Instead, Figure 5 shows a nearly

constant value of about 1.75×10^4 BTU/lbC for coals with apparent aromatic fractions ranging from 0.70 to 0.75 and a fall off on both sides of that f_a range.

This pattern can be understood as follows: As stated above, if coal were composed of only hydrocarbons, the trend would be to lower BTU/lbC for higher f_a values. This trend is responsible for the fall off of the curve for the highest three f_a values. However, organic compounds containing oxygen, but equivalent numbers of carbon atoms have lower heats of combustion than analogous hydrocarbons. The coals with the lowest observed f_a values, which might have been expected have the highest BTU/lbC values, also have the highest total oxygen contents (maf), and their lower BTU/lbC values may be associated with these high oxygen contents. The coals with highest f_a values (0.81, 0.95, and 1.0) have very low oxygen contents, and there is a roughly decreasing progression of oxygen contents as f_a increases from 0.59 to 1.0. Hence, there are two competing influences on the BTU/lbC parameter, giving rise to the broad maximum at about 1.75×10^4 BTU/lbC.

REFERENCES

1. Pines, A., Gibby, M. G., and Waugh, J. S. J. Chem. Phys., v. 56, 1972, p. 1779.
2. Pines, A., Gibby, M. G., and Waugh, J. S. J. Chem. Phys., v. 59, 1973, p. 569.
3. Bartuska, V. J., Maciel, G. E., Schaefer, J., and Stejskal, E. O. Fuel, v. 56, 1977, p. 354.
4. VanderHart, D. L., and Retcofsky, H. L. Fuel, v. 55, 1976, p. 202.
5. Retcofsky, H. L. and VanderHart, D. L. Fuel, v. 57, 1978, p. 421.
6. a) Lowe, I. J. Phys. Rev. Letters, v. 2, 1959, p. 285.
   b) Kessemeier, H., and Norberg, R. E. Phys. Rev., v. 155, 1967, p. 321.
7. Andrew, E. R. Progr. Nucl. Magn. Reson. Spectrosc., v. 8, 1971, p. 1.
8. Schaefer, J., and Stejskal, E. O. J. Amer. Chem. Soc., v. 98, 1976, p. 1031.
9. Maciel, G. E., Bartuska, V. J., and Miknis, F. P. Fuel (in press).
10. Maciel, G. E., Bartuska, V. J., and Miknis, F. P. Fuel, v. 57, 1978, p. 505.
11. Maciel, G. E., Bartuska, V. J., and Miknis, F. P. Fuel (in press).
12. Miknis, F. P., Maciel, G. E., and Bartuska, V. J. Org. Geochem. (in press).
13. Resing, H. A., Garroway, A. N., and Hazlett, R. N. Fuel, v. 57, 1978, p. 450.
14. Noggle, J. H., and Schirmer, R. E. The Nuclear Overhauser Effect, Academic Press, New York, 1971.
15. Farrar, T. C., and Becker, E. D. Pulse and Fourier Transform NMR, Academic Press, New York, 1971.
16. Whitehurst, D. D. "Organic Chemistry of Coal," J. W. Larsen, Ed., ACS Symposium Series, v. 71, Amer. Chem. Soc., Wash., D.C., 1978.

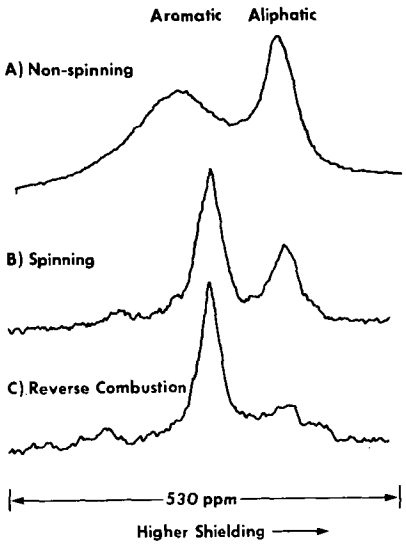

Figure 1. ^{13}C NMR Spectra of Hanna, Wyoming Coal

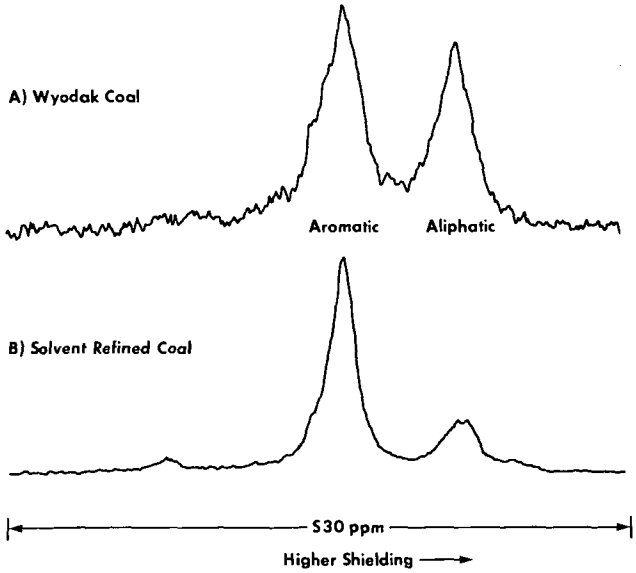

Figure 2. ^{13}C NMR Spectra of Wyodak Coal and SRC Product

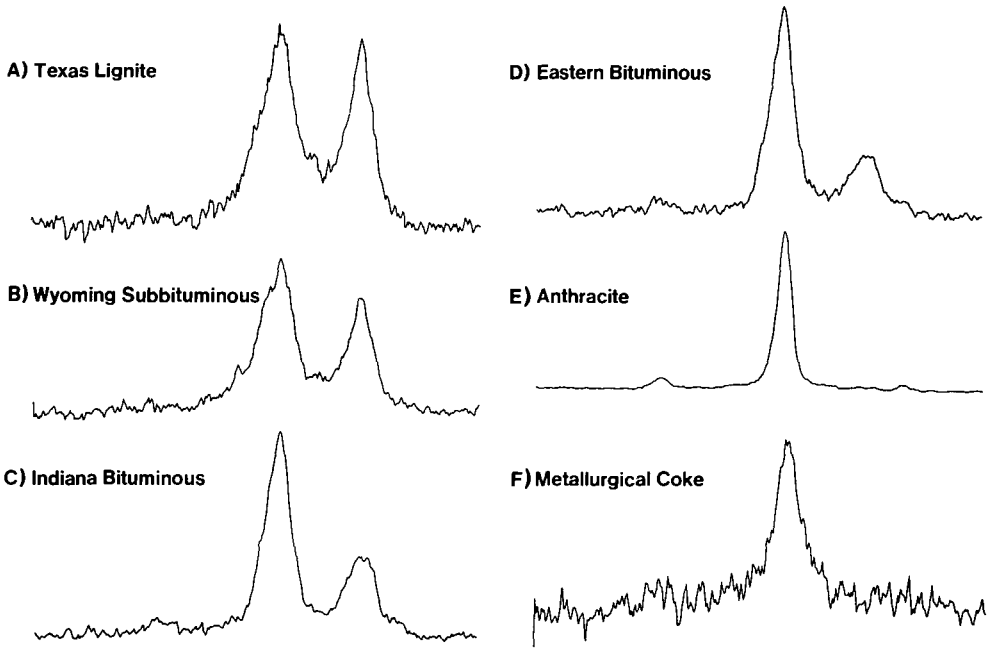

Figure 3. ^{13}C NMR Spectra of Coals of varying rank

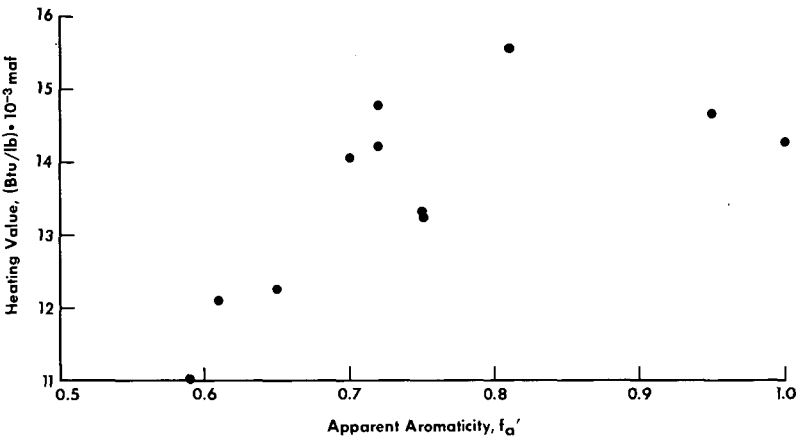

Figure 4. Plot of heating value versus aromaticity

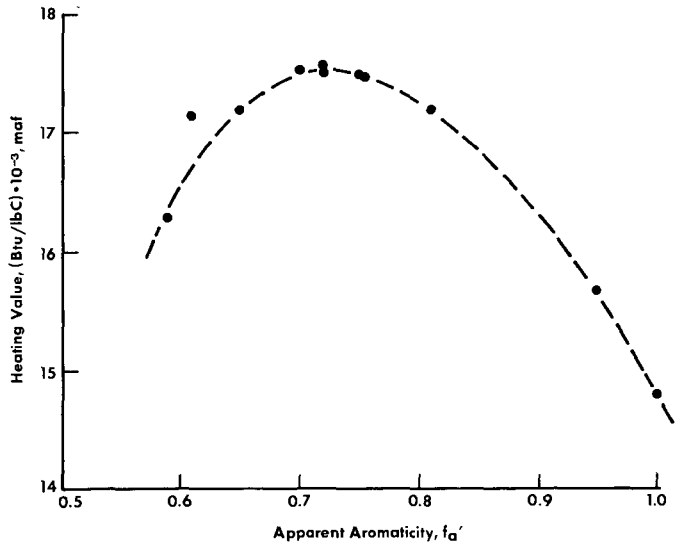

Figure 5. Plot of heating value/pound of carbon versus aromaticity

THE EFFECTS OF T_1 AND NOE CONSIDERATIONS IN QUANTITATIVE APPLICATIONS OF CARBON-13 NMR TO THE ANALYSIS OF COMPLEX HYDROCARBON MIXTURES

Terry D. Alger, Ronald J. Pugmire, W. David Hamill, Jr., and David M. Grant

Departments of Chemistry and Mining and Fuels Engineering, University of Utah, Salt Lake City, Utah 84112

I. Introduction

Since the signal intensities of a nuclear magnetic resonance spectrum are dependent upon the number of given nuclei present in a compound, nuclear magnetic resonance can be a strong analytical tool for quantifying the amounts of material present in a sample. In many compounds of interest which contain carbon, carbon-13 magnetic resonance (cmr) spectra are of particular value as an analytical tool since the spectra can be void of multiplet structure due to ^{13}C-^{13}C splittings (if carbon is in natural abundance only) and can be void of multiplet structure due to ^{1}H-^{13}C splittings (if noise-modulated proton decoupling techniques are used). Moreover, a range of chemical shifts of over 200 ppm for common functional groups assist greatly in resolving individual peaks in any given spectrum (1). Thus under such experimental conditions, each ^{13}C nuclear environment is represented by a single ^{13}C resonance. In complex mixtures of hydrocarbons resulting from coal liquification, these qualities of cmr make ^{13}C spectra particularly useful. Such coal mixtures can contain hundreds of compounds, and may be quite viscous. In such mixtures, ^{13}C spectra have been used by various workers to quantify the amount of a given compound, as well as to quantify the amount of aromaticity in given coal derivative samples (2-4).

Nevertheless, there are some problems attendant with the ^{13}C nmr technique and the usefulness of the ^{13}C signal intensity as a quantifiable parameter. To begin with, ^{13}C nuclei in natural abundance amount to only about 1.1%. In complex mixtures of multiple compounds, signal sensitivity therefore becomes a problem. Fourier transform methods of data acquisition with repeated pulse sequences and data storage for signal averaging, has somewhat overcome such complications (4). However, such Fourier techniques themselves lead to other problems. To ensure that the time necessary to store sufficient transients is not inordinately long, it is desirable to repeat the pulse sequence as rapidly as possible. Nevertheless, the delay time between successive pulse sequences (individual transients) is dependent upon the spin-lattice relaxation times (T_1) of the ^{13}C system. If the next pulse sequence is begun before any given ^{13}C signal has had an opportunity to relax to its thermal equilibrium value, saturation effects occur, and the resultant ^{13}C signal intensity is not maximized. For hydrocarbon systems which contain a wide variety of carbon-13 relaxation times from fairly short (2 sec) to fairly long (200 sec), this creates a problem. Reasonable delay times of 1-10 seconds between successive 90° pulses would most likely saturate the ^{13}C signals with long relaxation times (200 sec) so that less than 10% of the possible signal would be observed. In contrast, delay times of 1-10 seconds with 90° pulses could permit nearly 90% of the signals to be observed if the relaxation times were short (2 sec). Under such variable saturation effects, the ^{13}C signal intensities would be difficult to relate to quantifiable results (4).

For hydrocarbon systems which result from coal derivatives, such wide variations in relaxation times are a reality. Spin-lattice relaxation times in acenaphthene have been reported to vary from 3.1 seconds for the ^{13}C nuclei with two protons attached, to about 150 seconds (5a,5b,5c) at the internal bridgehead carbon. A similar range of the spin-lattice relaxation times for the protonated and non-protonated carbons in pyrene has been observed. Since delay times of $5T_1$ are necessary to ensure complete relaxation following a 90° or 180° pulse (6), some other method must be found for taking ^{13}C signal intensities in

hydrocarbon systems with long relaxation times. Repeated pulse sequences (1,000 to 10,000 transients) with delay times of 1,000 seconds ($5T_1$) become prohibitively long to run (for example, 10,000 transients with delay times of 1,000 sec between transients would take 116 days per spectrum).

Another problem inherent in the proton-decoupled ^{13}C spectra relates to the Nuclear Overhauser Effect (NOE) experienced by the ^{13}C signals when the coupled ^{1}H nuclei are doubly irridated. It has been observed that ^{13}C intensities are enhanced when coupled ^{1}H signals are irridated by a saturating second frequency. The value of the NOE is determined by the ratio of S_∞/S_o. (The ^{13}C signal intensity after the proton decoupler has been on long enough to establish equilibrium is S_∞ S_o is the signal intensity without proton decoupling) (7). Depending upon whether a given nucleus is dominated by dipole-dipole relaxation, or by other relaxation mechanisms, the value of NOE can vary from 3 to 1, respectively (8,9). In the hydrocarbon systems of coal derivatives, it appears that the NOE factors can vary over the maximum ranges (being about 3 if protons are directly attached, and as low as 1-2 if no protons are attached). Hence, variations in NOE enhancements of ^{13}C signal intensities representing the same number of ^{13}C nuclei could vary over a magnitude of 1-3 (8). This is hardly acceptable for quantitative studies. Thus, some means of either quickly determining the NOE factors for each ^{13}C signal must be found, or else some means of eliminating the NOE enhancement must be used.

In an effort to address the preceeding problems we have obtained T_1 and NOE values on a number of model compounds (polycyclicaromatic hydroaromatic, and alkylated aromatic hydrocarbons) which are thought to have representative values similar to those found in complex hydrocarbon mixtures. The T_1 and NOE values thus obtained provide valuable information on relaxation processes, range of values expected, and details of molecular motion.

II. Experimental

The T_1 and NOE data were taken at 25 MHz and 75 MHz on Varian XL-100-15 and SC-300 FT spectrometers, respectively. T_1's were obtained by the inversion recovery method (10) while NOE values were obtained by a two point gated decoupling method.

III. Results and Discussion

We have obtained T_1 and NOE data on napthlalene, tetralin, acenaphthene, pyrene, symmetrical hexahydropyrene, phenanthrene, 1,2,3,4,5,6,7,8, octahydrophenanthrene, xanthone, and phenyloctane. This group of compounds represent a set of structural types representative of many moieties known to occur in coal derived liquids. In terms of general relaxation considerations the data can be considered, for convenience, in terms of protonated and non-protonated carbons. Protonated carbons are found, within experimental error, to exhibit essentially a full nuclear overhauser effect and the dipolar relaxation mechanism thus is dominant (11). The T_1 values at 25 MHz for all protonated carbons examined fall in the range of 2-11 second. Similar values are observed at 75 MHz. The non-protonated carbons, however, fall in the range 28-240 seconds at 25 MHz with the higher numbers associated with the PAH's where the $1/r^6_{C-H}$ term in the relaxation expression rapidly alternates the efficient carbon-hydrogen intramolecular dipolar relaxation mechanism.

Some very interesting results are observed for the non-protonated carbons at 75 MHz. The T_1 values are shortened considerably indicating significent contributions made by chemical shift anisotropy at high fields. Using the rate expression (11)

$$\frac{1}{T_1} = \frac{1}{T_1^D} + \frac{1}{T_1^{CSA}} + \frac{1}{T_1^o} \qquad 1)$$

and assuming that $1/T_1^o$ approaches zero for the systems in question (which, based on the low and high field data, is justified), one can readily calculate dipolar

contributions of 88, 413, and 127 seconds, to the relaxation rates at C-9,10,C-11, and C-12, respectively by assuming isotropic motion of the molecules. The chemical shift anisotropy term is 88, 73, and 54 seconds, respectively for these carbons. In the case of pyrene the contribution from chemical shift anisotropy is even greater with contribution of 35 and 38 seconds for carbons 11,12,13,14 and 15,16 respectively. Hence, relaxation constraints are much less severe at high fields than those encountered using iron core magnet NMR technology.

Based on the data obtained to date, we estimate that the non-protonated carbons at C-15,16 in pyrene represent the longest T_1 values one would expect to encounter. Using mixtures of these compounds we have varied spectrometer operating conditions in order to arrive at an optimal set of parameters for use on coal derived liquids. Details of the results of these studies at 25 and 75 MHz will be forthcoming.

Acknowledgment

We gratefully acknowledge support for this work from the Department of Energy under contract ER-78-S-02-5006 and a National Institutes of Health Regional Resources grant RR-574.

REFERENCES

1. J. Strothers Carbon-13 NMR Spectroscopy, Academic press, New York, London 1972.

2. H. L. Retcofsky, F. K. Schweighardt and M. Hough, Anal. Chem., 49 585 (1977).

3. R. J. Pugmire, D. M. Grant, K. W. Zilm, L. L. Anderson, A. G. Oblad, and R. E. Wood, Fuel, 56, 295 (1977).

4. a) R. G. Ruberto, D. C. Cronauer, D. M. Jewell, and K. S. Seshadr, Fuel, 56, 25 (1977); b) Ibid., 56, 17 (1977); c) K. S. Seshadri, R. G. Ruberto, D. M. Jewell, and H. R. Malone, Div. Fuel Chem., 20, 38 (1977).

5. a) J. N. Shoolery and W. C. Jankowski, Varian Applications Note NMR-73-4, August, 1973; b) J. N. Shoolery, Varian Instrument Applications, Vol. 10, Number 3, 1976; c) J. N. Shoolery, "Some Quantitative Applications of ^{13}C NMR Spectroscopy," in Progress in Nuclear Magnetic Resonance Spectroscopy, Permagon Press Ltd., Oxford, England (1977).

6. R. K. Harris, and R. H. Newman, Journal of Magnetic Resonance 24 449 (1976).

7. J. R. Lyerla and D. M. Grant, MPT International Review of Science Physical Chemistry, Series One, 4 155 (1972).

8. a) T. D. Alger, D. M. Grant, and R. K. Harris, Journal Physical Chemistry, 76, 281 (1972); b) A. J. Jones, D. M. Grant, and K. F. Kuhlmann, J. Amer. Chem. Soc., 91, 5013 (1969).

9. It should be noted, see Ref. 7 for a complete description, that if the liquid is not in the region of motional narrowing,

$$\text{i.e., } (\omega_{\alpha\beta}^{2}\,\tau_{c}^{2} \ll 1),$$

the NOE will not be equal to 3 even if the relaxation is totally dipole-dipole dependent (transition probabilities and hence relaxation mechanisms are related to:

$$W_{\alpha\beta} = \gamma^{2}\, H^{*}_{Loc}(t)\, H_{Loc}(t)\, \left(\frac{2\tau_{c}}{1 + \omega_{\alpha\beta}^{2}\tau_{c}^{2}}\right)$$

10. R. Freeman and H. D. W. Hill, J. Chem. Phys., 53, 4103 (1970).

11. K. F. Kuhlmann and D. M. Grant, J. Chem. Phys., 55, 2998 (1971).

TABLE I

Relaxation Parameters in Pyrene and Acenaphthene

COMPOUND	POSITION	25 MHz T_1	25 MHz n(±0.2)	75 MHz T_1	75 MHz n(±0.2)
Acenaphthene	1,2	3.1±0.2	3.0	3.1	1.95
	3,8	5.6±0.8	2.8	6.0±0.4	1.85
	4,7	5.6±0.8	2.8	6.6±0.5	1.85
	5,6	6.4±0.9	2.8	6.5±0.4	1.85
	9,10	87±10	2.3	44±2	1.0
	11	208±30	1.8	62±7	0.4
	12	128±10	2.1	38±3	0.4
Pyrene	1,3,6,8	8.0±0.4	1.9	4.9±0.4	2.0
	2,7	6.8±0.2	1.9	4.5±0.3	2.0
	4,5,9,10	7.2±0.8	1.9	5.4±0.2	2.0
	11,12,13,14	135±10	1.2	26.2±1.4	0.51
	15,16	240±30	0.6	35.1±3.5	0.17

Hydrogenation Reactivity of Petrographic Composition of Coal

Y. Nakata*, S. Ueda*, Y. Maekawa* and M. Shibaoka**

*Government Industrial Development Laboratory, Hokkaido
41-2, Higashi-Tsukisamu, Toyohiraku,
Sapporo, 061-01, Japan

**CSIRO, Fuel Geoscience Unit, P.O.Box 136, North Ryde,
N. S. W., Australia 2113

Introduction

With special regard to the characteristics of high pressure hydrogenation of the petrographic composition of coal, in the past reports by Bergius[1], Wright et al[2], Fisher et al[3] are available, and more recently we have reports on the results of work by Given, Davis and Mitchell et al[4)-7]. According to these reports, among the 3 maceral groups of coal, namely vitrinite, exinite and inertinite, it has been pointed out that the reactivity of vitrinite and exinite are high.

Among the coals produced in Australia, while there are rather large number of coals with a relatively high inertinite content, and whereas the main component of inertinite is semifusinite, generally the scarcity of fusinite is characteristic. While it is generally accepted that the hydrogenation reactivity of fusinite is low, no reports regarding semifusinite seen to be available.

In the present report we conducted liquefaction experiments by hydrogenation reaction on hand picked vitrinite concentrates and inertinite concentrates of Bayswater seam coal (N.S.W., Australia), and the respective features of liquefaction reaction were clarified and a comparative investigation was made between the two.

Experimental

The samples used in the experiments were vitrinite concentrates and inertinite concentrates hand picked from Bayswater seam coal of high volatile bituminous rank. The petrographic, proximate and ultimate analyses of the hand-picked samples are given in Table 1. In the experiments we used a batch type autoclave with an inner volume of 500 cc as the hydrogenation apparatus. In the once experiment, we inserted 10 g of dry sample coal, 1 g of red mud catalyst, 0.1 g sulfur promoter together with 10 steel balls for agitation, and the hydrogenation reaction was conducted under an initial hydrogen pressure of 100 kg/cm^2 at reaction temperatures of 400°C and 450°C respectively and by changing the reaction time from 0-150 minutes. In the case where vehicle oil was used, we applied decrystalized anthracene oil.

Among the reaction products, the gas was dealt with gas chromatography and the composition thereof was measured. Regarding the liquid and solid products, using n-hexane, benzene were fractionated into oil-1(O_1), oil-2(O_2), asphaltene(A), and organic benzene insolubles (O.B.I). The conversion was calculated from total pro product(gas+O_1+O_2+A). In addition O.B.I. was subjected to extracting tests using pyridine. The details of the above are as seen in our previous report[8].

Results and discussion

In Fig. 1 is shown the changes by reaction time of the yield of each fraction

of hydrogenation products of vitrinite and those of inertinite are shown in Fig. 2.

Even at a reaction temperature of 400°C the reaction of vitrinite proceeds and the conversion increases with the reaction time however the conversion of inertinite does not exceed 15% or thereabouts. However, in the case where vehicle oil is added to inertinite, even under identical reaction conditions the conversion increases markedly to 45% or thereaboute.

When this vehicle oil is used, this conversion is attained by the nominal reaction time zero. From the previous paper[9], it may be considered that the coal hydrogenation reaction with vehicle oil proceeds by the chemical reaction controlling. Therefore, it may be understood that the initial stage reaction rate of inertinite is very fast. However, thereafter ever what the reaction time is increased, no increase in the conversion was recognized, and it is surmized that the portion which can react under certain given conditions is restricted. Whereas the equilibrium conversion is higher than 400°C a similar tendency is seen when the reaction temperature is 450°C. This point is that which differs from vitrinite in which a gradual increase is seen with the increase in reaction time. However, when the distribution of reaction products in viewed, the distribution of gas, oil and asphaltene in both cases is relatively similar.

Further, hydrogen consumption of both cases in hydrogenation is as shown in Table 2, it may be seen that in the case of inertinite approximately 2 fold values are seen. The molecular weight of the reaction products of both cases are as seen in Table 3. When the reaction temperature becomes 450°C, a relative fairly good coincidence is seen between the vitrinite and inertinite, however when the reaction temperature is 400°C, it may be noted that the reaction products from inertinite show higher values. The H-NMR spectra of oil-1 and oil-2 of inertinite at 400°C are shown in Fig. 3; as may be seen an approximately similar pattern is recognized. Similarily the H-NMR spectra of oil-1 of inertinite at 150 minutes, 400°C, and oil-1, oil-2 of vitrinite at 30 minites, 400°C as shown in Fig. 4 show a similar pattern.

Thus from the above, it may be surmized that product from the liquefaction of the main parts of both sample coal have a relatively similar composition.

Conclusion

1) The reaction rate of vitrinite shows a gradual increase with the reaction time, however in the case of inertinite, the reaction does not proceed beyond a given value. This given value shows an increase with the rise in reaction temperature and the reaction rate is fast up till the time that this value is attained.

2) The hydrogen consumption is larger in inertinite.

3) It may be surmized that the liquefaction products from the main part of both sample coal have a relatively similar composition.

References

1) Bergius,F., Gluckauf,61, 1317 (1925)
2) Wright,C.C., and Sprunk,G.C., Penn. State Coll. Min. Ind. Exp. Stat. Bull. 26 (1939)
3) Fisher,C.H., Sprunk,G.C., Eisner,A., O'Donnell,H.J., Clarke,L., and Storch,H. H., U.S. Burean Mines Tech. Paper 642 (1942)
4) Given,P.H., Cronauer,D.C., Spackman,W., Lovell,H.L., Davis,A., and Biswas,B., Fuel, 54, 34 (1975)
5) Given,P.H., Cronauer,D.C., Spackman,W., Lovell,H.L., Davis,A., and Biswas,B., ibid, 54, 40 (1975)

6) Davis,A., Spackman,W., and Given,P.H., Energy Sources, 3, 55 (1976)
7) Mitchell,G.D., Davis,A., and Spackman,W., Liquid Fuels From Coal, Academic Press, p.p 255-270 (1977)
8) Maekawa,Y., Ueda, S., Hasegawa,Y., Yokoyama,Y., Hiroki,E., Yoshida,Y., Nenryo Kyokai-Shi (J. Fuel Soc. Japan) 49, 908 (1970)
9) Maekawa,Y., Shimokawa,K., Ishii,T., Takeya,G., Kogyo Kagaku Zasshi (J. Chem. Soc. Japan, Ind. Chem. Section), 73, 2347 (1970)

Table 1 Petrographic, Proximate and Ultimate Analysis of Bayswater Seam Coal

Sample	Maceral analysis (%)					Proximate analysis (%)				Ultimate analysis (%)				
	Vitrinite	Exinite	Miorinite	Semi-fusinite	Fusinite	Moisture	Ash	Volatile matter	Fixed carbon	C	H	N	S	O
Vitrinite concentrate	99	0.5	0.5	tr	tr	3.4	1.6	32.9	62.1	83.0	5.3	2.0	0.5	9.2
Inertinite concentrate	0.5	5	4	90	0.5	4.5	16.2	20.8	58.5	85.0	4.1	1.9	0.3	8.7

Table 2 Hydrogen consumption of vitrinite and inertinite hydrogenation

Sample	R.T °C	Rt min.	H_2 consumption wt % of coal	wt % of coal/conversion
Vitrinite	400	0	0.75	6.1×10^{-2}
"	"	30	1.24	5.6 "
"	"	60	3.42	7.0 "
"	"	90	2.95	4.5 "
"	"	120	3.52	4.9 "
"	"	150	4.22	5.4 "
"	425	60	4.84	6.9 "
"	450	0	1.37	2.7 "
"	"	30	4.20	5.4 "
"	"	60	5.40	6.1 "
Inertinite	400	0	2.05	1.8×10^{-1}
"	"	30	2.64	1.6 "
"	"	60	1.39	1.4 "
"	"	150	2.95	2.5 "
"	410	60	1.30	1.3 "
"	425	60	2.80	1.4 "
"	435	60	2.23	0.6 "
"	450	0	1.38	1.1 "
"	"	30	1.67	4.9 "
"	"	60	5.05	0.9 "
"	"	90	4.72	0.9 "
"	"	120	4.99	0.9 "
"	"	150	5.86	1.0 "

Table 3 Moleculer weight of inertinite and vitrinite hydrogenation product

Raw Sample	R.T °C	Rt min.	Product oil-1	oil-2	Asphaltene
Vitrinite	400	0	340	500	-
"	"	30	-	-	680
"	"	60	320	450	660
"	"	90	300	360	700
"	"	120	-	420	760
"	"	150	420	530	770
"	425	60	290	450	750
"	450	0	340	460	580
"	"	30	280	480	800
"	"	60	300	370	850
Inertinite	400	0	490	460	470
"	"	30	470	500	520
"	"	60	420	530	530
"	"	150	400	580	-
"	410	60	440	550	630
"	425	60	340	440	580
"	435	60	-	370	620
"	450	0	370	630	590
"	"	30	350	420	590
"	"	60	340	510	830
"	"	90	350	370	650
"	"	120	350	440	690
"	"	150	320	420	690

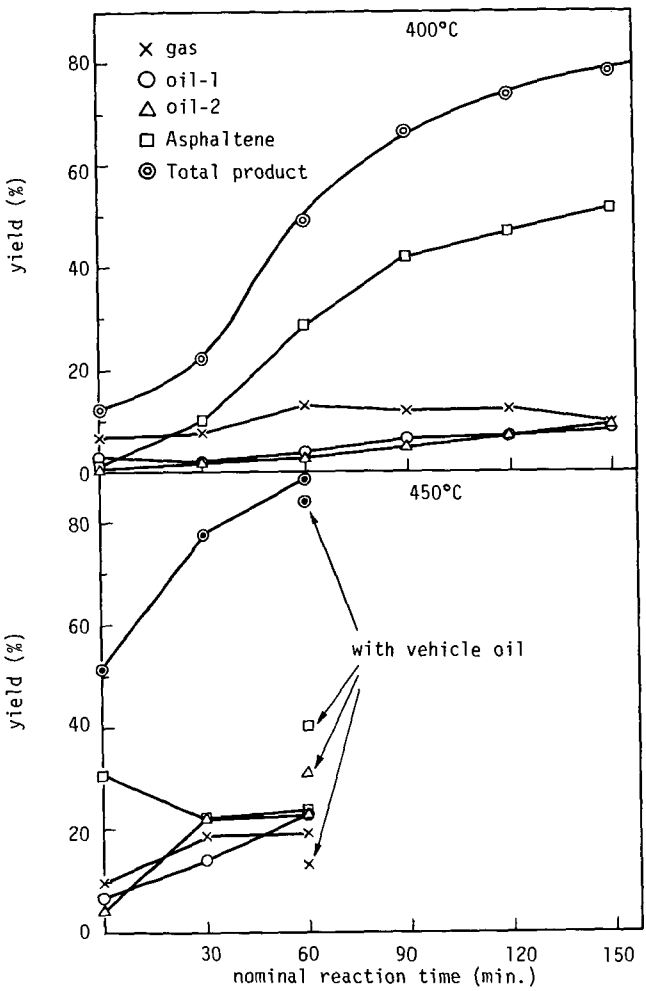

Fig. 1 Distribution of hydrogenation products from Bayswater vitrinite at 400°C, 450°C

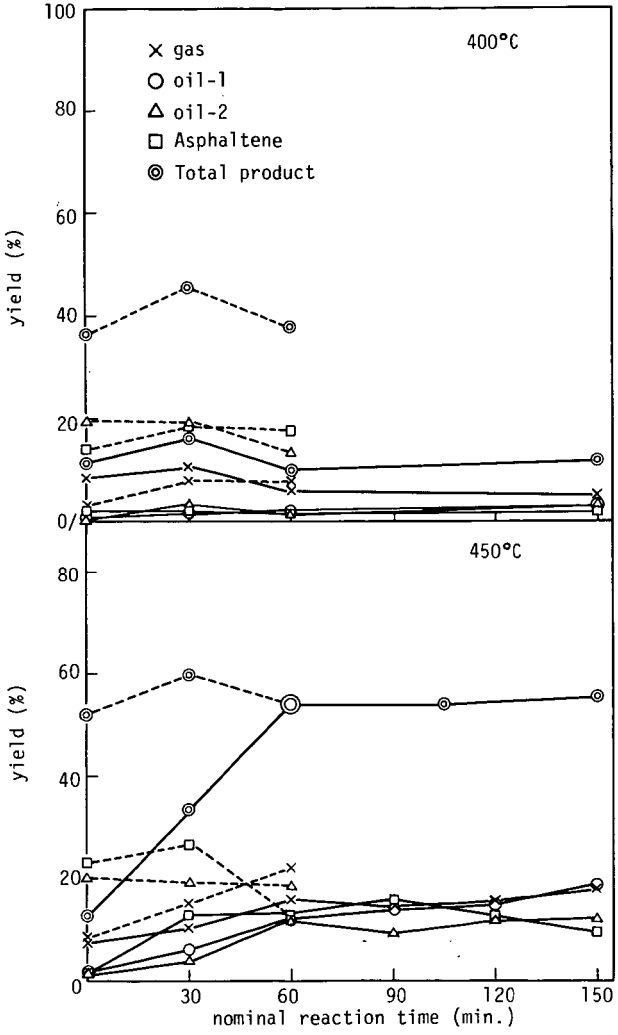

Fig. 2 Distribution of hydrogenation products from Bayswater inertinite at 400°C, 450°C

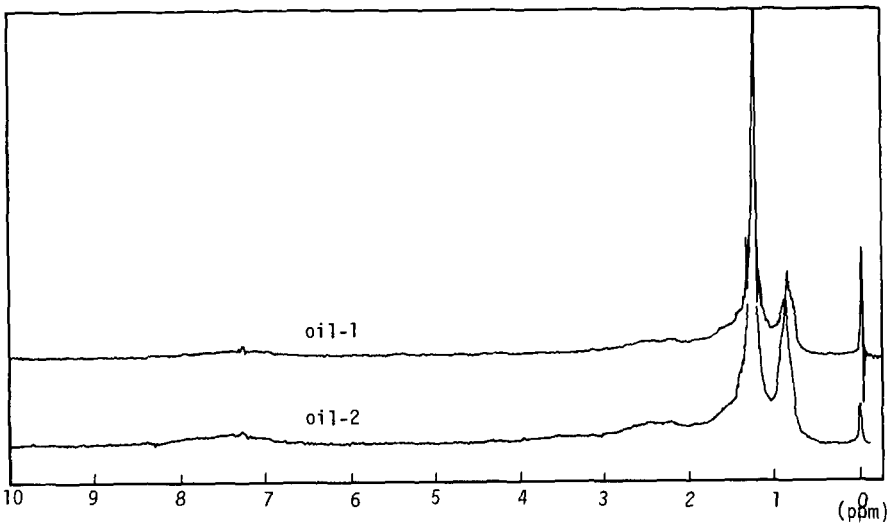

Fig. 3 H-NMR spectra of oils from inertinite hydrogenation at 400°C(Rt:30 min.)

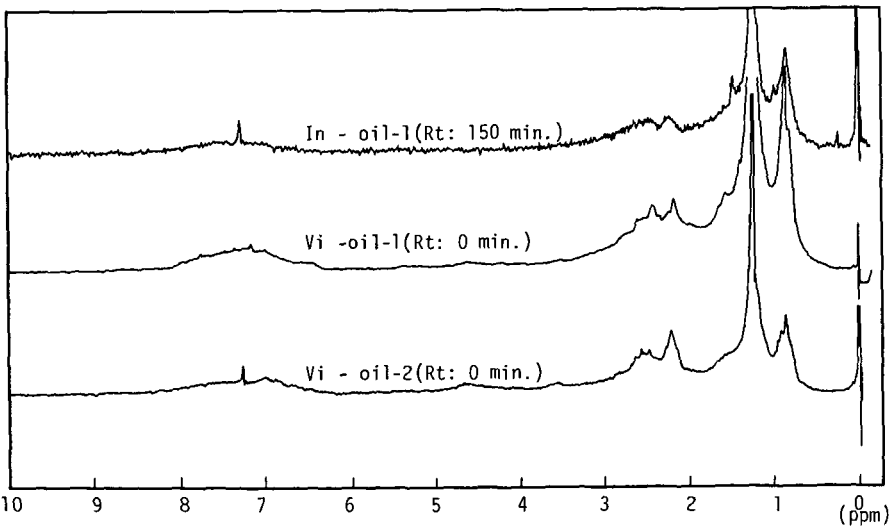

Fig. 4 H-NMR spectra of oils from inertinite and vitrinite hydrogenation at 400°C

STRUCTURAL ANALYSIS OF COALS AND COAL DERIVATIVES USING REFERENCE POLYMERS AND THE C-H-O TERNARY DIAGRAM

J.F. Stephens

CSIRO Fuel Geoscience Unit
North Ryde, N.S.W., Australia 2113

INTRODUCTION

The C-H-O ternary diagram is a most effective tool for dealing with the complexities of the chemical structure and reactivity of coals and coal derivatives. Three papers submitted recently discuss the geochemistry of coals(1), the structure of coals(2) and an overview of the conversion of brown coal to oil(3) with its aid. Previously there has been only limited use of the ternary diagram in coal chemistry(4,5) except in the form of the van Krevelen H/C vs O/C diagram(6) which is a simplified version of the C-H-O ternary diagram.

The full C-H-O ternary diagram has been found to offer a clearer and more quantitative approach to problems in coal chemistry than the van Krevelen diagram. It has been of particular value in conceptualizing model molecules of coals and coal derivatives. In the theoretical approach described here these model molecules are in essence 'hybrid polymers' assembled from a wide range of reference polymers which report in the same general area of the C-H-O ternary diagram as coals(2). The reference polymers are based upon the structures of benzene, naphthalene, anthracene (phenanthrene), pyrene and dibenzanthracene as representative of the likely benzenoid structures in coal. These aromatic structures have been modified by a variety of substituents such as aliphatic chains of various lengths and hydroxyl groups as well as ortho-attached alicyclics, furan and cyclopentadiene, and the monomer structures have been linked together either directly or via ether or carbonyl groups. Varying degrees of polymerization, from the dimer to the infinite polymer of these structures, were plotted on C-H-O ternary diagrams as shown in Figure 1, where, as an example, the disposition within a segment of the C-H-O ternary diagram of reference polymers incorporating the furan structure is shown. Each inverted triangle, such as JKL, indicates the distribution of a family of polymers with the same substituent/s on each monomer unit. From right to left in Figure 1 the substituents associated with each triangle are: none, methyl, alicyclic ring plus hydroxyl, alicyclic ring and lastly hexyl aliphatic chain. The relative positions of the individuals in each family are the same within their respective triangles as illustrated in greater detail for the unsubstituted family of the triangle JKL on the right of Figure 1. The simplest individual in the family, the dimer of furan, reports at the left hand end of the baseline (J) while the infinite polymer of furan reports at the right hand end (K), with polymers of intermediate degree reporting at points along the baseline, the distance between them getting smaller with each increase in degree of polymerization. The lines within the triangle give the locations of the corresponding polymers incorporating benzene, naphthalene, anthracene (phenanthrene) and dibenzanthracene, each group occupying a line further and further removed from the base of the triangle. The polymers incorporating pyrene report on a line to the right of the triangle. The data given in Figure 1 also do duty for the corresponding thiophen structures, the difficulty of the presence of nitrogen and sulphur in coal composition being overcome by replacing them with their valence equivalents, C+H for N and O for S.

The 'law of levers' is used to assemble model coal molecules(1,7). This 'law' is the formal expression of the observation that when two or more substances are compounded together then the product has a composition that is intermediate to those of the contributing substances. Moreover the composition of the product is closer to that of the major contributor than to that of any of the others. Thus as it applies here: the total product of compounding together any quantities of any

numbers of members of a ternary system lies at the centre of gravity of their distribution on the ternary diagram. This also holds in reverse, for the decomposition of a member of a ternary system into its constituent parts.

The simplest example of the 'law of levers' is the compounding of two substances D and E into a product F in the C-H-O ternary system. This is expressed as follows.

$$\alpha \begin{pmatrix} C \\ H \\ O \end{pmatrix}_D + (1-\alpha) \begin{pmatrix} C \\ H \\ O \end{pmatrix}_E = \begin{pmatrix} C \\ H \\ O \end{pmatrix}_F$$

D and E lie at the end of a line given unit length in the ternary diagram; F, the product of their compounding, lies on the line between them at the fractional distance α from E and $(1-\alpha)$ from D. If F lies close to E then α is small and D makes only a small contribution to the composition of F while E makes a correspondingly larger contribution.

In this communication the 'law of levers' is used both notionally and by way of calculation in the application of the C-H-O ternary diagram and reference polymers to three aspects of coal science and technology.

THE CHEMICAL AND STRUCTURAL MATURATION OF AUSTRALIAN VITRINITES

It has been found that concentrates of Australian vitrinites cluster into three major compositional groups labelled x, y and z in order of increasing maturity(1). Model structures x', y', y'' and z' with compositions corresponding to the median values of each of these groups were assembled by linking together reference polymers in linear assemblies, it being assumed that the required molecular masses were infinite.

The application of these procedures led to each model coal structure having its maximum or close-to maximum possible aromatic character. These model structures are presented as lists of relative proportions of structural components per 1000 carbon atoms in Table 1. Their ternary coordinates and the coordinates of the median compositions of the corresponding cluster of vitrinites are also listed. Structures y' and y'' were assembled to demonstrate the effect on aromaticity of changing proportions of alicyclic to aliphatic structures.

The compositions of the models were expressed as molecular formulae, each containing 1000 carbon atoms. The ternary diagram and the 'law of levers' were then used to establish the reactions of Equations 1 to 3 by which coal of composition x could mature to y and then to z, forming the new structures y''' and z'' from x'.

$$\underset{x'}{C_{1000}H_{908}O_{92}} \rightarrow 0.973(\underset{y'''}{C_{1000}H_{790}O_{78}}) + 16.1H_2O + 26.8CH_4 \qquad 1)$$

$$\underset{y'''}{C_{1000}H_{790}O_{78}} \rightarrow 0.965(\underset{z''}{C_{1000}H_{731}O_{39}}) + 31.8H_2O + 7.3CO \qquad 2)$$

$$\underset{y'''}{C_{1000}H_{790}O_{78}} \rightarrow 0.969(\underset{z''}{C_{1000}H_{731}O_{39}}) + 30.4H_2O + 4.0CO_2 \qquad 3)$$

The elimination of methane and water in these reactions leads to an increase in bonding in the residues so that the formation of y''' proceeds via the introduction of 43 new bonds into the residue of x' while further maturation to z'' requires the formation of a further 30 to 33 bonds. The structure x' contains 69 linearly linked substructures per 1000 carbon atoms so that each of the substructures of x' forms on average 1.25 new bonds on changing to y''', increasing to 2.12 to 2.17 on changing to z''.

X-ray diffraction studies of coals by Cartz and Hirsch(8) and by Hirsch(9) suggest that there is only a slow increase in aromatic character in the bituminous coal range until the rank of ~89% carbon is attained when a comparatively abrupt change in molecular structure, including a rapid increase in aromatic character, occurs.

Coupling this X-ray diffraction data with the above structure modelling based solely on compositional data suggests
(a) that the substructures in bituminous vitrinite molecules consist principally of two or three-ring aromatic structures often including furan or cyclopentadiene moieties, and
(b) that in high rank bituminous vitrinites each substructure can be bonded on average to as many as four other neighboring substructures.

COAL HYDROGENATION

The Australian Coal Industry Research Laboratories have surveyed the hydrogenation potential of a wide range of Australian coals in recent years using a batch autoclave procedure(10). Their work can be divided into two parts, an initial small program in which carbon black feed stock oil was used as the hydrogenation vehicle and a second larger program in which tetralin was the vehicle. The essential differences between these two programs can be seen in Figure 2 where the positions of the average atomic compositions of the feed coals, the vehicles and the products of both series of experiments are plotted.

The first program was characterized by the use of some high rank feed coals and probably a limited transfer of hydrogen to the coals via the carbon black feed stock oil. Indeed application of the 'law of levers' to the relative dispositions of the reaction components on the ternary diagram suggests strongly that redistribution of the hydrogen already in the coals was a most significant aspect of the reactions. Thus both the insoluble residues and the distillation residues are significantly depleted in hydrogen relative to the feed coals while the hydrogen enriched fraction of the coals, the oil and the recovered solvent, probably also enriched in hydrogen, could not be separated by distillation.

In the second program, in which tetralin was employed as the vehicle, all reaction products except the insoluble matter contained more hydrogen and less oxygen than the feed coals. The tetralin vehicle was also recovered at the end of these reactions with only slight changes to its composition. While a significant proportion of the hydrogen consumed in these reactions was lost in by-product molecules such as water and methane, another substantial proportion contributed to the formation of the coal extracts. As can be seen by further application of the 'law of levers' to Figure 2 most of this hydrogen formed part of the 42 atomic percent of the coal extract which in the average case distilled as oil, leaving a distillation residue only marginally enriched in hydrogen with respect to the parent coal.

This analysis highlights the role that the vehicle plays in reactions designed to obtain liquid fuels from coals.

ASPECTS OF THE SUPERCRITICAL-GAS EXTRACTION OF A COAL

Bartle, Martin and Williams(11) have examined the chemical nature of a supercritical-gas (toluene) extract of a low rank coal (~83% carbon) from the Markham Main seam, United Kingdom. The extract was obtained at the Coal Research Establishment of the British National Coal Board. This work is significant for the insight it permits into the structure of coal as well as for the opportunity it opens up of liquefying coal under mild conditions.

The extract, which constituted 17% of the original coal, was first fractionated by solution and chromatographic techniques. The fractions were then characterized by

elemental and functional group analysis, ^{1}H nmr spectroscopy and isopiestic molecular weight determinations. These data were supplemented by ^{13}C nmr, mass and ir spectroscopy. Within the frameworks of empirical formulae provided by the elemental analysis and the molecular weight determinations, the ^{1}H nmr spectroscopy data were used to generate structural models for the various fractions of the extract. The method of model building used by Bartle, Martin and Williams(11) was based principally on nine factors (derived from the ^{1}H nmr data) of which five are referred to here. These are

i) AlkC - the number of aliphatic and alicyclic carbon atoms in a structure.
ii) RJ(CH_2) - the number of ring joining CH_2 groups in a structure.
iii) C_R - the number of aromatic ring carbons in the 'average equivalent hydrocarbon' (aeh) corresponding to a structure.
iv) C_J - the number of ring joining carbons in the aeh.
v) H_R - the number of hydrogen atoms in the unsubstituted nucleus of the aeh.

Complete understanding of the meaning of these definitions requires reference to the work of Bartle, Martin and Williams(11) and to that of Bartle and Smith(12,13) who originated much of this technique when studying the structure of tars.

In the present study these factors were divided by $\overline{C}$, the number of carbon atoms in the formula of the structure in question. This enabled ready comparison of the factors between structures of different composition, organization and size.

The factors C_R, C_J and H_R were used by Bartle, Martin and Williams(11) to define aromatic nuclei for their model structures. This was achieved by using a three dimensional rectangular graph on which these three factors for the various fractions of the extracts were compared with those for a wide range of representative aromatic hydrocarbon types. The representative aromatic hydrocarbon type selected by this comparison was then made into a complete model structure by the addition of other structural details defined by the other factors. Two aspects of this work have been reexamined by the present author with the aid of the C-H-O ternary diagram. First the composition of the various fractions of the extract are compared with those of the macerals of the parent coal using the analytical data of Given, Peover and Wyss(14). Second, new model structures are suggested for the largest fraction of the extract, Band A_1.

Origins of Fractions of Extract

In Figure 3 the four fractions known as Bands A, B, A_1 and B_1, which constitute over 80% of the extract, are shown to cluster around the position of exinite while the remainder of the extract, the benzene insoluble fraction, reports near the position of the vitrinite. In fact the weighted mean composition of Bands A, B, A_1 and B_1 reports at almost the same position as that of the exinite, the two sets of C-H-O ternary coordinates being 0.46759, 0.49686, 0.03555 and 0.46728, 0.49837 and 0.03435 respectively. This close match may be somewhat fortuitous as the petrographic purity of the exinite used for elemental analysis was given as 88%. Nevertheless, it is very probable that the greater part of the supercritical-gas extract came from the exinite of the parent coal.

The benzene insoluble fraction lies on the line joining the position of the vitrinite to that of the benzyl radical $C_6H_5CH_2^{\cdot}$(0.500,0.500,0.0), suggesting strongly that this fraction was derived from the vitrinite by reaction with benzyl radicals from the toluene solvent. Application of the 'law of levers' gives a 13.5 atomic percent benzyl contribution to the composition of the benzene insoluble fraction, that is ~2.2 atomic % of the whole extract. While Bartle, Martin and Williams expressed the opinion that the extract was formed from the coal by mild pyrolysis during the supercritical-gas extraction process, they also reported the formation of a minor amount of bibenzyl which they attributed to some pyrolysis of the toluene used as solvent. In these circumstances some reaction of the coal with the hydrogen and benzyl radicals from the toluene must occur. The minor amount of hydrogen released may well

have played a significant but as yet unidentified role in the process, just as the benzyl radicals apparently did.

The Chemical Structure of Band A_1 Fraction

The factors derived from ^1H nmr data by Bartle, Martin and Williams(11) provide a close specification of molecular structure, particularly when combined with compositional and molecular weight data.

The C-H-O ternary diagram and the reference polymers have been used to evaluate the structure suggested for the average molecule of the Band A_1 fraction by Bartle, Martin and Williams as well as to suggest other structures that meet the specifications either alone or in mixtures with other structures.

The procedure used by the present author to assemble the model structures from the reference polymers depended on knowing the distribution of the reference polymers on the C-H-O ternary diagram and the use of the 'law of levers' for guidance in choosing combinations likely to have the right composition. In order that the somewhat indefinite molecular weight specifications were met, the model molecules were assembled mainly from halves of reference dimers though, in a few cases, the model molecules were assembled from thirds of trimers. On several occasions, when the compositions of the model molecules so assembled were not quite as required, minor structural changes such as the addition or subtraction of substitutional groups (e.g. $-CH_2-$ and $-O-$) were made so that compositional requirements were met. Once a model molecule had been assembled, its five structural factors AlkC, $RJ(CH_2)$, C_R, C_J and H_R were compared with the experimental values for the Band A_1 fraction. On some occasions the model molecules were rearranged in attempts to improve the agreement between the calculated and experimental values. This, however, was never a straightforward matter as the factors are not independent but are related in a complex manner. After some initial exploration four satisfactory results were obtained quite rapidly, two being individual model molecules and the two others being groups of four different model molecules with satisfactory average factors. The structures of these model molecules are given in Figures 4 and 5 and their compliance with the experimentally determined values of the factors are indicated by the error bar graphs in Figure 6. These model molecules satisfy the constraints as well, and probably better than, the model molecule proposed by Bartle, Martin and Williams, particularly with respect to composition. A moderate change in the structure, namely the replacement of four alicyclic carbon atoms and their hydrogens with four aliphatic carbon atoms and their hydrogens virtually eliminates this comparatively small compositional defect in the Bartle, Martin and Williams model molecule, a simplified version of which appears in Figure 5.

All the model molecules have a certain general similarity confirming that the factors derived from the ^1H nmr data coupled with compositional and molecular weight data can only arise from a narrow range of molecular structures. Improvement in molecular weight determinations would appear to be the major need for further restricting and thus improving the choice of structures. The structural features of these model molecules are most easily appreciated by inspection of those labelled M and N in Figure 5. These were formed by 'averaging' the previously formed model molecules. Both M and N are needed as the 'average' includes only half of an alicyclic ring. Two features stand out. First, the dominance of aliphatic over alicyclic components in the non-aromatic part of the structures. Second, the extended nature of the aromatic cores of the molecules which, however, would probably yield derivatives of mainly naphthalene and benzene on degradation because they incorporate pentacyclic structures.

The aliphatic portions of all the model molecules are shown in Figures 4 and 5 as single chains for convenience only. Their real distribution would be quite diverse(11) and could well extend to cross-linking. This could occur either

between otherwise unattached aromatic sub-structures or within a single structure, taking a partly alicyclic form incorporating some other number of carbon atoms than the usual five or six. Either of these possibilities would probably require a simplification of the aromatic portion of the structure, such as the opening of a pentacyclic ring, for the maintenance of the structural factors near the required values.

CONCLUDING REMARKS

The C-H-O ternary diagram has been shown previously to provide most useful insights into the chemistry of fossil fuels. Here it has been employed in conjunction with a series of reference polymers to generate information on the structural aspects of both coal maturation and the derivation of liquid fuels from coal.

The use of the C-H-O ternary diagram with the reference polymers provides a planar system of analysis which reduces the need for the three dimensional rectangular system used by Bartle, Martin and Williams(11) to interpret the structural factors derived from their ^{1}H nmr data. It is both easy and useful to work out the structural factors as each model molecule of correct composition is formed. Often the results indicate the changes needed to a trial model to produce a better one. Alternatively the results may indicate plainly that particular types of trial models cannot be improved. The molecular structures suggested both in this communication and by Bartle, Martin and Williams are remarkably specific. They should be accepted with a modicum of caution as no allowance has been made for the normal uncertainty of compositional data or for some assumptions made of necessity by Bartle, Martin and Williams in the interpretation of their ^{1}H nmr data.

REFERENCES

1. J.F. Stephens, Fuel, submitted (1978).
2. J.F. Stephens, Fuel, in preparation.
3. H.A.J. Battaerd, and D.G. Evans, Fuel, submitted (1978).
4. W. Francis, "Coal : Its Formation and Composition", E. Arnold, London, 1954, p.304.
5. T.K. Ghosh, Fuel, 50, 218 (1971).
6. D.W. van Krevelen, "Coal, Typology, Chemistry, Physics, Constitution", Elsevier, Amsterdam, 1961.
7. G. Masing, "Ternary Systems" (Trans by B.A. Rogers), Dover, New York, 1944.
8. L. Cartz, and P.B. Hirsch, Trans. Roy. Soc., 252(A), 557 (1960).
9. P.B. Hirsch, Proc. Roy. Soc., 226(A), 143 (1954).
10. Australian Coal Industry Research Laboratories, Reports No. PR75-6, PR75-14, PR76-8, PR77-1, PR77-8, PR77-15 (1975-77).
11. K.D. Bartle, T.G. Martin and D.F. Williams, Fuel, 54, 226 (1975).
12. K.D. Bartle and J.A.S. Smith, Fuel, 44, 109 (1965).
13. K.D. Bartle and J.A.S. Smith, Fuel, 46, 29 (1967).
14. P.H. Given, M.E. Peover and W.F. Wyss, Fuel, 39, 323 (1960).

Table 1

Proportions of Structural Features Constituting C_{1000} Linearly Linked Model Coal Molecules Together with Their Ternary Coordinates and Those of the Median Coals Aimed At

Structural features	x'	y'	y''	z'
benzene	27.3	13.5	15.7	0
naphthalene	30.3	18.9	23.6	0
anthracene	6.1	18.9	18.3	6.4
dibenzanthracene	3.0	8.1	7.9	32.1
cyclopentadiene	12.1	8.1	10.5	9.6
furan	9.1	10.8	10.5	9.6
aliphatic - CH_2	142.4	56.8	162.3	118.6
alicyclic - CH_2	157.6	162.2	0	25.6
-O-as hydroxyl and ether	48.5	46.0	41.9	16.0
>C = O groups	27.3	21.6	26.2	12.8
quinone oxygens	6.1	0	0	0
		Coordinates		
Model coal molecule				
C	0.50000	0.53546	0.53501	0.56522
H	0.45455	0.42258	0.42297	0.41304
O	0.04545	0.04197	0.04202	0.02174
Median coal				
C	0.50000	0.53500	0.53500	0.56500
H	0.45400	0.42300	0.42300	0.41300
O	0.04600	0.04200	0.04200	0.02200

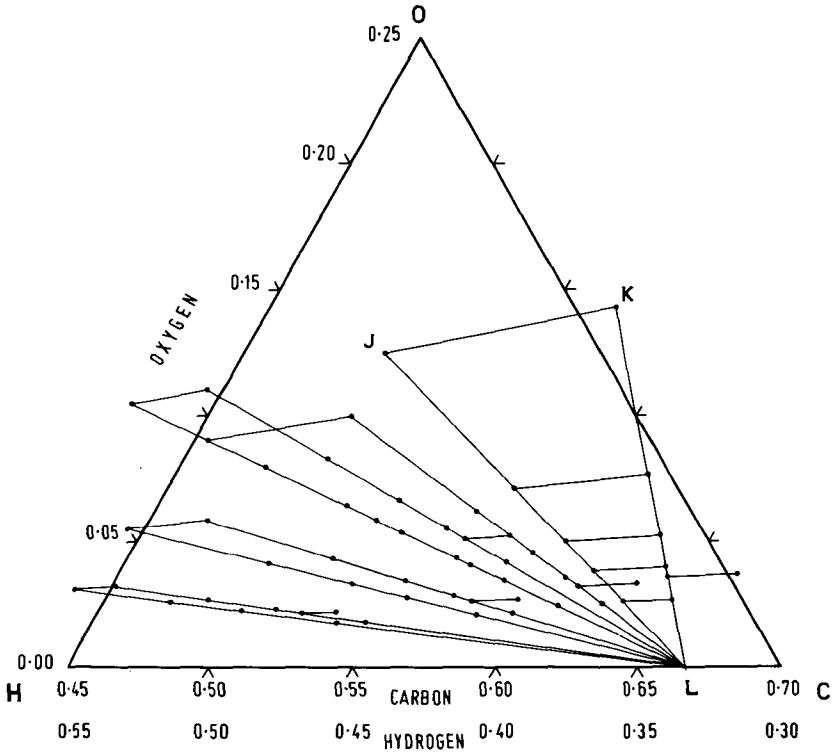

Figure 1. The distribution of the furan-containing reference polymers on a segment of the C-H-O ternary diagram. C, H and O values given as atomic fractions.

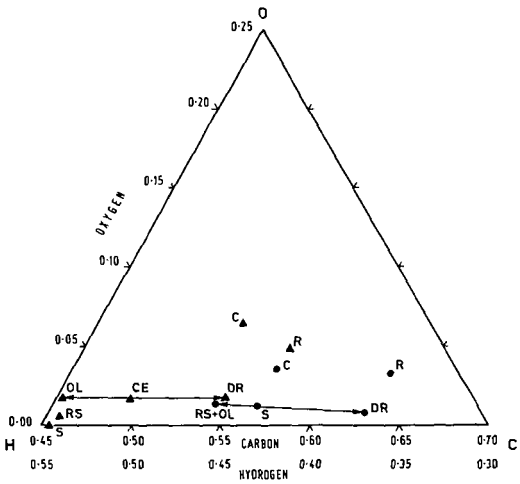

Figure 2. ACIRL coal hydrogenation results. ▲, components in tetralin experiments; ●, components in carbon black feed stock experiments; CF, coalfeed; S, solvent; RS, recovered solvent; CE, coal extract; OL, oil; DR,distillation residue; R, insoluble residue.

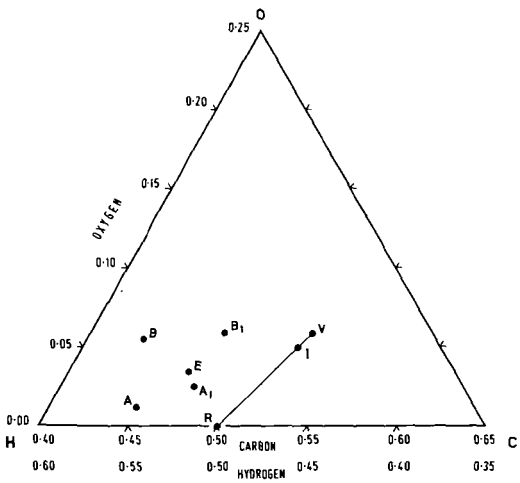

Figure 3. Super critical-gas extraction of coal. Locations of Bands A, B, A_1, B_1. I, benzene insolubles; R, benzyl radical; E, Markham Main exinite; V, Markham Main vitrinite.

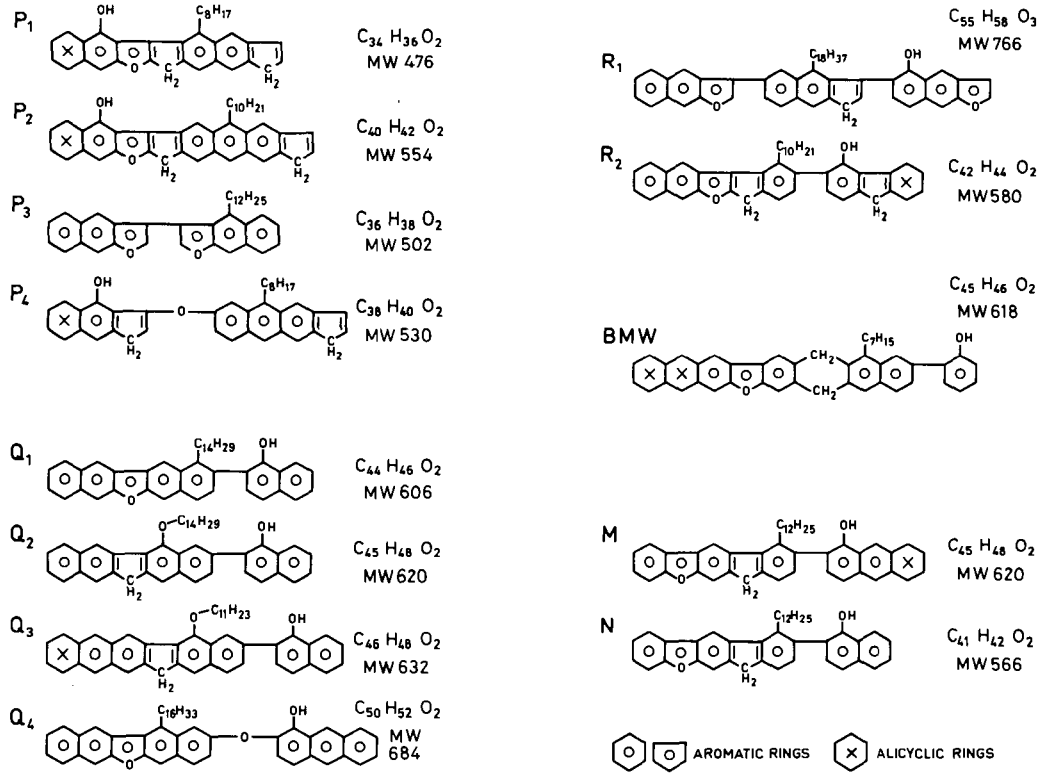

Figures 4 and 5. Structures of model molecules with compositions approaching that of Band A_1.

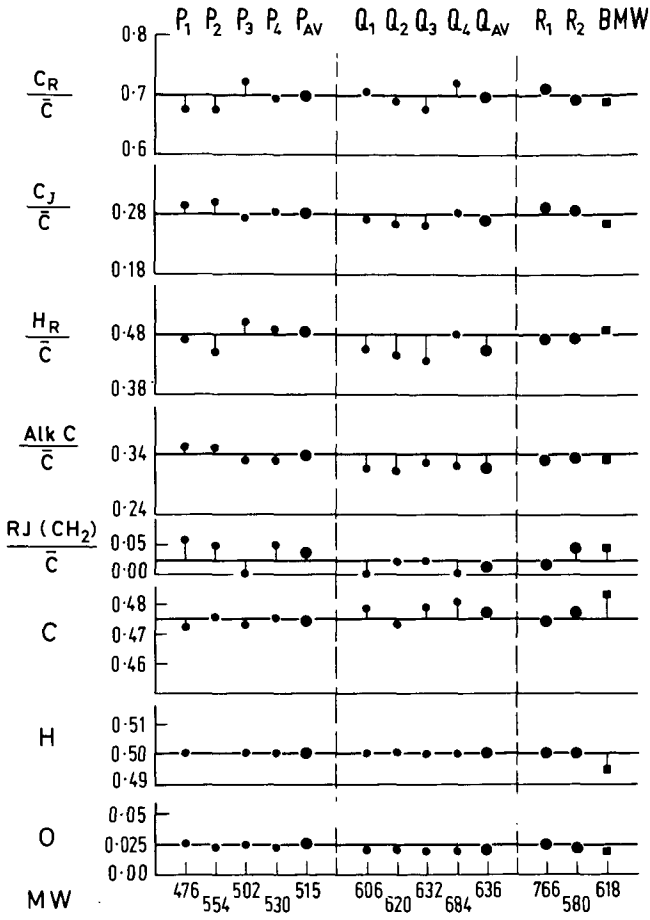

Figure 6. Error bar graphs of structural factors and compositions for the model molecules of Figures 4 and 5 and the averages, P_{AV} and Q_{AV}, for two groups of them.

THE INTERACTIONS OF GASES WITH COAL: STRUCTURAL INFERENCES*

E. L. Fuller, Jr.

Chemistry Division
Oak Ridge National Laboratory
Oak Ridge, Tennessee 37830

Current and proposed efficient uses of coal involve the interaction of fluid phases with coal or coal chars. This study deals with the mode of interaction of gases with coal from the standpoint of analyses related to the structure of coal and implications pertinent to mechanisms of fluid phase reactions. "Coal is an amorphous substance and it is difficult to define its structure.... The fundamental chemistry of coal liquefaction will probably remain poorly understood until coal structure is better defined."(1) There is considerable effort to define this structure in terms of internal surface area and microporosity in studies of vapor (2) (3) (4) and liquid (5) interactions. Microgravimetric sorption equipment and techniques (6) have been used to elaborate the thermodynamics and kinetics described in this text. The coal, high-volatile A-bituminous Illinois No. 6, was obtained at the mine face and stored in argon prior to grinding (< 200 mesh) in argon.

Sorption-desorption isotherms are given in Figures 1-3 for (a) N_2 [classical vapor for surface area determinations],(7) (b) CO_2 [often suggested as a means of determining the "effective area" of coal],(2) and (c) H_2O [of interest because of its inherent content in coal and its potential use as a reactant at elevated temperatures]. Classical BET (7) analyses of the data indicate a marked disparity in the apparent specific surface area of this coal: 2.8, 128, and 68.2 m^2/gm for N_2, CO_2, and H_2O respectively. (The N_2 value is consistent with the predominant 1-10 μm size distribution observed microscopically.) These values vary markedly and seem to be "dominated by dipolar and London forces" as noted in related studies.(5)

Alternate analyses of the isotherms can be performed in terms of the sorption potential: $\varepsilon = -RT \ln P/P_o$ (Polyani, circa 1914).(8) Various relationships between this quantity and the sorbate concentration, Γ, have been used.(8)

In terms of the chemical (9) and physical structure (10) of coal [polynuclear aromatic rings with methylenic linkages with numerous polar functional groups, oriented to some extent in parallel layers] one can readily envision the energetics of the sorption process to follow a distribution of the type (11) (12) $\varepsilon = \varepsilon^\circ e^{-a\Gamma}$. If we were to view the substrate as a yielding "soft" electronic structure (extensive pi bond network with the polar entities rather randomly distributed), we would anticipate considerable energetic (electronic) perturbation by the sorption processes. Then a distribution like that above would be expected to apply. Such a model is akin to the image forces induced in the mobile electrons when sorption occurs on metals.(13) Our experimental results follow the trends inherent in this model for each of the gases. The data for water is shown in Figure 4. Many have attributed the variation of sorption capacity to temperature effects on the diffusion rate by virtue of very large activation energy for diffusion into the coal matrix.(14) Our kinetic results were not amenable to interpretation in terms of diffusion mechanisms. However good adherence to a mass action second order (15) was noted. An example is given in Figure 5 for one incremental pressure change employed in the construction of the water isotherm. One should note that this data was obtained under isobaric, controlled pressure, conditions ($\pm 0.0001\ P_o$) for the time required to evaluate the steady state condition at each chosen pressure. The technique and evaluation

*Research sponsored by the Office of Basic Energy Sciences, Division of Material Sciences, U. S. Department of Energy under contract W-7405-eng-26 with the Union Carbide Corporation.

procedures are outlined elsewhere.(16) Carbon dioxide results were more complex and indicated that there were two second order processes in play.

With such assurance that we are dealing with steady state conditions, based on this kinetic continuity and accountability, we can confidently attribute the desorption retention to structural changes induced in the coal matrix. This retention is totally removed in vacuo [10^{-10} P_o] albeit quite slowly [24+ hours]. Such behavior could arise if trace amounts of a second vapor, i.e., H_2O in N_2, were adsorbed. We have employed $99.999_5\%$ N_2 and have not noted the retention phenomena on rigid substrates in this microgravimetric system. Many related systems show a similar retention where there is a "change in 'structural' arrangement in the molecular network".(17)

We can gain further insight into the process in terms of the molecular properties of the sorbate molecules. If there are induced effects in the substrate, one would anticipate the magnitude of the energy of interaction to be proportional to energy arising from the intermolecular forces between two sorbate molecules in the gas phase.(18) There is good correlation between the dispersion ($\frac{3}{4}\alpha^2 h\gamma$) and electrostatic ($\frac{2}{3}\frac{\mu^4}{kT}$) energies and the ε° term inherently evaluated in our treatment of the sorption isotherms in the form of Figure 4. The correlation is shown in Figure 6.

These results are to be contrasted with that predicted for sorption onto a rigid ("hard") electrostatic field (13) and noted experimentally as a first power relation (19) in polarizability (α) and second power in dipole moment (μ).

In light of these studies and the marked swelling properties of coal, even on CO_2 and CH_4 sorption,(20) we must question the existence of a fixed definable pore structure and/or internal surface area of coal. Further analyses on this and coals of varied rank are warranted. One would anticipate that the results might range from the marked sorption swelling of cellulosic materials to the intercalation phenomena noted for graphite.(17)

Acknowledgment: This work is the result of the diligent and concientious efforts of the members of the Massachusetts Institute of Technology School of Chemical Engineering Practice, M. M. Alger, O. K. Chow, M. Z. Khan, and S. M. Senkan.

References

1. W. H. Wiser and L. L. Anderson, Ann. Rev. Phys. Chem. 26 339 (1975).

2. J. Medik, Fuel 56 131 (1977).

3. K. Tomkow et al., Fuel 56 101 (1977).

4. Z. Spitzer et al., Fuel 56 313 (1977).

5. J. W. Larson et al., Fuel 57 309 (1978).

6. E. L. Fuller, Jr. et al., Prog. Vac. Sci. Tech. 3 71 (1974) and 1 265 (1972).

7. S. Brunaur, P. H. Emmett and E. Teller, J. Am. Chem. Soc. 60 309 (1938).

8. A. W. Adamson, "Physical Chemistry of Surfaces," Wiley, p. 575 (1976).

9. (a) G. R. Hall and L. B. Lyon, Ind. Eng. Chem. 56 36 (1962); (b) W. H. Wiser, Ref. 1 (1975).

10. P. B. Hirsch, Proc. Roy. Soc. 226A 143 (1955).

11. J. H. deBoer and C. Zwikker, Z. Phys. Chem. B3 407 (1929).

12. R. S. Bradley, J. Chem. Soc. (1936) 1799.

13. W. A. Steele, "The Interactions of Gases with Solid Surfaces," Ch. 2, Pergamon (1974).

14. S. P. Nandi and P. L. Walker, Fuel 43 385 (1964).

15. S. W. Benson, "The Foundations of Chemical Kinetics," McGraw-Hill (1960).

16. E. L. Fuller, Jr., "Microgravimetric Studies of Catalysts in Microweighing in Vacuum and Controlled Environments," editor, A. W. Czanderna, Elsevier (in press, 1978).

17. P. J. Sereda and R. F. Fedlman, Ch. 24 in "The Solid-Gas Interface," editor, E. A. Flood, Vol. II, Marcel Dekker (1967).

18. J. O. Hirschfelder et al., "Molecular Theory of Gases and Liquids," Ch. 13, Wiley (1954).

19. E. L. Fuller, Jr. and P. A. Agron, "Reactions of Atmospheric Vapors with Lunar Soils," ORNL-5129, March 1976.

20. (a) H. Briggs and R. P. Sinha, Proc. Royal Soc. Edin. 53 48 (1933); (b) A. Czaplinski, Arch. Gorn. 16 227 (1971); (c) E. A. Flood and R. H. Heyding, Can. J. Chem. 32 660 (1954).

FIG. 1. Nitrogen 77 K

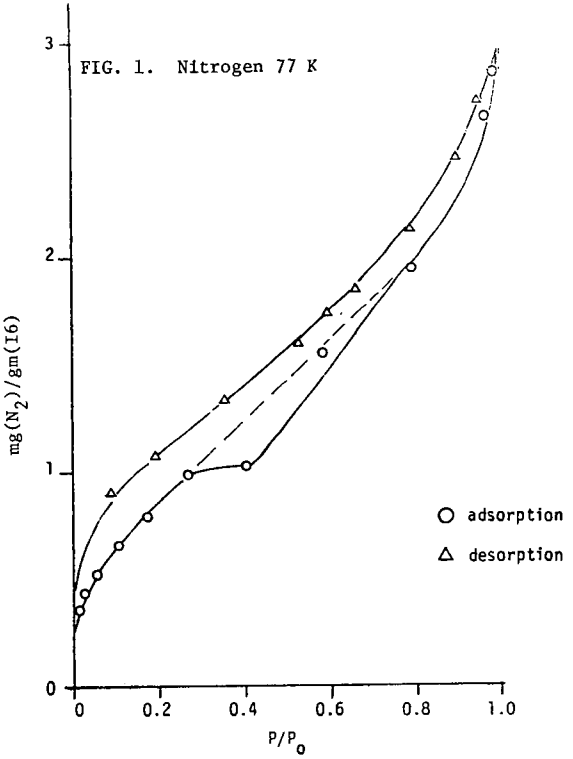

FIG. 2. Carbon Dioxide 195 K

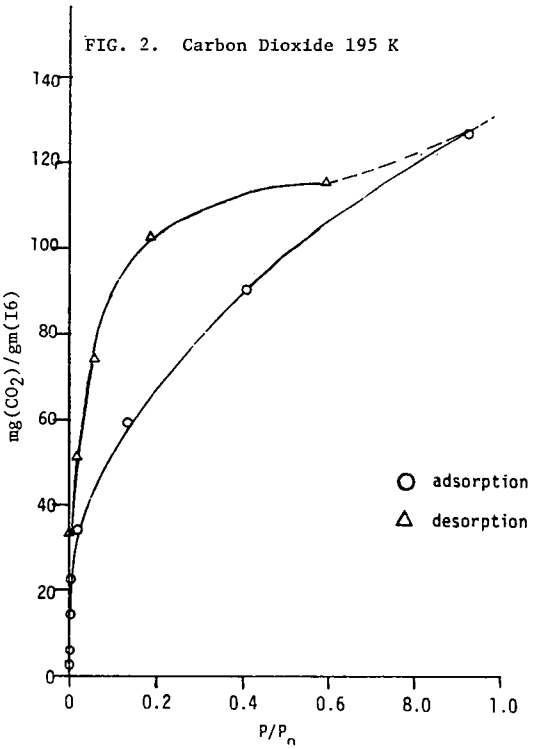

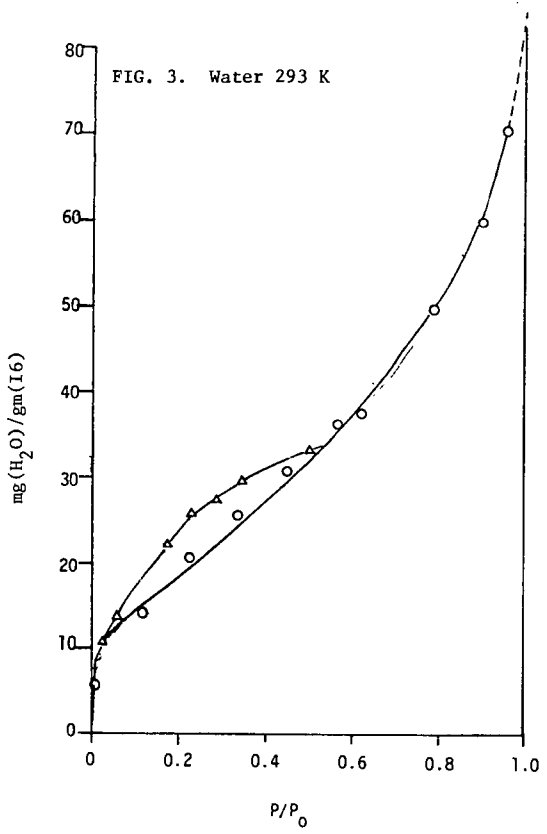

FIG. 3. Water 293 K

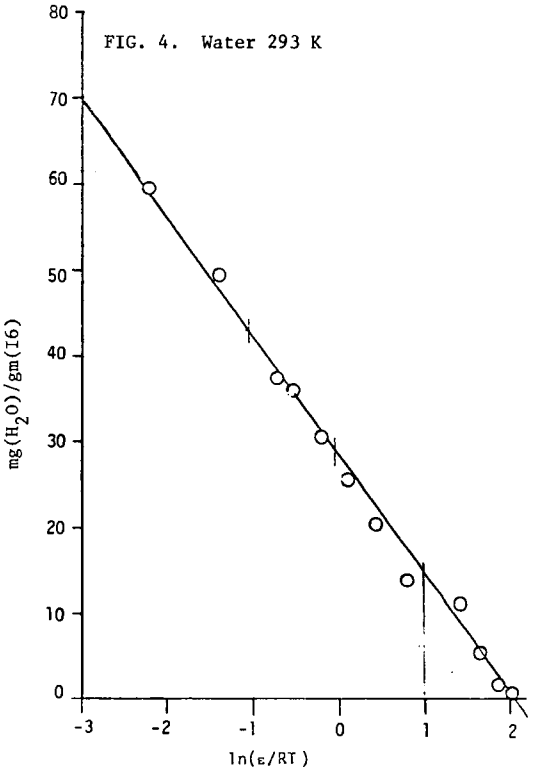

FIG. 4. Water 293 K

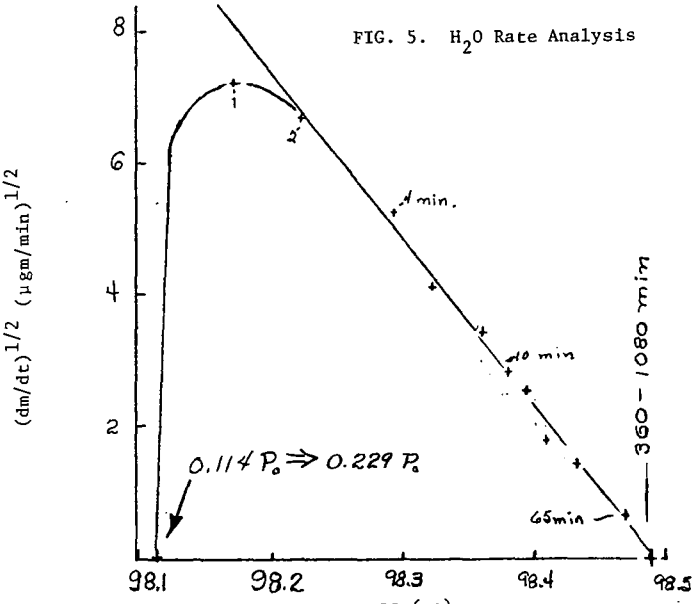

FIG. 5. H_2O Rate Analysis

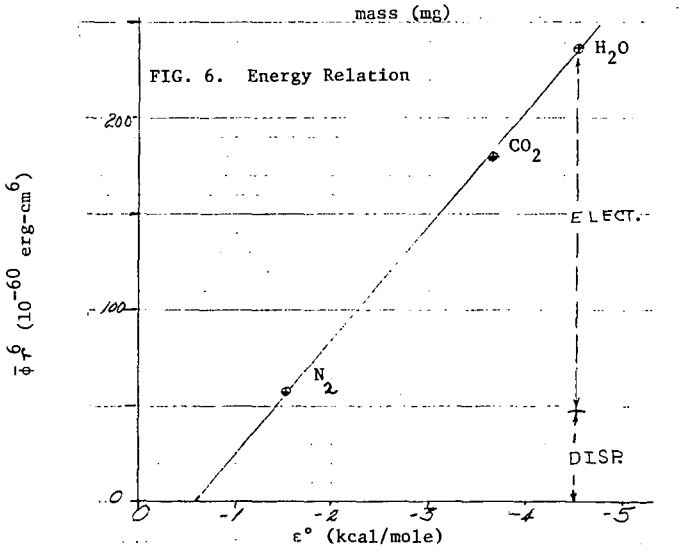

FIG. 6. Energy Relation

Coal Hydrogenation Char as Blending Agents for Coke Production

Ralph E. Wood and David M. Bodily

Department of Mining and Fuels Engineering
University of Utah
Salt Lake City, Ut 84112

Metallurgical coke, necessary in the production of "hot metal" in the conventional blast furnace, requires large quantities of coal with specific physical properties. These coals are expensive because of their relative scarcity in comparison with non- or marginally coking coal. For many years blast furnace practice, the world over, has utilized minimum amounts of premium coals by blending coals with different properties to produce a mix that will give an acceptably strong and porous coke.[1] In some areas of the world, Japan for example, as many as 15 different coals may be blended to provide an acceptable mix.[2] These coals are purchased in Canada, Australia and the United States and only small quantities of Japanese coals are used because of their marginal coking quality. Practice in the United States requires the use of minimum quantities of premium coals and maximum use of marginally coking coals.

As an example of the U.S. situation, U.S. Steel's Geneva Works, near Provo, Utah, uses a blend of three coals to produce coke with a stability factor (percentage of the original coke remaining at a preselected screen size, following a fixed tumbling sequence) that is known to be required for iron production with a fixed blast furnace ore, limestone and coke feed. Captive coal from U.S. Steel's Geneva, Utah, and Somerset, Colo., mines (nearly equivalent in coking properties) are blended with 20% to 30% of coal from the Mid-Continent Coal & Coke Co. mine at Coal Basin, Colo. The Geneva and Somerset coals are high volatile bituminous in rank, with very low fluidity (1-5 dial divisions per minute in a Grisler Plastometer) and only minimum coking character as evidenced by a Free-Swelling Index of no more than 1. The Coal Basin coal is a medium volatile bituminous material with plasticity of more than 20,000 dial divisions per minute and a Free-Swelling Index of 3 or 4.

The present study is a laboratory scale examination of the possibility of using coal liquefaction char residues as a blending material with marginally coking coals to enhance the desired properties of the resulting coke.

Experimental

Standard blends of U.S. Steel, Geneva, Utah, coal and Mid-Continent Coal & Coke Co., Coal Basin coal were used as the base case for comparison with cokes produced using Geneva coal with added amounts of residual chars produced in the University of Utah's entrained-flow coal liquefaction reactor.[3] Proximate and ultimate analyses of the reference coals and the tested chars are shown in Table 1 and 2. The hydrogenation reactor conditions, as well as pertinent information with respect to the production of chars are included in Table 3. Properties of resultant cokes tested were Free-Swelling Index, strength, CO_2 burnoff rate and combustion temperature. Because only small quantities of char are available it was not possible to make strength or stability tests at the scale ordinarily required. Free-Swelling Index measurements were made on coke buttons resulting from ASTM test D720 applied to coals and blends.[4] Strength comparisons were made by measuring the pressure in pounds required to break the coke buttons produced in ASTM test D720, a dead weight gage was used for this measurement. Since this test was performed at such a small scale the results can be considered to be qualitative in nature and large-scale tests would be required for actual extrapolation to blast furnace operation.

Carbon dioxide burnoff rates were measured by heating coke samples (1 gram) at

900° C in a flowing stream of CO_2 for 1 hour[5]. Traces of oxygen were removed from the gas by passing it over a bed of hot copper turnings. The combustion temperatures were measured by heating a 1-gram coke sample in a stream of oxygen and noting the temperature at which a sudden increase in temperature was observed[6].

For each of the measurements made, a series of 3 to 6 replicates were made in an effort to improve the confidence in the final answer.

Results and Discussion

The original impetus for this study followed observation that some coal liquefaction chars show extreme swelling in the standard volatile matter test (ASTM Test D-3175-77). Some of these chars swell sufficiently to fill the entire crucible and thus indicate high fluidity in the plastic temperature zone. Figure 1 shows the Free-Swelling Index (FSI) of a variety of residual coal hydrogenation liquefaction chars as a function of the conversion level. These measurements were made with a single starting coal, Clear Creek, Utah, from Island Creek Coal Co.'s Utah #2 mine. The indication is that higher conversion leads to higher FSI numbers. Obviously, this function must peak out and descend with very high conversion when the remaining organic matter is insufficient to provide fluidity. However, in the 60- to 80%-conversion range the FSI numbers approach those of acceptable blending coals.

Figure 2 shows the effect on FSI of blending Coal Basin coal and two different chars with Geneva Coal. R-71 and R-85 chars were produced from the same starting coal. R-71 represents a conversion of 75% of the coal matter to liquids and gases while R-85 represents a conversion of 25%. The lower conversion char does not affect the FSI while the high conversion char produces the same change in FSI and as does the addition of the accepted blending coal. If FSI were the only criterion required for blending material then R-71 would make a good substitute for Coal Basin coal in the Geneva coke starting material.

In Figure 3 are shown the pressures required to break the coke buttons prepared in the FSI tests. In this case the low conversion char (R-85) produces coke buttons that are harder than those produced by the reference coal. The high conversion char (R-71) produces coke buttons that are weaker. It is tempting to say that a high conversion char should be added for increasing the plasticity of the blend and that a low conversion char should be added for strength. However, these tests are yet to be performed.

Table 4 contains the CO_2 burnoff rates of cokes produced at 70, 80 and 90% Geneva coal concentration for the reference coal and the two chars. The low conversion char approximates the standard blend in burnoff rate at 70% but is higher at 80 and 90%. The high conversion char is higher in burnoff rate at all concentrations.

Table 5 contains a similar comparison for combustion temperatures. At 70% concentration of Geneva coal the standard additive is considerably better (has a higher combustion temperature). At 80 and 90% the low conversion char has no advantage but the high conversion char is at least equal to the standard additive.

Addition of a high conversion char such as R-71 would result in addition of ash materials to the product coke. This is not desirable because of the additional slag produced in the blast furnace as well as the additional heat required from the coke to melt the slag produced by the ash. Considering the material of this study, a 20%-addition of Coal Basin coal would increase the ash from 5.0 to 5.3%. A 20%-addition of R-71 (22.1% ash) would increase this from 5.0 to 8.4%.

A formidable problem with the addition of these particular chars to coals for production of metallurgical coke is that $ZnCl_2$ was used as a catalyst in the hydrogenation-liquefaction procedure. Zinc is a very troublesome element

if present in blast furnace feed materials. Its compounds are reduced in the hot portion of the blast furnace, the metal is volatilized to the cooler portions of the upper area of the furnace. It tends to condense as ZnO and blocks small passageways such that the flow of gases may be seriously restricted. The oxide also tends to react chemically with Al_2O_3 in the firebrick lining of the furnace. This causes expansion and spalling of the brick surface. Chlorine is likewise an undesirable component of blast furnace materials because of its corrosive effects[7].

The data of Table 6 show the effect of successive leaching steps on the zinc content of the high conversion char (R-71). Seven leaches with HCl will reduce the $ZnCl_2$ equivalent concentration to 0.3% or 0.15% Zn. As a 20% component of the coal blend this would constitute only 0.03% Zn and would be quite acceptable.

It is apparent that some coal liquefaction chars do possess physical and chemical characteristics that would be desirable in coal blends used for the production of metallurgical grade coke. These are fluidity, strength and combustion temperature. The CO_2 burnoff rate was not improved by the addition of the chars used in this study.

ACKNOWLEDGEMENT

This work was supported by the U.S. Department of Energy, contracts EE-77-5-03-1484 and E(49-18)-2006.

REFERENCES

1. W. Beimann, H.S. Auvil and D. C. Coleman, High Temperature Carbonization, H. H. Lowry, Ed., "Chemistry of Coal Utilization, Wiley, N.Y., 1963, Ch. 11.

2. T. Miyazu, Y. Okuyama, N. Suzuki, T. Fukuyama and T. Mori, Nippon Kokan Technical Report--Overseas, December 1975, p. 1.

3. R. E. Wood and W. H. Wiser, Ind. Eng. Chem., Process Des. Devel., 15 (1), 144, (1976).

4. American Society for Testing and Materials, 1977 Annual Book of ASTM Standards, Part 26, 1977, p. 244.

5. W. K. Kinzer and R. E. Kusner, Proc. Ironmaking Conf., Iron & Steel Soc., AIME, Vol. 34, 2 (1975).

6. General Motors Corp., Test Methods for Coke, GM 4444-P.

7. H. E. McGannon, Ed., The Making, Shaping and Treating of Steel, U.S Steel Corp., Pittsburgh, PA, 1971., Ch. 15.

Table 1. - Proximate analysis of coals and chars

	% H_2O	% Ash	% Volatile matter	% Fixed carbon
Coal Basin, Colo.	1.1	6.5	24.0	68.4
Geneva, Utah	3.2	5.0	39.6	52.2
R-71	2.4	22.1	24.8	50.7
R-85	2.7	8.4	39.6	49.3

TABLE 2. - Ultimate analysis of coals and chars

	% C	% H	% N	% S	% O	% Zn
Coal Basin, Colorado	84.3	5.0	2.1	0.7	1.4	--
Geneva, Utah	72.0	5.0	1.7	.7	15.6	--
R-71 Clear Creek, Utah coal char	49.2	3.7	1.8	.4	6.8	16.0
R-85 Clear Creek, Utah coal char	72.8	5.4	1.8	.7	4.9	6.0

TABLE 3. - Hydrogenation conditions and product description for Clear Creek, Utah coal chars used in this study.

	R-71	R-85
Coal sample weight, grams	852.3	626.6
Weight $ZnCl_2$ grams	57.1	41.6
Weight ash, grams	90.6	59.8
Total sample, grams	1,000	728
Particle size, mesh	-100+200	-200
Temperature, ° C	493	493
Pressure, H_2	1,800 psi	1,800 psi
Reactor length, ft	66	86
Average residence time	50 sec	10 sec
% Solids (after toluene extraction)	24.3	74.1
% Liquids produced	71.9	19.4
% gases	3.8	6.5
% Conversion	75.7	25.9

TABLE 4. - CO_2 burnoff rate of coal-char blends

% Geneva coal	70 mg/g/min	80 mg/g/min	90 mg/g/min
Coal Basin Coal	3.25	4.33	5.00
R-85	2.97	5.75	6.31
R-71	4.70	4.80	8.67

TABLE 5. - Combustion temperatures of coal char blends, ° C

% Geneva Coal	70	80	90
Coal Basin Coal	687	660	611
R-85	649	603	594
R-71	647	670	654

TABLE 6. - Effect of Zn removal from char on FSI

Char R-71 16.0% $ZnCl_2$ content

No. of Conc HCl leaches*	%$ZnCl_2$	FSI
1	11.5	5.5
2	8.6	5.5
3	5.6	5.5
4	3.5	5
5	1.9	5
6	0.5	4
7	0.3	4

* Each leach 1 hour at boiling temperature (12 m HCl)

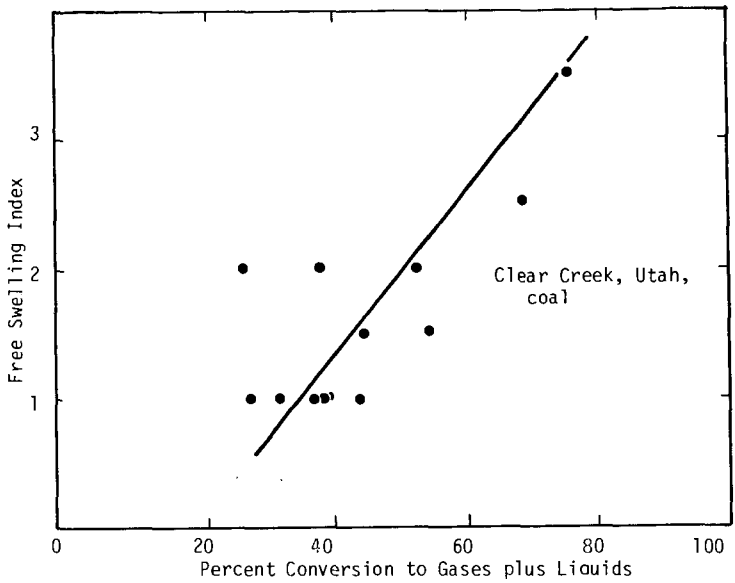

Figure 1. Capicity Hydrogenation Chars vs. Conversion Level.

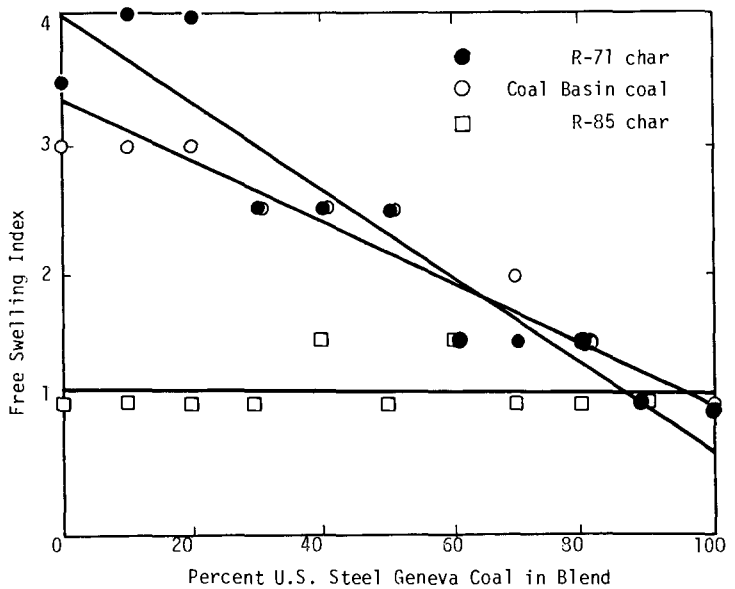

Figure 2. Swelling Capacity of Coal Blends.

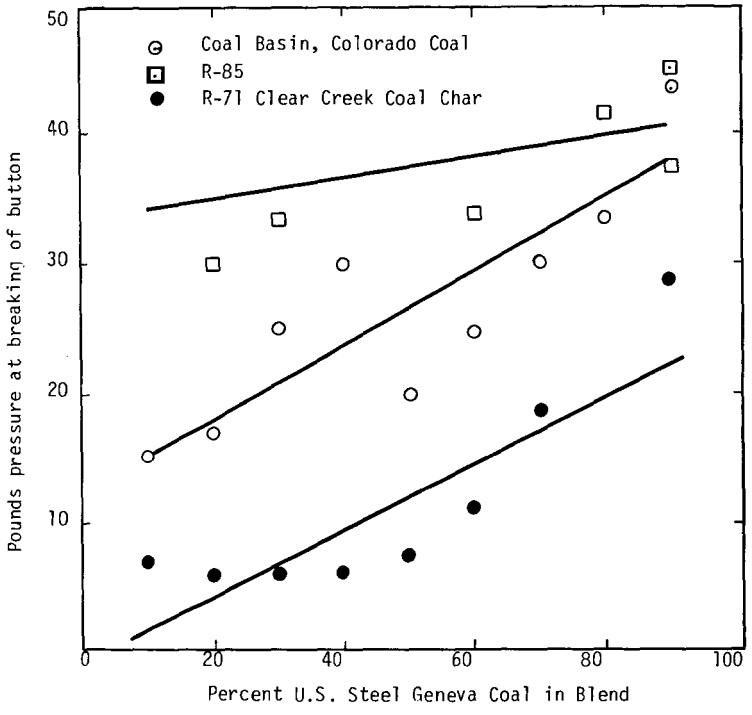

Figure 3. Breaking Pressure in Pounds for Volatile Matter Test Button.

The Initial Stage of Coal Hydrogenation in the Presence of Catalysts

Ryoichi Yoshida* and David M. Bodily

Department of Mining and Fuels Engineering
University of Utah
Salt Lake City, Ut 84112

Introduction

Several factors are important in the development of an hydrogenation process for the economic conversion of coal to a liquid fuel.[1,2] These include a better understanding of the structure of coal, the effective use of hydrogen and/or alternate reducing gases and the development of cheaper or more active catalysts.

This paper is concerned with the initial stage of coal hydrogenation, where the reactivity is greatly affected by the chemical structure characteristics of the coal and the conversion per unit of hydrogen consumed is high.[3,4] Several catalysts are studied and reactivity in an entrained-flow hydrogenation reactor and the chemical structure of the products are determined.[5]

Experimental

Clear Creek, Utah, coal was hydrogenated in a short-residence, entrained-flow reactor.[5] Zinc chloride, Co-Mo/Al_2O_3, presulfided red-mud and red-mud plus sulfur were used as catalysts. The coal particle size was -100+200 mesh and the catalyst ranged from 6.4% for $ZnCl_2$ to 10.7% for the other catalysts. The coal was also hydrogenated without catalyst. The temperature ranged from 400° C to 500° C and the hydrogen pressure was held at 1,800 psi. Residence time (8-372 sec) was varied by choice of the tube length (12-36 m). A typical analysis of Clear Creek, Utah, coal is shown in Table 1.

Products were separated by stepwise extraction using hexane, toluene and pyridine. The extraction scheme is shown in Figure 1.

Determination of C, H and N for each product was carried out by a micro method using a Perkin-Elmer 240 CHN Analyzer. Proton NMR spectra were measured at 90 MHz and 300 MHz. Molecular weights were determined by vapor pressure osmometry on Corona Wescan 117 Molecular Weight Apparatus.

Results and Discussion

The yields of hydrogenation products are shown in Table 2. Comparison of the initial stage of hydrogenation for 8-12 sec at 500° C in the presence of different catalysts and without catalyst shows conversions of about 20% for all samples. A catalytic effect on conversion and product distribution is not apparent. This indicates that at least 20% of Clear Creek, Utah, coal converts noncatalytically into liquid and gas. This is similar to the results obtained on Japanese coals[6,7].

In Figure 2 the effect of temperature and time at 500° C on conversion and product distribution using $ZnCl_2$ catalyst is shown. The effect of temperature during short residence times of 8 to 12 sec is not large. Conversions increase from 6% to 18% with the increase of temperature from 400° to 500° C. However, the effect of time at 500° C is large. For example, conversions increase from 18% to 35% during the period from 8 to 21 sec. The effect of reactor length on conversion at 500° C

* On leave from the Government Industrial Development Laboratory, Hokkaido, Sapporo Japan.

is also shown in Figure 2, using $ZnCl_2$ catalyst the conversions increase from 18% to 75% with an increase in reactor length from 12 m to 36 m. Using the other catalysts and with no catalyst the conversions are merely ca.20% at 36 m reactor length. This indicates that $ZnCl_2$ is a very active catalyst in the initial stage of hydrogenation.

These results suggest that in this reactor the reaction up to 500° C and 12 sec proceeds noncatalytically except when a very active catalyst is used. About 20% of the coal takes part in the reaction. At 500° C and after 12 sec, the reaction proceeds catalytically and is greatly affected by residence time.

In Figure 3 and 4 the results of ultimate analysis of each product are shown. The H/C atomic ratio decreases with increasing conversion, especially up to 20% conversion. The changes in liquid (oil + asphaltene -I) and asphaltene-II are remarkable. The O,N,S/C atomic ratio increases with conversion up to 20% conversion, and it is nearly constant in spite of the progress of conversion in the reaction beyond 20% conversion. At about 20% conversion the H/C ratio of each product for $ZnCl_2$ catalyst is lower than for other catalysts. This suggests that $ZnCl_2$ catalyzes reactions which decrease the H/C ratio.

Comparison of a typical proton NMR spectra of liquid (oil+asphaltene-I) measured at 90 MHz and 300 MHz shows two new bands in the aliphatic region at 1.5 ~ 1.8 ppm and 2.0~2.1 ppm in the 300 MHz spectra.[8] The hydrogen distribution of each product was obtained from NMR spectra. Hydrogens bound to aromatic carbons, Ha, and hydrogens bound to carbons α to aromatic rings, $H\alpha$, increase and the hydrogens bound to aliphatic carbons β or further from aromatic rings, Ho, decrease with increasing conversion.

Structural analysis was performed using the equation of Brown and Ladner[6,7,9]. Results of these calculations are shown in Figure 5. The carbon aromaticity, fa, increases and the aromatic hydrogen-to-carbon ratio of the hypothetical unsubstituted aromatic material, Hau/Ca, decreases with the increase of conversion. Up to 20% conversion the changes in liquid (oil + asphaltene-I) and asphaltene-II are significant. The main differences in the chemical structure between liquid (oil + asphaltene-I) and asphaltene-II are the average number of aromatic rings in the unit structure (Hau/Ca) and fa. At about 20% conversion the degree of substitution of ring carbons, σ, of each product using $ZnCl_2$ catalyst is lower, and fa is higher than those obtained with the other catalysts. This suggests that $ZnCl_2$ catalyses reactions which decrease σ and increase fa, e.g., dealkylation. This ability of $ZnCl_2$ may be related to the high activity in the initial stage of hydrogenation.

It is concluded that a continuous distribution exists in the structural units of coal. The units taking part in the noncatalytic reaction up to about 20% conversion are characterized by higher H/C ratio, lower O,N,S/C ratio, higher content of aliphatic hydrogen ($H\alpha$ + Ho), lower fa and 1-2 aromatic rings. In the catalytic reaction (greater than 20% conversion) the units taking part in the reaction are characterized by lower H/C ratio, higher content of Ha, higher fa and larger number of aromatic rings.

Acknowledgement

This work was supported by the U.S. Department of Energy, Contract E(49-18)-2006.

REFERENCES

1. G. R. Hill and L. B. Lyon, Ind. Eng. Chem., 54 (6), 36 (1962).

2. A. G. Oblad, Catal. Rev.-Sci. Eng., 14 (1), 83 (1976).

3. R. Yoshida, Y. Maekawa, T. Ishii and G. Takeya, Nippon Kagaku Kaishi (J. Chem. Soc., Japan, Chem. Ind. Chem.), 1972 (10), 1885.

4. R. C. Neavel, Fuel, 55, 237 (1976).

5. R. E. Wood and W. H. Wiser, Ind. Eng. Chem., Process Des. Devel., 15, 144 (1976).

6. R . Yoshida, T. Ishii and G. Takeya, Nippon Kagaku Kaishi (J. Chem. Soc. Japan, Chem. Ind. Chem.), 1972 (10), 1892.

7. R. Yoshida, Y. Maekawa and G. Takeya, Nenryo Kyokaishi (J. Fuel Soc. Japan), 51, 1225 (1972).

8. K. D. Bartle and D. W. Jones, Fuel, 48, 21 (1969).

9. J. K. Brown and W. R. Ladner, Fuel, 39, 87 (1960).

Table 1. - Analysis of Clear Creek, Utah, coal

Ultimate analysis (%, d.a.f.)				Atomic ratio		Proximate analysis (%)			
C	H	N	O(diff)	H/C	O,N,S/C	Moisture	Ash	Volatile matter	Fixed carbon
76.1	5.5	1.6	16.8	0.87	0.18	0.83	6.50	45.42	47.25

Table 2. Yield of products from hydrogenation

Catalyst	Temp, (°C)	Tube length (m)	Time (sec)	Product distribution (% d.a.f.) Liquid: Aqueous phase	Oil	Asphaltene-I	Total	Gas	Residue: Asphaltene-II	Toluene insolubles	Conversion (%,d.a.f.)
$ZnCl_2$	400	36	13	1.7	1.3	0.6	3.6	2.0	0.6	93.8	6.2
	450	36	13	4.0	2.7	3.0	9.7	3.2	2.5	84.6	15.4
	500	12	8	4.2	4.4	3.4	12.0	2.0	3.7	82.3	17.7
		18	21	4.9	7.9	11.2	24.0	3.5	8.0	64.5	35.5
		24	8	3.9	4.8	4.8	13.5	2.9	2.3	81.3	18.7
		36	372	7.4	35.1	3.7	46.2	11.0	17.0	25.8	74.2
Co-Mo	500	36	12	3.3	6.3	4.1	13.7	2.6	2.9	80.8	19.2
Presulfided red-mud	500	36	12	4.5	5.3	6.5	16.3	4.1	2.5	77.1	22.9
Red-mud plus sulfur	500	36	12	4.3	4.5	7.5	16.3	3.3	2.5	77.9	22.1
No	500	36	10	2.9	5.5	5.1	13.6	3.4	3.0	80.0	20.0

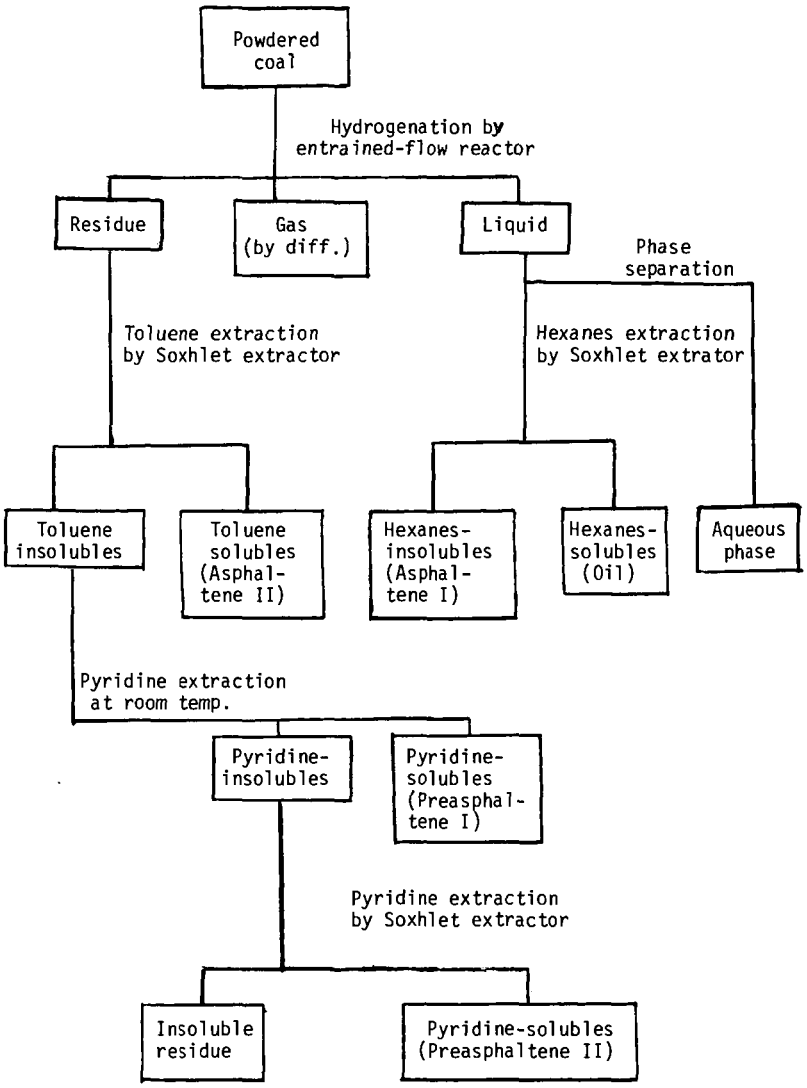

Fig. 1 - Flow diagram of product separation

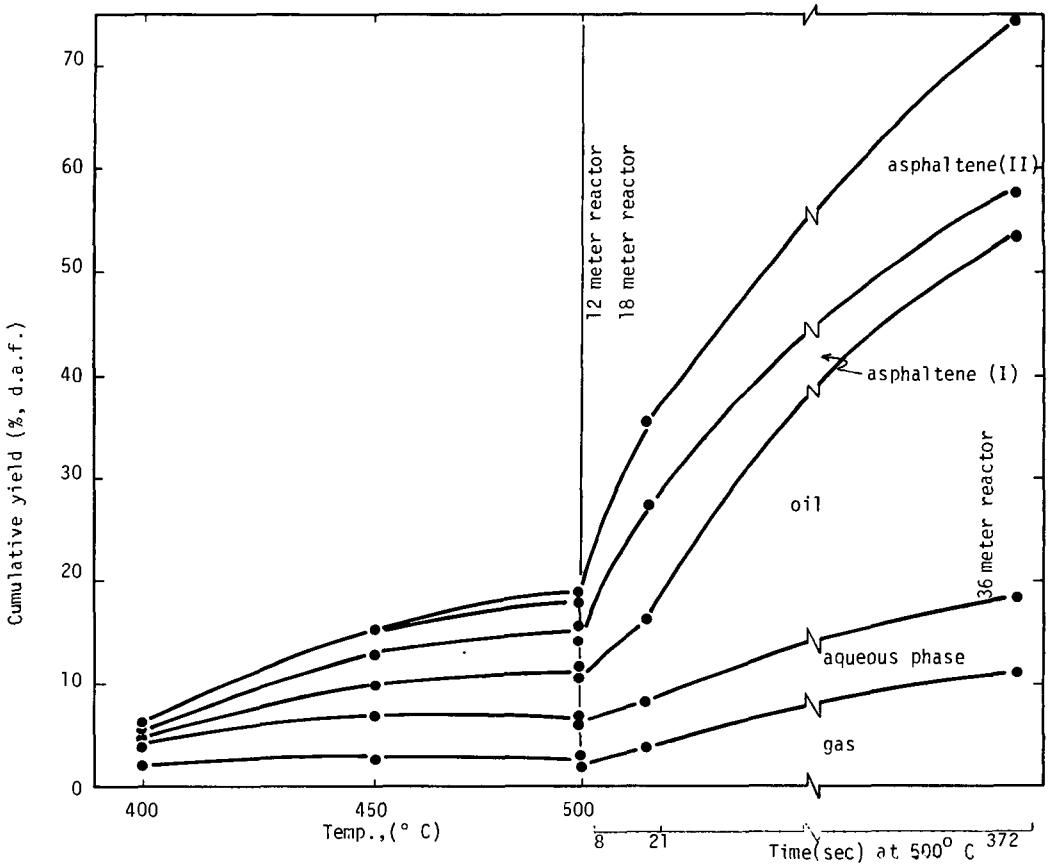

Figure 2. Effects of temperature and time on hydrogenation with $ZnCl_2$ catalyst.

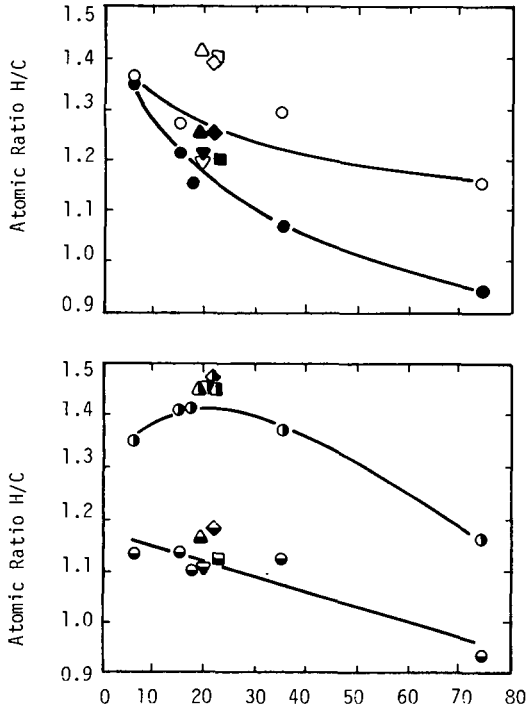

Figure 3. H/C Ratio of Products Versus Conversion

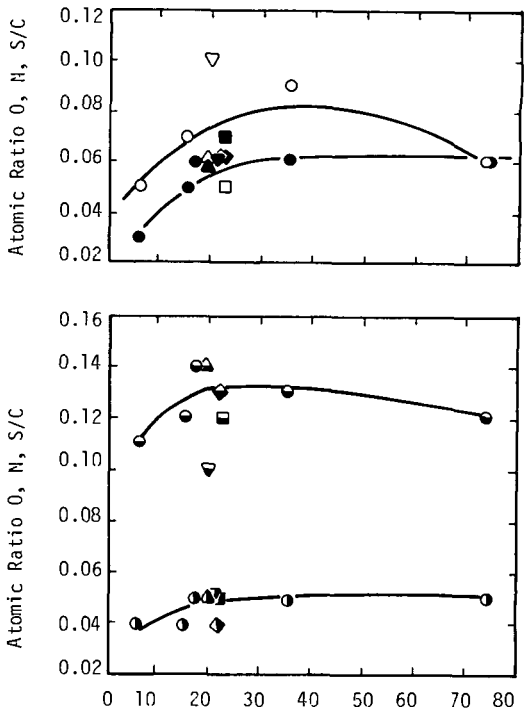

Figure 4. O, N, S/C Ratio of Products Versus Conversion

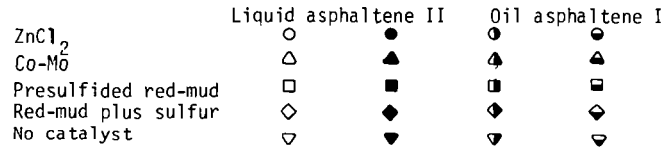

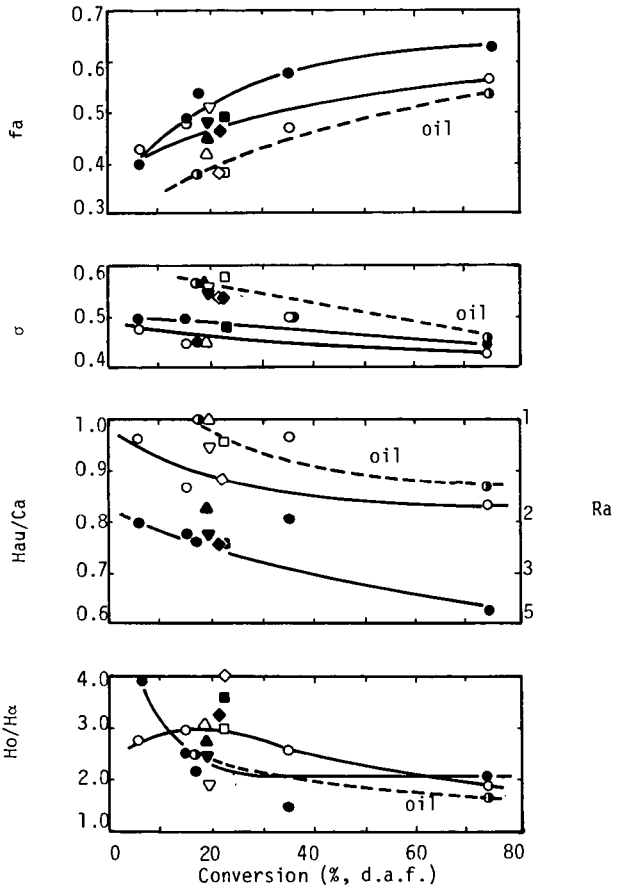

Figure 5. Change of Structural Parameters of Products with Conversion

	Liquid	Asphaltene-II	Oil
$ZnCl_2$	○	●	◑
Co-Mo	△	▲	
Presulfided red-mud	□	■	
Red-mud plus sulfur	◇	◆	
No catalyst	▽	▼	